

**The Tethered Agonist Approach to Mapping Ion-Channel Proteins—
Toward a Structural Model for the Agonist-Binding Site of the
Nicotinic Acetylcholine Receptor**

Thesis by

Lintong Li

In Partial Fulfillment of the Requirements

for the Degree of

Doctor of Philosophy

California Institute of Technology

Pasadena, California

2002

(Submitted July 5, 2002)

© 2002

Lintong Li

All Rights Reserved

Acknowledgements

I am finally here, right before finishing my 24 years of student life. I am happy and excited about beginning new explorations but will miss being a student, especially the time I have spent here at Caltech. I wish I could stay here longer and have additional learning opportunities. I am writing this to thank people here as well as to record memories of my Caltech life.

First of all, I would like to thank my advisor, Professor Dennis A. Dougherty. I am fortunate to be able to study at Caltech, and even more fortunate to have Dennis as my advisor. I am very grateful to Dennis for his guidance, encouragement, support and understanding. As a scientist, he amazes me with his scientific insights. As a mentor, he has taught me above all how to do good science. As an advisor, he has encouraged me through frustrating research times and has supported me in scientific and life decisions. I deeply appreciate his patience and I am always impressed by his ability to understand me, sometimes before I could even express myself clearly.

I would also like to thank my mentor in Biology, Professor Henry A. Lester, for his advice and support. I have certainly benefited a great deal from all the discussions I had with him and the great ideas he provided me. I have learned a lot from his challenging and insightful questions for me in our “Unnatural” meetings. I also appreciated all his time and advice.

I thank all the other members of my committee. I thank Professor Robert H. Grubbs for his advice. I learned a lot about carbohydrate chemistry from the joint group meeting that we have had with Professor Linda Hsieh-Wilson's group. I am very grateful to Professor Sunney I. Chan for his support.

My graduate study has been so much enjoyable and fruitful because of many talented colleagues and friends I have met here at Caltech. I feel lucky to have met Dr. Wenge Zhong at the beginning of my graduate studies. I learned organic chemistry and molecular biology from him and completed my first chemical reactions, injection and recording with his assistance. I have benefited from the practical advice he has given me since then. Gabriel S. Brandt also taught me a lot of biology, helped me in many ways, and is always very patient and thoughtful. He is full of ideas, which are probably proportional to the papers filling up his desk. It is always fun to chat with Josh A. Maurer; more importantly, he has answers to all kinds of questions and is a good resource of information. Niki M. Zacharias is always a warmhearted girl; I will never forget the group baby shower she organized for me, nor the hospital visit from her, Gabe, Josh and Don right after the birth of my son. Donald E. Elmore is the group computer guy (well, sure more than that) and is also always there when I need a favor. I enjoyed the company of Dr. David S. Dahan during recording experiments, especially his optimistic spirit in front of tedious experiments and frustrating results. I appreciate E. James Petersson for his help with troubleshooting the HPLC, and his time to show me how to use Environmental Engineering's HPLC-MS. Sarah L. Monahan is such a talented and versatile girl who enjoys many different activities that I wish I could. I am sure I will see

her photographs somewhere in the future. Darren L. Beene has the most diverse experience among the people I have met here, from Alaska to Germany, from a fisherman to a cook. I wish a great fatherhood for him. I had so much fun talking with my new officemate Steve A. Spronk about everything from fantasy baseball to religion. Tingwei Mu is the youngest in our group now. I enjoyed the time when we talked in our native language about many things except soccer, which he is a fan of and I am not. Amanda L. Cashin is just starting her exciting research in our group.

Thanks also go to other former members of our “Unnatural” group. Marcus C. Sarofim is smart and speaks really fast. I am sure he will have a bright future. Both Dr. Justin P. Gallivan and Dr. Pamela A. England are great scientists. Dr. Vince Liptak is pursuing a new career in patent law. I also thank all the help from Drs. Jennifer C. Ma, Sarah M. Ngola, Seth A. Miller and Jesse Lin, who graduated soon after I joined the group.

I also want to thank many members of the Lester group. Dr. Hong Dang is a great rig captain and biologist who made Hartline I such a nice rig. I bothered him with many questions and problems that he answered and solved for me in almost every case. Dr. Ming Li and I have so many similar interests that we can’t stop talking whenever we see each other. Dr. Ping Li is always fun to talk to. I thank Purnima Deshpande and Shannan Boss for organizing a baby shower for me. I appreciate all the help and suggestions I have got from Dr. Cesar Labarca, Purnima Deshpande, Vanna Santoro, Dr. Yanhe Tong, Dr. Baljit Khakh, Dr. Yongxin Li, Hairong Li, Dr. Chi-Sung Chiu, Dr.

Wenmei Shi, Donghong Ju, Pam Fong, Kira Kostenko, Jason Sydes and Dr. Irina Sokolova. I also thank Shannan Boss and Linda Clark for helping with scheduling.

My life here in the last five years wouldn't have been this memorable without the friendship that I have shared with my good friends, Dr. Suzie Hwang Pun, Dr. Winston Pun, Dr. Sidao (Stone) Ni, Dongdong (Dorothy) Niu, Dr. Xindong Liu, Ning Liu, Jiehui Wang and Dr. Wen Li. We have had so much great time together and so many good memories. I will always cherish our invaluable friendship. I would also like to thank the friends I have met at FIS (Fellowship of International Students) at Lake Avenue Church, especially Perlita Lim for all her caring and kindness. I thank Aileen Chang for her advice on choosing a research group after I came to Caltech.

I thank Dr. Wenge Zhong for preparing the compounds Tyr-O3Q and Lysyl-carbamylcholine discussed in Chapter 2 and 3, respectively. I thank Niki M. Zacharias and Caroline Gibbs for preparing the compound Tyr-O3tBu discussed in Chapter 2. I thank Deqiang Zhang for assistance in the docking studies discussed in Chapter 3. I thank Professor Dennis A. Dougherty for proofreading this thesis.

I have reserved my final thanks for my family. I can't thank my parents enough for the unconditional love they have given me. They have supported me in all these years both emotionally and physically. I thank my son, George, who has given me all the joys that nobody else could give me. Finally, I want to thank my husband, Deqiang Zhang, who is the foundation stone of my life.

Abstract

The integral membrane proteins of neurons and other excitable cells are generally resistant to high-resolution structural tools. In this thesis we present our efforts to probe the structure of the agonist-binding site of the nicotinic acetylcholine receptor (nAChR) using the tethered agonist approach, which combines chemical synthesis, the nonsense suppression methodology for unnatural amino acid incorporation and electrophysiology.

In Chapter 2, we present the results of incorporating a series of tethered quaternary ammonium derivatives of tyrosine into the nAChR using the *in vivo* nonsense suppression methodology for incorporating unnatural amino acids site-specifically. At three sites, a constitutively active receptor results, but the pattern of activation as a function of chain length is different. At position $\alpha 149$, there is a clear preference for a three-carbon tether, while at position $\alpha 93$ tethers of 2-5 carbons are comparably effective. At position $\gamma 55/\delta 57$, all tethers except the shortest one can activate the receptor. Based on these and other data, a model for the binding site of the receptor can be developed by analogy to the acetylcholine esterase crystal structure.

In Chapter 3, we report evidence that the N-terminal extracellular domain of nAChR is closely related to acetylcholine binding protein (AChBP), whose crystal structure was solved in May 2001. Based on the model obtained from docking acetylcholine into the structure of AChBP, we designed and incorporated a new tethered agonist, lysyl-carbamylcholine. Incorporation of this tethered agonist at several positions

produced constitutively active receptors, with significant activity seen at α 192, α 193, and γ 119/ δ 121. These results demonstrated that the loop E residue γ 119/ δ 121 on the complementary subunit is very near the agonist-binding site. We also investigated the role of an intersubunit hydrogen bond, which was seen in the crystal structure of AChBP. Incorporation of tryptophan analogs that abolish the hydrogen bonding abilities slowed the desensitization of the receptor, which implied that this hydrogen bond might play a key role in the allosteric transitions of desensitization.

In Chapter 4, we describe our efforts to prepare a short tethered agonist and the results of incorporating it into nAChR at α 198 by chemical modification of cysteine mutants introduced by nonsense suppression methodology. Methanethiosulphonate ethyltrimethylammonium (MTSET) modification resulted in constitutive activity, which suggested the closeness of α 198 to the agonist-binding site.

In Chapter 5, methods in molecular biology, electrophysiology and molecular docking, and the synthesis of amino acids and dinucleotide dCA-amino acids are summarized.

Table of Contents

Acknowledgements.....	iii
Abstract.....	vii
List of Figures.....	xii
List of Schemes.....	xv
List of Tables.....	xvi
Chapter 1. Introduction.....	1
1.1 Chemical Approaches to Exploring Molecular Neurobiology.....	2
1.2 The Nicotinic Acetylcholine Receptor (nAChR).....	7
1.3 The Agonist-Binding Site of nAChR.....	13
1.4 The Crystal Structure of Acetylcholine Binding Protein (AChBP).....	17
1.5 Reference.....	21
Chapter 2. Mapping the Agonist-Binding Site of the nAChR by Tethered Agonists– Identification of Residues Contributing to the Binding of the Quaternary Ammonium Group of Acetylcholine.....	28
2.1 Introduction.....	29
2.2 Incorporation of Tyr-OnQ into the nAChR.....	33
2.3 Incorporation of an Isosteric, Neutral Tether.....	38
2.4 Discussion.....	41
2.5 Reference.....	49

Chapter 3. Identification of Additional Residues Near the Agonist-Binding Site by a Tethered Agonist and Investigation of the Effect of an Intersubunit Hydrogen Bond on the nAChR Desensitization—Further Evidence that the N-terminal Extracellular Domain of nAChR Is Closely Related to AChBP.....	52
3.1 Introduction.....	53
3.2 Docking Studies.....	57
3.3 Incorporation of Lysyl-carbamylcholine at γ Leu 119/ δ Leu 121 Resulted in Significant Constitutive Activity of the Receptor.....	61
3.4 Investigation of the Effect of an Intersubunit Hydrogen Bond on Desensitization.....	70
3.5 Conclusions and Future Directions.....	76
3.6 Reference.....	78
Chapter 4. Efforts Toward Preparing a Short Tethered Agonist and Its Introduction into nAChR by Chemical Modification.....	80
4.1 Introduction.....	81
4.2 Efforts toward Preparing a Short Tethered Agonist—MTSET-Modified Cysteine.....	82
4.3 MTSET-Modification of Cysteine Incorporated by Nonsense Suppression Resulted in Constitutively Active Receptors.....	89
4.4 Reference.....	92

Chapter 5. Methods in Molecular Biology, Electrophysiology and Molecular Docking, and Synthesis of Amino Acids.....	93
5.1 Methods in Molecular Biology and Electrophysiology.....	94
5.2 Methods for Molecular Docking.....	98
5.3 Synthesis of Amino Acids and dCA-Amino Acids.....	101
5.4 Reference.....	113
 Appendix I.....	 116

List of Figures

Figure 1.1. Schematic of synaptic transmission.....	3
Figure 1.2. The fundamental protocol for <i>in vivo</i> nonsense suppression methodology for incorporating unnatural amino acids site-specifically into proteins.....	6
Figure 1.3. The structure of nAChR.....	9
Figure 1.4. Transitions between the four states of the nAChRs.....	11
Figure 1.5. The structure of nAChR with a blowup of the agonist-binding site that was mapped based on biochemical studies.....	15
Figure 1.6. The structure of AChBP.....	19
Figure 2.1. Plot of $\log[EC_{50}/EC_{50}(\text{wild type})]$ vs. quantitative cation- π binding ability at $\alpha 149$ for the fluorinated tryptophans.....	30
Figure 2.2. Schematic of the quaternary ammonium of ACh positioned over the 6-ring of α Trp 149 and the structure of Tyr-O3Q.....	31
Figure 2.3. Representative recording trace of voltage-clamp currents for an individual oocyte expressing mutant nAChR with Tyr-O3Q incorporated at $\alpha 149$	34
Figure 2.4. The standing current is partially occluded by additional ACh.....	35
Figure 2.5. Tethered agonist relative efficiencies for Tyr-OnQ as a function of n (the number of methylene groups in the side chain) at positions $\alpha 149$, $\alpha 93$, and $\gamma 55/\delta 57$	38
Figure 2.6. Structure of Tyr-O3Q and Tyr-O3tBu.....	39
Figure 2.7. Results of incorporation of Tyr-O3tBu compared with that of Tyr-O3Q at three sites of nAChR.....	39
Figure 2.8. Binding of nAChR by ^{125}I - α -bungarotoxin measured by γ counter.....	40

Figure 2.9. Western blots of nAChR.....	41
Figure 2.10. The evolving view of the nAChR agonist-binding site.....	48
Figure 3.1. The deduced structure of the agonist-binding site of the nAChR.....	55
Figure 3.2. Two different views of docked ACh in the binding site of AChBP.....	60
Figure 3.3. The structure of acetylcholine, carbamylcholine and lysyl-carbamylcholine.....	62
Figure 3.4. The electrophysiological results of incorporation of lysyl-carbamylcholine into nAChR at γ Leu 119/ δ Leu 121 on three different experiment dates.....	63
Figure 3.5. The relative effectiveness of lysyl-carbamylcholine at γ Leu 119/ δ Leu 121 on three different experiment dates.....	64
Figure 3.6. Comparison of the effectiveness of the two tethered agonists at γ Leu 119/ δ Leu 121.....	65
Figure 3.7. The results of incorporation of Tyr-OnQ (n=2-5) and Tyr-O3tBu at γ Leu 119/ δ Leu 121.....	66
Figure 3.8. The relative effectiveness of tethered agonist lysyl-carbamylcholine at α Cys 192 and α Cys 193.....	68
Figure 3.9. Structures of tryptophan and its analogues.....	71
Figure 3.10. Representative traces in the desensitization experiments.....	72
Figure 3.11. The weighted rate constants for desensitization of wild-type and mutant nAChRs.....	73
Figure 3.12. ACh-induced current for wild-type and mutant nAChRs with tryptophan analogs at α Trp 149.....	74

Figure 3.13. Representative dose-response measurements for wild-type and mutant nAChRs with tryptophan analogs at α Trp 149.....	75
Figure 4.1. The structure of MTSET-modified cysteine.....	81
Figure 4.2. A schematic of the electronic effect of the quaternary ammonium on the instability of the ester bond.....	85
Figure 4.3. Amino acids containing a short chain with a quaternary ammonium group at the end.....	86
Figure 4.4. The representative traces in the electrophysiological experiment.....	90
Figure 4.5. The inward current resulted from the MTSET-modification of the mutant nAChR with cysteine at α 198 in the presence or absence of the Leu9'Ser mutation in β subunit.....	91

List of Schemes

Scheme 4.1. The synthetic route for N-NVOC-S-[(2-trimethylammonium)-ethylthio]-cysteine cyanomethyl ester.....	83
Scheme 4.2. The disproportionation of the disulfide of N-NVOC-S-[(2-trimethylammonium)-ethylthio]-cysteine cyanomethyl ester.....	83
Scheme 4.3. Synthesis of dCA- N-NVOC-S-[(2-trimethylammonium)-ethylthio]-cysteine beginning with the coupling of N-NVOC-S-trityl-cysteine cyanomethyl ester with dCA followed by the deprotection of trityl group and the reaction of MTSET.....	84
Scheme 4.4. Synthesis of N-NVOC-S-[(2-trimethylammonium)-ethylthio]-cysteine....	86
Scheme 4.5. The method of coupling the N-protected amino acid with dinucleotide dCA using CDI in aqueous solution.....	87
Scheme 4.6. The method of coupling the N-protected amino acid with NPS-protected dinucleotide dCA using CDI in anhydrous DMSO.....	88
Scheme 5.1. Synthesis of dCA-amino acid.....	102
Scheme 5.2. Synthesis of Tyr-OnQ.....	104
Scheme 5.3. Synthesis of 5-amino tryptophan.....	108

List of Tables

Table 3.1. Interaction energies (kcal/mol) between ACh and the five aromatic residues in the binding site.....	59
Table 3.2. The channel opening rate constants and the equilibrium binding constants of the nicotinic ligands for the embryonic mouse muscle nAChR.....	62
Table 3.3. The EC ₅₀ values and Hill coefficients for wild-type and mutant nAChRs with tryptophan analogs at α Trp 149.....	75

Chapter 1

Introduction

1.1 Chemical Approaches to Exploring Molecular Neurobiology

As an integral part of modern biology, neuroscience has benefited from research in all different fields, such as physics, chemistry, mathematics, anatomy, physiology and medicine. Our group has been trying to develop detailed insights into the structure and function of the molecules of memory, thought and sensory perception, using chemical approaches. This thesis presents work that is a small portion of these efforts. We will begin with discussion on neuroscience in general and introduce the molecules of the brain. We will then describe some chemical approaches that have been developed and used to study these molecules.

The human brain is a remarkably complicated structure (1, 2). There are roughly 10^{12} neurons in a human brain, and there is great diversity among them, with perhaps 1,000 different types of neurons. There are two million miles of axons. A ‘typical’ neuron makes connections (synapses) with 10^3 – 10^4 other neurons. This means that there are 10^{15} – 10^{16} synapses in the human brain. Altogether it makes the human brain the most complex structure, natural or artificial, on Earth (3).

Moving toward molecular issues, much of the action occurs at the synapse (4). The brain is about cell-cell communication, and the synapse is the gap between two cells (Figure 1.1). Synaptic transmission is mediated by small neurotransmitter molecules such as acetylcholine, dopamine and serotonin. These neurotransmitters are released from the presynaptic neuron, traverse the synaptic gap, and are then recognized and

processed by receptors on the surface of the postsynaptic neuron. One class of receptors is the G protein-coupled receptor class, in which ligand binding leads to activation of G proteins and which usually operates in a time frame of seconds (3). The activated G proteins act as second messengers to regulate the metabolism of the cell, as well as by directly affecting channel proteins. These ‘slow’ G protein-coupled receptors play a role in modulating synaptic transmission, cell excitability, and sensory systems. The other class of receptors is the ligand-gated ion channels (Figure 1.1), which on ligand binding undergo a fast conformational change to open an integral pore within a time frame of 1–100 ms (3). The majority of synaptic transmission in the brain is mediated by these ‘fast’ receptors. These receptors, and other neuroproteins such as ion-channels and neurotransmitter transporters, are proteins with a tremendous diversity of structure, but a few common features.

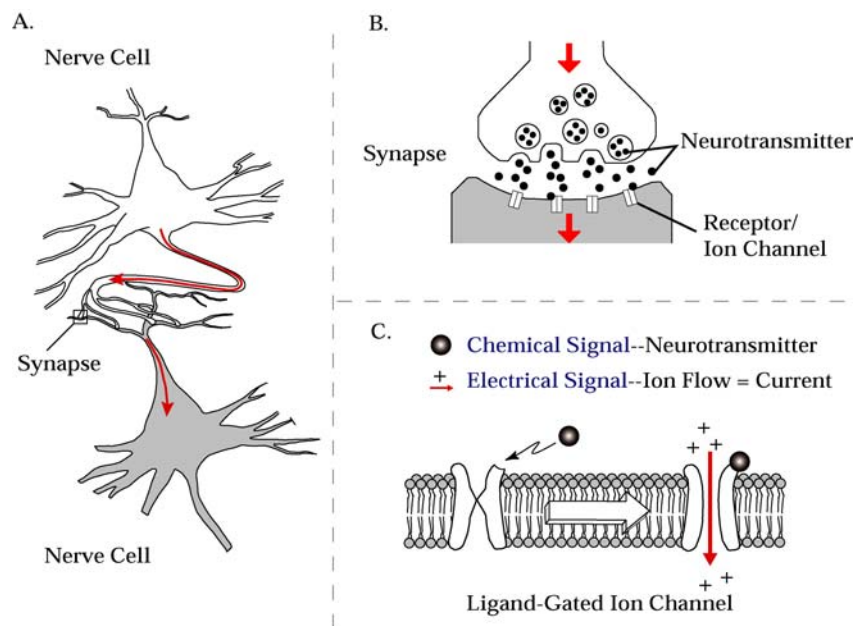


Figure 1.1. Schematic of synaptic transmission. A. Two neurons and the synapse between them. The red arrow indicates the direction of the action potential. B. The blowup of a synapse. C. Ligand-gated ion channel.

First, they are all integral membrane proteins. That is, they are not membrane-anchored or structures with just one membrane-spanning segment like the family of hormone receptor molecules. Neuroproteins typically cross the membrane many times, some containing 12 or more transmembrane segments. Often more than half of the protein is embedded in the membrane. Second, many, but not all, neuroproteins are multi-subunit systems. Often four or five individual proteins, each with several transmembrane segments, combine to form the functional system. Because of these features, it is in general difficult to accumulate significant quantities of pure, properly folded, functional neuroproteins. They are therefore not amenable to high-resolution structural methods, such as x-ray crystallography or NMR spectroscopy. For some systems, very useful low-resolution images are available, but atomic-scale detail is not.

In the absence of high-resolution structural data, important and fundamental insights into the mechanism underlying channel gating have been gained from structure-function studies at the molecular level. To do so, we need two tools: a way to modify rationally the structures of the neuroreceptors and a means to evaluate the functional consequences of the structural changes. For the latter, modern electrophysiological methods have enabled the measurement of the electrical activity of a single cell, even of a single ion channel molecule. As for the way to vary the structure of the neuroproteins, traditional site-directed mutagenesis has been a very valuable tool. However, it is restricted to the 20 natural amino acids, and therefore only allows limited structural variation. In order to introduce more chemical probes with diverse structures, chemical modification of natural amino acid has been commonly used. One of the most widely

used methods is the substituted-cysteine accessibility method (SCAM). SCAM is an approach to the characterization of channel (5, 6) and binding-site structures (7) that probes the environment of any residue by mutating it to cysteine, and by characterizing the reaction of the cysteine with sulfhydryl-specific reagents. Among these reagents, the methanethiosulphonates (MTS) are attractive because of their small size and their specificity for sulfhydryls (8). SCAM has been successfully used to identify channel-lining residues, to determine the potentially different environments of these residues in the open and closed states of the channel, to locate selectivity filters and gates, and to map the binding sites of channel blockers (9). In spite of all the success, SCAM has several limitations. First of all, it relies on cysteine mutation and therefore is restricted by the extent of the tolerance of the cysteine substitution in the protein. Second, it is limited to those positions that are accessible by the modification reagent. Furthermore, it lacks site-specificity if there are more than one cysteine in the protein. Finally, there might be complications due to side reactions related to the chemical modification.

In contrast, the nonsense suppression method for incorporating unnatural amino acids into proteins (Figure 1.2) has opened up essentially limitless possibilities to conduct a wide range of studies into protein structure and function. For over a decade, a diverse array of unnatural amino acids have been incorporated site-specifically into a variety of proteins. The methodology was developed and used in the *in vitro* translation system by Schultz's group (10) and a few other groups (11). Our group, in collaboration with Prof. Henry Lester, have taken a step further and adapted it into the *in vivo* translation system using the *Xenopus* oocyte (12, 13) to study the integral membrane proteins that play a

central role in molecular neurobiology. This methodology allowed us to perform more systematic structure-function studies when we use unnatural amino acid analogs with only subtle changes compared with the natural amino acids (14, 15). We also incorporated unnatural amino acids with more dramatic changes, for example, caged tyrosine (16, 17) and biocytin (18). More remarkably, we even incorporated α -hydroxy acids to make the backbone mutation to investigate the change of secondary structure during channel gating (19). In the work presented in this thesis we sought to generalize a potentially powerful tool—the tethered agonist approach—for mapping the agonist-binding site of the ligand-gated ion channels. This approach has been applied successfully to probe the structure of the agonist-binding site of the prototype ligand-gated ion channel—the nicotinic acetylcholine receptor. We will discuss this in more detail in the following chapters.

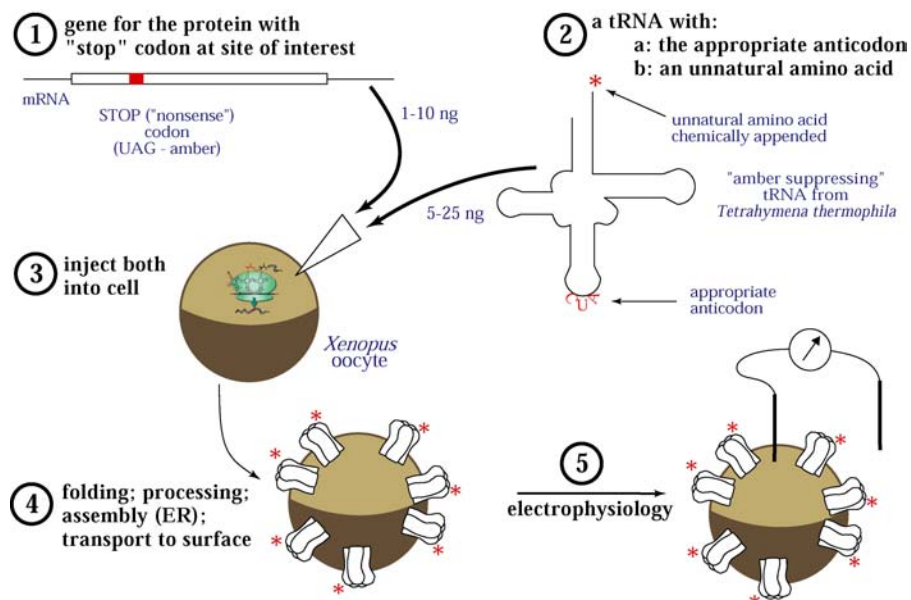


Figure 1.2. The fundamental protocol for *in vivo* nonsense suppression methodology for incorporating unnatural amino acids site-specifically into proteins.

1.2 The Nicotinic Acetylcholine Receptor (nAChR)

The nicotinic acetylcholine receptor (nAChR) belongs to a superfamily of ligand-gated ion channels, which mediate intercellular communication by converting the neurotransmitter signal released from the nerve ending into a transmembrane ion flux in the postsynaptic neuron or muscle fiber. The superfamily includes nAChR, 5-hydroxytryptamine type 3 (5-HT₃) receptors, γ -aminobutyric acid type A (GABA_A) and GABA_C receptors, glycine receptors and invertebrate glutamate and histidine receptors (8). All members of the superfamily share sequence homologies as well as structural and functional features.

The identification of the nAChR was made possible largely by a few wonders of the animal world (20). First, the electric organ of fish offers both an extremely rich and homogeneous source of synaptic material, and single cells (or electroplaques) for pharmacological studies. Second, because of its exquisite selectivity and high affinity, an α -toxin from the venom of the snake *Bungarus* enabled the isolation and purification of nAChR from the electric organ (21).

There are both muscle-type and neuronal-type nAChRs. The muscle receptors function at the neuromuscular junction as well as electric organs of certain rays and eels, while the neuronal receptors function in the central neural system. Their physiological properties include the activation response to fast application of acetylcholine (ACh) in the millisecond timescale resulting in the opening of the ion channel, as well as the slow

decrease or even full abolition, of the electrical response referred to as desensitization, following a prolonged application of nicotinic agonists and antagonists. The different nAChRs mediate the pharmacological actions of drugs, such as the effects of curare on muscle and of nicotine in brain, including addiction in smokers. The nAChRs are also involved in analgesia, enhanced cognition, memory and attention, and therefore also serve as the target for a number of promising pharmaceuticals for pain, memory enhancement, and the treatment of Alzheimer's and Parkinson's diseases (22). The role of desensitization in cholinergic neurotransmission under normal physiological conditions is uncertain, but is evident both in some pathological conditions and in neurotransmission by other neurotransmitters (23).

The muscle-type nAChR is a heteropentamer of ~300 kDa with a stoichiometry of $(\alpha 1)_2\beta 1\gamma\delta$ in electrocytes and fetal muscle and $(\alpha 1)_2\beta 1\varepsilon\delta$ in adult muscle. The overall shape and dimensions of the complex have been visualized by electron microscopy (EM) (Figure 1.3A). In the embryonic muscle-type nAChR (24), the subunits are arranged clockwise in the circular order of $\alpha\gamma\alpha\beta\delta$, as viewed from the synaptic cleft, like barrel staves around a central channel pore with a diameter of ~25 Å at the synaptic entry (25-27). Sequence analysis reveals homologies between the nAChR subunits from electric organ, skeletal muscle and brain of higher vertebrates, including humans (28). There are 12 known types of vertebrate neuronal ACh receptor subunit: $\alpha 2$ – $\alpha 10$ and $\beta 2$ – $\beta 4$. When expressed heterologously, $\alpha 7$, $\alpha 8$ and $\alpha 9$ can form functional homopentamers (29–32). By contrast, the $\alpha 2$ – $\alpha 6$ and $\alpha 10$ neuronal subunits form functional complexes only when coexpressed with β -subunits or with other α -subunits (33–36).

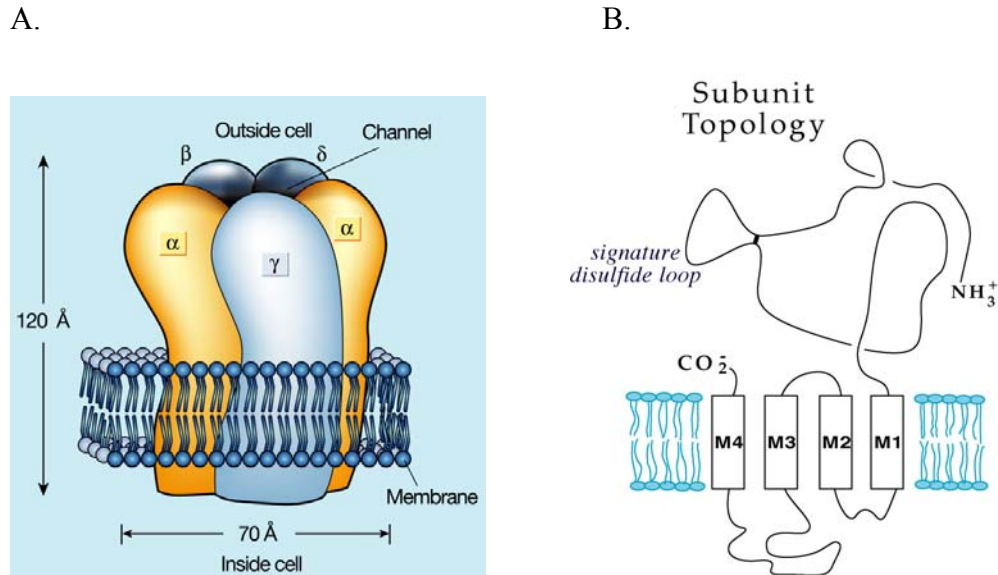


Figure 1.3. The structure of nAChR. A. The overall layout of the nAChR, based on the 4.6 Å resolution structure by cryo-electron microscopy studies (26, 27). (Figure adapted from ref. (37).) B. The transmembrane topology of each subunit. The four transmembrane regions are indicated as M1, M2, M3, and M4, respectively.

All nAChR subunits share a similar hydrophathy profile (Figure 1.3B), with a large N-terminal hydrophilic domain (comprising ~210 amino acids) that faces the synaptic cleft and carries the ACh-binding site, four ~20-amino acid hydrophobic transmembrane stretches (the second of which, M2, lines the ion channel), and a hydrophilic cytoplasmic loop that contains the phosphorylation sites and is involved in receptor biosynthesis, assembly, transport, clustering, anchoring, and modulation.

Attempts to solve the entire structure of nAChR failed, for the reasons discussed earlier. Structural studies were thus limited to electron microscopy (EM) down to 4.6 Å resolution (27) and to the recombinant N-terminal synaptic domain of nAChR. Circular

dichroism revealed a high content of β -sheet structure in the isolated extracellular domain of the $\alpha 1$ -subunit of the mouse muscle receptor (38), a finding consistent with recent EM images that revealed tunnels in the $\alpha 1$ -subunit N-terminal domain of *Torpedo* receptor that were framed by seven twisted β strands running approximately perpendicular to the membrane plane (27). In addition, secondary structure predictions suggested an immunoglobulin-like folding, almost exclusively of β sheets, for the N-terminal domain of the nicotinic receptor (39). High-resolution data at the atomic level are now available for ACh binding protein (AChBP) (see section 1.4).

The residues located at the interface are not well conserved among nAChRs and probably contribute to the diversity of subunit combinations. By contrast, specific interactions (e.g., hydrophobic, polar, hydrogen bonds) have to be at least partially conserved to mediate common features of the allosteric transitions. The nAChRs are allosteric, in that they are oligomeric, contain multiple agonist-binding sites, noncompetitive antagonist sites, and gates that interact at a distance (~ 20 - 40 Å between the binding sites and the ion channel based on fluorescence transfer measurements (40)) through changes in the quaternary structure of the receptor. In response to ACh, single nAChR molecules undergo a conformational transition to an open channel low-affinity state, associated with slower modulatory transitions to (or from) desensitized, closed and high-affinity states. Four functional states have been described in nAChRs (Figure 1.4): the resting (closed) state (R), the active open state (O), the fast-onset desensitized (closed) state (I), and the slow-onset desensitized (closed) state (D) (41-48). The resting state is the most stable state in the absence of agonist, and the slow-onset desensitized

state is the most stable state in the presence of agonist. The open state and the fast-onset desensitized state are metastable states, in that their concentrations rise transiently and reach a very low value at equilibrium. The nAChRs also open, albeit rarely, and desensitize in the absence of agonist. Many models have been developed to fit the kinetics of agonist binding, channel opening and closing, and desensitization. One of them is the Monod-Wyman-Changeux (MWC) model of allosteric interactions (49, 50). The MWC theory has been extended to accommodate multiple functional states and quasi-symmetry (46, 48) since most nAChRs are asymmetrical heteromers.

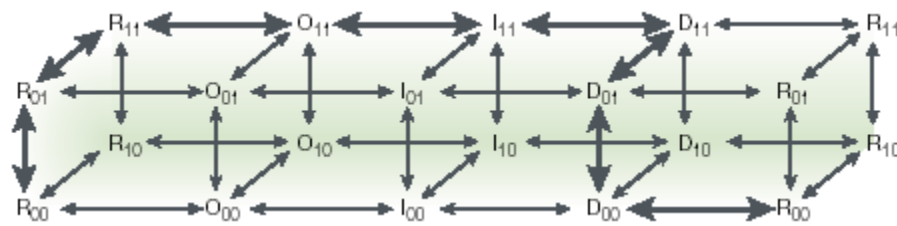


Figure 1.4. Transitions between the four states of the nAChRs. It is assumed that the two agonist-binding sites are different. The subscripts indicate the state of occupation of the sites: 00, unoccupied; 01 or 10, singly occupied; 11, doubly occupied. Heavy arrows indicate a principal reaction pathway. (Figure adopted from Ref. 8.)

Although the requirement for a conformational change that links agonist binding to the opening of the ion channel portion of the receptor (gating) has been obvious, the details have remained elusive. The allosteric transitions of the protein underlying the physiological ACh-evoked activation and desensitization possibly involve movement of the extracellular domain of each subunit, linked to a reorganization of the transmembrane domain responsible for channel gating. One of the structural elements in the extracellular

domain that is thought to be involved in gating is a disulfide bond. The nAChR family is also known as Cys-loop receptors because all family subunits contain a pair of disulfide-bonded cysteines (128 and 142 in nAChR α 1) that are separated by 13 residues in their amino-terminal extracellular domains. This disulphide bond is also called the 'signature loop' that defines this group of proteins. For the gating mechanism associated with the transmembrane domains, two competing models have been proposed. In one model, transmembrane helices are postulated to rotate as rigid bodies, removing a leucine side chain from a blocking position and opening the channel (51). In a competing proposal, the transmembrane segments M1 and M2 slide past each other and convert from a relatively unstructured form to a well-defined α helix (52, 53).

Although the structures of the membrane and cytoplasmic domains are less well determined compared with the extracellular domain, the channel lining and the determinants of selectivity have been mapped. The location and structure of the gates remain to be established. Studies by EM (26), spectroscopic (54, 55) and computational (39) methods as well as chemical labeling and mutagenesis indicate that the membrane-spanning segments are not completely α -helical, as originally predicted, but seem to be a mixture of α -helix, β -strand, and irregular secondary structures (8). The approximate arrangement of the membrane-spanning segments is known: M2 and part of M1 line the central lumen, and M3 and M4 are in contact with lipid. Specific M2 residues (2', 6' and 9' counting from the cytoplasmic, amino-terminal end of M2) that line the channel have been identified by photolabeling with noncompetitive inhibitors (56, 57). SCAM has also been used to identify residues that are exposed to water, which in the membrane domain

include the channel lining residues (5, 58-61). It should be noted that the picture is dynamic. Many residues that line the channel, that are associated with the gates and even with the protein–lipid interface, are in different environments in the different functional states.

Except for an anion-selective invertebrate nAChR (61), all known nAChRs are cation selective, as are 5-HT₃ receptors. All other Cys-loop receptors are anion selective. Cation-selective nAChRs are permeable to monovalent and divalent cations. In muscle-type nAChR, the ratio of permeabilities P_{Ca}/P_{Na} is ~ 0.2 (62). A short (~ 6 Å in length) narrow (7-8 Å in diameter) section, which is at the cytoplasmic end of the channel, selects for ion charge and size, and determines conductances (63-67). This region also contains the resting gate (52, 68). The conductance ratios were most sensitive to mutations of polar residues at the 2' position (63, 65), which is therefore likely to be in the narrowest part of the channel and to constitute part of the selectivity filter.

1.3 The Agonist-Binding Site of nAChR

The agonist-binding sites of the nAChR are located at subunit interfaces (21). The muscle-type receptor has two distinct ACh-binding sites (located at interfaces between the α and γ , and the α and δ , subunits). Photoaffinity labeling and mutagenesis studies have identified a number of residues as being crucial for ligand binding. Affinity labeling experiments performed with a series of competitive antagonists of different chemical structures show that all probes label primarily the $\alpha 1$ subunits, and to a lesser

extent the γ and δ subunits. This supports an asymmetric location of the binding site with respect to the interface. It is thus proposed that the $\alpha 1$ subunits form the 'principal component,' while γ or δ subunits contribute to the 'complementary component' of the nicotinic binding site (21). The principal part is composed of α -subunit residues—contributing to the so-called 'loops' A (W86 and Y93) (69), B (W149 and Y151) (70) and C (Y190, C192, C193 and Y198) (71, 72), whereas the neighboring subunit residues—contributing to the 'loops' D (γ W55/ δ W57) (73), E (γ L109/ δ L111 and γ Y111/ δ R113) (74, 75) and F (γ D174/ δ D180) (76), form the complementary part of the binding pocket (Figure 1.5). In all the photoaffinity labeling studies that identified the above residues, different agonists and antagonists photolabeled various residues to different extents, some with significant amounts of labeling, some with weak labeling. Results from mutagenesis studies are consistent with the findings of the photoaffinity labeling studies. Mutations of the loops A–C residues affected the binding of both agonists and competitive antagonists (77-80). Mutations of the loop D residues affected agonist binding and gating, but had little effect on antagonist binding (81). By contrast, mutations of loop E residues only affected competitive antagonist binding, but not agonist binding or gating (75, 82, 83). These results are consistent with the notion that the loops A–D are the main component of the agonist-binding site, while the loops E and F are less important and more remote.

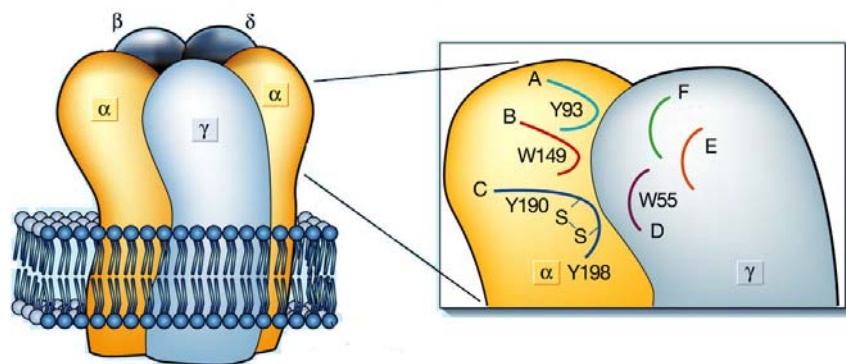


Figure 1.5. The structure of nAChR with a blowup of the agonist-binding site that was mapped based on biochemical studies. The one at the α and γ subunit interface is shown, there is an equivalent one at the α and δ subunit interface. (Image adapted from ref. 27.)

All the residues mentioned above, especially those in loops A-D, are considered the key residues that contribute to ligand binding. Among them, most of them are aromatic residues—tyrosine or tryptophan. This has led us to propose that cation- π interactions might be important in binding the positively charged quaternary ammonium group of ACh. Extensive studies by our group have established that one of the aromatic residues— α Trp 149—is the cation- π site (14). We will discuss this in more detail in Chapter 2. In our earlier studies we investigated the roles played by three tyrosine residues— α 93, α 190, and α 198—by unnatural amino acid mutagenesis, we found some interesting results but no indication of a cation- π interaction (12, 15). We found that the hydroxy group of α Tyr 93 plays a crucial role, and a variety of tyrosine analogues are functional at α Tyr 198, while α Tyr 190 is an especially delicate site.

Besides the aromatic residues, there are a pair of adjacent cysteines, α Cys192 and α Cys 193, which form a highly unusual disulfide bond (84). This disulfide bond is characteristic of all nAChR α -subunits and absent in non- α subunits. A crosslinking experiment with a 9 Å bifunctional reagent reacting with the reduced α Cys192-193 not only identified a carboxylate residue δ Asp 180—the only negatively charged residue that has been shown to participate agonist binding—but also provided information on the distance between the two subunits within the agonist-binding site.

In the muscle-type nAChR, the two agonist-binding sites are not equivalent. In heterologously expressed combinations of subunits, the complex of α - and γ -subunits had a higher affinity for competitive antagonists, whereas the complex of α - and δ -subunits had a higher affinity for agonists (85). In complete receptor complexes, the two sites also bind agonists with different affinity (86). In addition, nAChRs are known for their pharmacological diversity. Different types of receptors bind different agonists or antagonists with different affinities. All the biochemical studies support the notion that variable residues located in the vicinity of the affinity labeled amino acids are the major elements contributing to the pharmacological diversity of the nAChRs (21). The emerging picture is that the binding site consists of a conserved core of aromatic residues, and that variable amino acids neighboring these positions, as well as several amino acids from the nonconserved loops E and F, confer on each receptor subtype its individual pharmacological properties.

Although there have been plenty of biochemical and electrophysiological studies on nAChR, the structure at atomic resolution has been missing. Recently, a high resolution structure of a protein that is homologous to the extracellular domain of the receptor has revealed the binding sites and subunit interfaces in great detail.

1.4 The Crystal Structure of Acetylcholine Binding Protein (AChBP)

Our knowledge of the structure of the nAChR, especially the extracellular domain, has been greatly advanced by the solution of the high-resolution structure of a snail ACh-binding protein (AChBP). In May 2001, Sixma and coworkers reported the discovery, cloning, physiological characterization, and crystal structure of AChBP (87, 88). AChBP is a small soluble protein that is stored and produced in snail glia cells and secreted in an ACh-dependent manner into cholinergic synapses, where it acts as a protein buffer and modulates synaptic transmission by binding ACh. AChBP binds agonists and competitive antagonists of the nAChR, including ACh, nicotine, epibatidine, (+)-tubocurarine and α -bungarotoxin, resembling the α 7-subtype of nAChR, albeit with a higher affinity for most of the ligands. AChBP is homologous to the extracellular domain of the nAChR—the region that contains the agonist-binding site. The structure of AChBP reveals in great detail the nature of the ligand binding domains and the subunit interfaces of the nAChR. Moreover, the structure is completely consistent with 40 years of biochemical studies of the agonist-binding site of the nAChR (see 3.1 for more details).

AChBP forms a homopentamer. Each subunit contains 210 amino acids and is 20-24% identical to the aligned sequences of the amino-terminal, extracellular domain of the nAChR subunits. However, AChBP lacks the transmembrane and intracellular domains present in the ligand-gated ion channels superfamily. Nearly all the residues that are conserved within the nAChR family are also present in AChBP. The characteristic disulphide bond referred to as the Cys-loop is present in the AChBP subunit, but there are only 12 intervening residues in place of the 13 that are found in the nAChR subunits. These residues are almost all different in AChBP compared with nAChR subunits. The Cys-loop consists of highly conserved hydrophobic residues in the nAChR family and is hypothesized to interact with some channel-forming elements. It is possible that this conserved loop is involved in coupling the extracellular domain of nAChR to the membrane region that is absent in the AChBP. In addition, the occurrence of the hydrophilic amino acids in the AChBP Cys-loop together with the presence of glycosylation sites, might be sufficient to yield a soluble homopentameric complex.

The crystal structure of AChBP reveals an oligomer of five identical asymmetric subunits arranged in an anticlockwise manner along the fivefold axis (Figure 1.6A). In three dimensions, the AChBP is 80 Å in diameter, 62 Å in height, with an axial channel that is ~18 Å in diameter. The size and shape of AChBP is consistent with cryo-electron microscopy data for the N-terminal domain of *Torpedo* nAChR (26, 27).

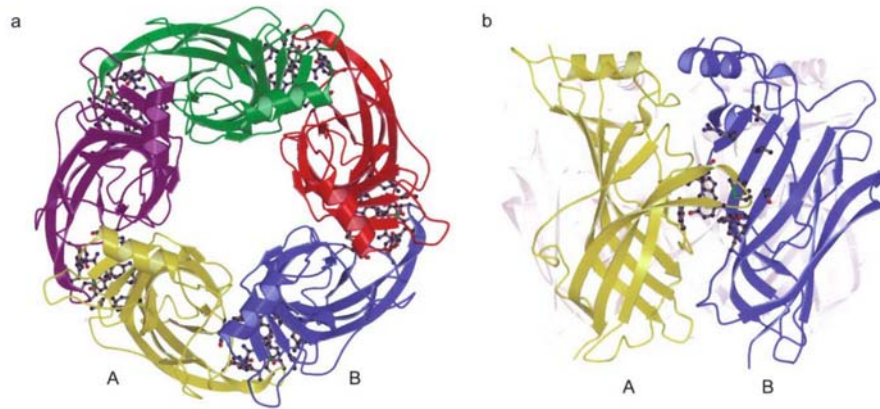


Figure 1.6. The structure of AChBP. A. The pentameric AChBP, viewed along the five-fold axis. Subunits are labeled anticlockwise in different colors, with A-B forming the plus and minus interface side, with the principal and complementary ligand-binding sites, respectively (ball-and-stick representation). B. Viewing the AChBP pentamer perpendicular to the five fold axis. The equatorially located ligand-binding site (ball-and-stick representation) is highlighted only in the A (yellow)-B (blue) interface. (Figures adapted from ref. 81.)

Each subunit of AChBP comprises an N-terminal α helix, two short 3_{10} helices and a core of ten β strands folded into a twisted β sandwich. The β strands are arranged with a uniquely modified immunoglobulin-like topology. The two twisted β sheets of the β sandwich are connected by the Cys-loop, which is close to the subunit carboxyl terminus at the ‘bottom’ of the cylindrical complex. In nAChR, the Cys-loop and the bottom of the complex are close to the extracellular surface of the membrane. The amino terminus of the AChBP subunit is at the opposite end of the cylinder (the ‘top’), placing the amino termini of the Cys-loop receptor subunits farthest from the membrane. The main immunogenic region (MIR) of the ACh receptor $\alpha 1$ -subunit aligns with AChBP

residues at the top of the cylinder. The secondary structure of the AChBP subunit closely resembles that predicted for the extracellular domain of the ACh receptor subunits (39).

The subunit interfaces are of considerable interest as they might play a crucial role in allosteric transitions. The plus side of the interface (Figure 1.6B) is framed essentially by loops, whereas the minus side mostly presents secondary structure elements. The residues located at the interface (88) are not well conserved among nAChRs and probably contribute to the diversity of subunit combinations. Hydrophobic residues in AChBP are essentially located inside the subunit interface whereas polar residues are exposed to the outside where they promote oligomerization.

In summary, the structure and function of the nAChR is becoming more and more clearly understood. In particular, the high-resolution structure of AChBP has brought tremendous insights to the knowledge of the receptor, especially the N-terminal extracellular domain which contains the agonist-binding site. In this thesis, we present our efforts to probe the structure of the agonist-binding site of the mouse muscle nAChR using the tethered agonist approach, which combines chemical synthesis, unnatural amino acid mutagenesis, electrophysiology, and computer modeling. On one hand, our results have been confirmed by the structural data of AChBP. On the other hand, our results have provided further evidence that AChBP is closely related to the extracellular domain of nAChR. Altogether our results provide detailed information on ACh binding, based on which the picture of how ACh binds to the agonist-binding site of nAChR is emerging.

1.5 Reference

1. Hall, Z. W. (1992) pp. 555, Sinauer Associates, Inc., Sunderland, MA.
2. Hille, B. (1992) *Ionic Channels of Excitable Membranes*, Sinauer Associates, Inc., Sunderland, MA.
3. Green, T., Heinemann, S. F., and Gusella, J. F. (1998) *Neuron* 20, 427-44.
4. Dougherty, D. A. (1998) *J. Phys. Org. Chem.* 11, 334-340.
5. Akabas, M. H., Kaufmann, C., Archdeacon, P., and Karlin, A. (1994) *Neuron* 13, 919-927.
6. Akabas, M. H., Stauffer, D. A., Xu, M., and Karlin, A. (1992) *Science* 258, 307-310.
7. Stauffer, D. A., and Karlin, A. (1994) *Biochemistry* 33, 6840-6849.
8. Karlin, A. (2002) *Nat. Rev. Neurosci.* 3, 102-114.
9. Karlin, A., and Akabas, M. H. (1998) *Methods Enzymol.* 293, 123-145.
10. Noren, C. J., Anthony-Cahill, S. J., Griffith, M. C., and Schultz, P. G. (1989) *Science* 244, 182-188.
11. Bain, J. D., Glabe, C. G., Dix, T. A., and Chamberlin, A. R. (1989) *J. Am. Chem. Soc.* 111, 8013-8014.
12. Nowak, M. W., Kearney, P. C., Sampson, J. R., Saks, M. E., Labarca, C. G., Silverman, S. K., Zhong, W., Thorson, J., Abelson, J. N., Davidson, N., Schultz, P. G., Dougherty, D. A., and Lester, H. A. (1995) *Science* 268, 439-442.
13. Nowak, M. W., Gallivan, J. P., Silverman, S. K., Labarca, C. G., Dougherty, D. A., and Lester, H. A. (1998) *Meth. Enzymol.* 293, 504-529.

14. Zhong, W., Gallivan, J. P., Zhang, Y., Li, L., Lester, H. A., and Dougherty, D. A. (1998) *Proc. Natl. Acad. Sci. USA* 95, 12088-12093.
15. Kearney, P. C., Nowak, N. W., Zhong, W., Silverman, S., K., Lester, H. A., and Dougherty, D. A. (1996) *Mol. Pharmacol.* 50, 1401-1412.
16. Miller, J. C., Silverman, S. K., England, P. M., Dougherty, D. A., and Lester, H. A. (1998) *Neuron* 20, 619-624.
17. Tong, Y., Brandt, G. S., Li, M., Shapovalov, G., Slimko, E., Karschin, A., Dougherty, D. A., and Lester, H. A. (2001) *J. Gen. Physiol.* 117, 103-18.
18. Gallivan, J. P., Lester, H. A., and Dougherty, D. A. (1997) *Chem. Biol.* 4, 739-749.
19. England, P. M., Zhang, Y., Dougherty, D. A., and Lester, H. A. (1999) *Cell* 96, 89-98.
20. Grutter, T., and Changeux, J. P. (2001) *Trends Biochem. Sci.* 26, 459-463.
21. Corringer, P.-J., Novere, N. L., and Changeux, J.-P. (2000) *Annu. Rev. Pharmacol. Toxicol.* 40, 431-458.
22. Paterson, D., and Nordberg, A. (2000) *Prog. Neurobiol.* 61, 75-111.
23. Jones, M. V., and Westbrook, G. L. (1996) *Trends Neurosci.* 19, 96-101.
24. Karlin, A., Holtzman, E., Yodh, N., Lobel, P., Wall, J., and Hainfeld, J. (1983) *J. Biol. Chem.* 258, 6678-6681.
25. Stroud, R. M., McCarthy, M. P., and Shuster, M. (1990) *Biochemistry* 29, 11009-11023.
26. Unwin, N. (1993) *J. Mol. Biol.* 229, 1101-1124.

27. Miyazawa, A., Fujiyoshi, Y., Stowell, M., and Unwin, N. (1999) *J. Mol. Biol.* 288, 765-786.
28. Le Novere, N., and Changeux, J.-P. (1995) *J. Mol. Evol.* 40, 155-172.
29. Anand, R., Conroy, W. G., Schoepfer, R., Whiting, P., and Lindstrom, J. (1991) *J. Biol. Chem.* 266, 11192-11198.
30. Cooper, E., Couturier, S., and Ballivet, M. (1991) *Nature* 350, 235-238.
31. Elgoyhen, A. B., Johnson, D. S., Boulter, J., Vetter, D. E., and Heinemann, S. (1994) *Cell* 79, 705-715.
32. Gotti, C. et al. (1994) *Eur. J. Neurosci.* 6, 1281-1291.
33. Vernallis, A. B., Conroy, W. G., and Berg, D. K. (1993) *Neuron* 10, 451-464.
34. Le Novere, N., Zoli, M., and Changeux, J.-P. (1996) *Eur. J. Neurosci.* 8, 2428-2439.
35. Ramirez-Latorre, J. et al. (1996) *Nature* 380, 347-351.
36. Elgoyhen, A. B. et al. (2001) *Proc. Natl. Acad. Sci. USA* 98, 3501-3506.
37. Dougherty, D. A., and Lester, H. A. (2001) *Nature* 411, 252-254.
38. West Jr., A. P., Bjorkman, P. J., Dougherty, D. A., and Lester, H. A. (1997) *J. Biol. Chem.* 272, 25468-25473.
39. Le Novere, N. et al. (1999) *Biophys. J.* 76, 2329-2345.
40. Herz, J. M., Johnson, D. A., and Taylor, P. (1989) *J. Biol. Chem.* 264, 12439-12448.
41. Katz, B., and Thesleff, S. (1957) *J. Physiol. (Lond.)* 138, 63-80.
42. Sakmann, B., Patlak, J., and Neher, E. (1980) *Nature* 286, 71-73.
43. Neubig, R. R., Boyd, N. D., and Cohen, J. B. (1982) *Biochemistry* 21, 3460-3467.

44. Heidmann, T., Bernhardt, J., Neumann, E., and Changeux, J.-P. (1983) *Biochemistry* 22, 5452-5459.
45. Auerbach, A. A. (1993) *J. Physiol. (Lond.)* 461, 339-378.
46. Edelstein, S. J., Schaad, O., Henry, E., Bertrand, D., and Changeux, J.-P. (1996) *Biol. Cybern.* 75, 361-379.
47. Auerbach, A., and Akk, G. (1998) *J. Gen. Physiol.* 112, 181-197.
48. Grosman, C., and Auerbach, A. (2001) *Proc. Natl. Acad. Sci. USA* 98, 14102-14107.
49. Monod, J., Wyman, J., and Changeux, J.-P. (1965) *J. Mol. Biol.* 12, 88-118.
50. Karlin, A. (1967) *J. Theor. Biol.* 16, 306-320.
51. Unwin, N. (1995) *Nature* 373, 37-43.
52. Wilson, G. G., and Karlin, A. (1998) *Neuron* 20, 1269-1281.
53. Karlin, A., and Akabas, M. H. (1995) *Neuron* 15, 1231-1244.
54. Gorne-Tschelnokow, U., Strecker, A., Kaduk, C., Naumann, D., and Hucho, F. (1994) *EMBO J.* 13, 338-341.
55. Methot, N., Ritchie, B. D., Blanton, M. P., and Baenziger, J. E. (2001) *J. Biol. Chem.* 276, 23726-23732.
56. Giraudat, J., Dennis, M., Heidmann, T., Chang, J. Y., and Changeux, J.-P. (1986) *Proc. Natl. Acad. Sci. USA* 83, 2719-2723.
57. Giraudat, J. et al. (1987) *Biochemistry* 26, 2410-2418.
58. Akabas, M. H., and Karlin, A. (1995) *Biochemistry* 34, 12496-12500.
59. Zhang, H., and Karlin, A. (1997) *Biochemistry* 36, 15856-15864.
60. Zhang, H., and Karlin, A. (1998) *Biochemistry* 37, 7952-7964.

61. Kehoe, J., and McIntosh, J. M. (1998) *J. Neurosci.* 18, 8198-8213.
62. Adams, D. J., Dwyer, T. M., and Hille, B. (1980) *J. Gen. Physiol.* 75, 493-510.
63. Villarroel, A., Herlitze, S., Koenen, M., and Sakmann, B. (1991) *Proc. R. Soc. Lond. B Biol. Sci.* 243, 69-74.
64. Konno, T., Busch, C., Von Kitzing, E., Imoto, K., Wang, F., Nakai, J., Mishina, M., Numa, S., and Sakmann, B. (1991) *Proc. R. Soc. Lond. B Biol. Sci.* 244, 69-79.
65. Imoto, K., Konno, T., Nakai, J., Wang, F., Mishina, M., and Numa, S. (1991) *FEBS Lett.* 289, 193-200.
66. Cohen, B. N., Labarca, C., Davidson, N., and Lester, H. A. (1992) *J. Gen. Physiol.* 100, 373-400.
67. Corringer, P. J., Bertrand, S., Galzi, J. L., Devillers-Thiery, A., Changeux, J. P., and Bertrand, D. (1999) *Neuron* 22, 831-43.
68. Wilson, G., and Karlin, A. (2001) *Proc. Natl. Acad. Sci. USA* 98, 1241-8.
69. Galzi, J. L., Revah, F., Black, D., Goeldner, M., Hirth, C., and Changeux, J.-P. (1990) *J. Biol. Chem.* 265, 10430-10437.
70. Dennis, M., Giraudat, J., Kotzyba-Hibert, F., Goeldner, M., Hirth, C., Chang, J.-Y., Lazure, C., Chrétien, M., and Changeux, J.-P. (1988) *Biochemistry* 27, 2346-2357.
71. Kao, P. N., Dwork, A. J., Kaldany, R. R. J., Silver, M. L., Wideman, J., Stein, S., and Karlin, A. (1984) *J. Biol. Chem.* 259, 11662-11665.
72. Middleton, R. E., and Cohen, J. B. (1991) *Biochemistry* 30, 6987-6997.
73. Chiara, D. C., Middleton, R. E., and Cohen, J. B. (1998) *FEBS Lett.* 423, 223-6.

74. Wang, D., Chiara, D. C., Xie, Y., and Cohen, J. B. (2000) *J. Biol. Chem.* 275, 28666-74.
75. Chiara, D. C., Xie, Y., and Cohen, J. B. (1999) *Biochemistry* 38, 6689-98.
76. Czajkowski, C., and Karlin, A. (1995) *J. Biol. Chem.* 270, 3160-3164.
77. Mishina, M., Tobimatsu, T., Imoto, K., Tanaka, K., Fujita, Y., Fukuda, K., Kurasaki, M., Takahashi, H., Morimoto, Y., Hirose, T., and et al. (1985) *Nature* 313, 364-9.
78. Galzi, J. L., Bertrand, D., Devillers-Thiery, A., Revah, F., Bertrand, S., and Changeux, J. P. (1991) *FEBS Lett.* 294, 198-202.
79. Sine, S. M., Quiram, P., Papanikolaou, F., Kreienkamp, H. J., and Taylor, P. (1994) *J. Biol. Chem.* 269, 8808-16.
80. Tomaselli, G. F., McLaughlin, J. T., Jurman, M. E., Hawrot, E., and Yellen, G. (1991) *Biophys. J.* 60, 721-7.
81. Xie, Y., and Cohen, J. B. (2001) *J. Biol. Chem.* 276, 2417-26.
82. Sine, S. M., Kreienkamp, H. J., Bren, N., Maeda, R., and Taylor, P. (1995) *Neuron* 15, 205-11.
83. Sine, S. M. (1997) *J. Biol. Chem.* 272, 23521-7.
84. Kao, P. N., and Karlin, A. (1986) *J. Biol. Chem.* 261, 8085-8.
85. Blount, P., and Merlie, J. P. (1989) *Neuron* 3, 349-57.
86. Prince, R. J., and Sine, S. M. (1999) *J. Biol. Chem.* 274, 19623-9.
87. Smit, A. B., Syed, N. I., Schaap, D., Minnen, J., Klumperman, J., Kits, K. S., Lodder, H., Schors, R. C., Elk, R., Sorgedragger, B., Brejc, K., Sixma, T. K., and Geraerts, W. P. M. (2001) *Nature* 411, 261-268.

88. Brejc, K., Dijk, W. J. v., Klaassen, R. V., Schuurmans, M., Oost, J. v. d., Smit, A. B., and Sixma, T. K. (2001) *Nature* 411, 269-276.

Chapter 2

Mapping the Agonist-Binding Site of the nAChR by Tethered Agonists– Identification of Residues Contributing to the Binding of the Quaternary Ammonium Group of Acetylcholine

2.1 Introduction

As discussed in Chapter 1, a large number of aromatic amino acids were identified as contributing to the agonist-binding site of the nAChR. This led us to propose that a cation- π interaction may be important in binding the quaternary ammonium group of ACh (1). The cation- π interaction is a general noncovalent binding force, in which the face of an aromatic ring provides a region of negative electrostatic potential that can bind cations with considerable strength (2, 3). In a biological context, it is the aromatic side chains of Phe, Tyr, and Trp that can be expected to be involved in cation- π interactions, and a large body of evidence indicates a prominent role for cation- π interactions in structural biology in general (2, 4, 5). The physical underpinnings of the cation- π interaction are now well understood, so that one can use *ab initio* quantum mechanical calculations on small model systems to predict with some confidence how modifications of an aromatic system should affect its cation- π binding ability (6, 7). This knowledge, combined with extensions to site-directed mutagenesis for *in vivo* unnatural amino acid incorporation (8-11) allows the systematic evaluation of potential cation- π binding sites.

Then the question is which, if any, of the aromatic residues involved in agonist binding undergoes a direct cation- π interaction with the agonist. Previously, we used unnatural amino acid mutagenesis to evaluate three conserved tyrosines at the agonist-binding site (Figure 1.5) (8, 12), with no results that suggested a cation- π interaction. However, theoretical studies of the cation- π interaction (7) and surveys of protein

structures (3, 5) clearly indicate that, of the natural amino acids, Trp presents the most potent cation- π binding site. We then studied the four different tryptophans implicated in ACh binding— α 86, α 149, α 184, and γ 55/ δ 57. Using nonsense codon suppression procedures, we incorporated and evaluated electrophysiologically a series of Trp derivatives (13, 14). The most intriguing data came from studies of the fluorinated Trp derivatives. The strongly electron-withdrawing fluoro substituent substantially weakens the cation- π interaction, while fluorine is generally considered to be a substituent that provides a negligible steric perturbation. Beginning with 5-F-Trp and moving on to di-, tri-, and tetrafluoro derivatives produces a series of closely related compounds with substantial electronic but minimal steric changes. Progressive fluorination at position α 149 leads to a systematic increase in EC_{50} . As shown in Figure 2.1, there is a compelling correlation between: a) *ab initio* quantum mechanical predictions of cation- π binding abilities; and b) EC_{50} values for ACh at the receptor for a series of tryptophan derivatives, which were incorporated into the receptor using the *in vivo* nonsense suppression method for unnatural amino acid incorporation.

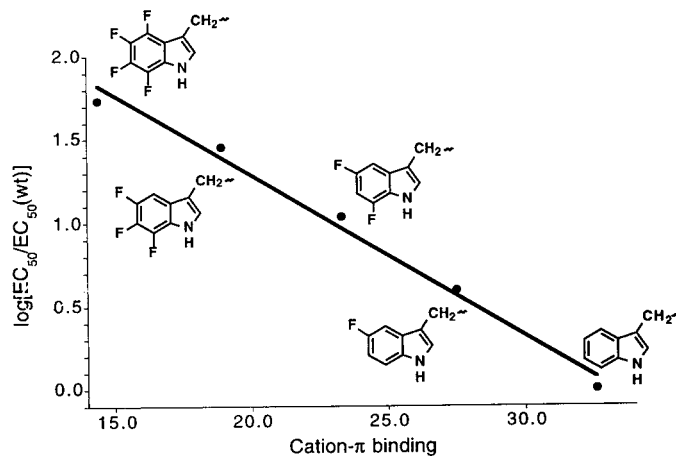


Figure 2.1. Plot of $\log [EC_{50}/EC_{50} (wild\ type)]$ vs. quantitative cation- π binding ability at α 149 for the fluorinated tryptophans.

Such a correlation is seen at one, and only one, of the aromatic residues—tryptophan-149 of the α subunit. This finding indicates that, on binding, the cationic, quaternary ammonium group of ACh makes van der Waals contact with the indole side chain of α tryptophan-149, providing the most precise structural information to date on this receptor. Note that the maximum in cation- π binding occurs over the six-membered ring of Trp (2, 6), and the calculated cation- π binding energies involve such a geometry, so the quaternary ammonium of ACh must be positioned over the 6-ring of α Trp 149 (Figure 2.2). This model suggests that any means of positioning a quaternary ammonium in close proximity to α Trp 149 might produce an active receptor. Thus, the unnatural amino acid Tyr-O3Q (Tyr- $O-(CH_2)_3-N(CH_3)_3^+$, see Figure 2.2) was prepared and incorporated at this position. The quaternary ammonium group in the side chain of Tyr-O3Q was meant to mimic the analogous functional group in ACh. Modeling clearly shows that the quaternary ammonium of Tyr-O3Q can achieve the same position as that proposed in the binding of ACh. Indeed, incorporation of Tyr-O3Q at position α 149 produces a constitutively active receptor, resulting in nicotinic receptor current even in the absence of ACh.

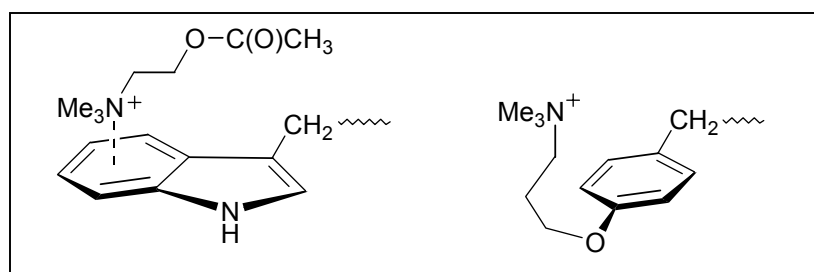


Figure 2.2. (Left) Schematic of the quaternary ammonium of ACh positioned over the 6-ring of α Trp 149. (Right) Structure of Tyr-O3Q, showing that the tethered quaternary ammonium can be positioned in roughly the same location as the quaternary ammonium of ACh.

The tethered agonist strategy has a distinguished history with the nAChR. In pioneering experiments, tethered agonists were introduced into the nAChR using chemical modification of Cys residues created by reduction of the Cys 192-193 disulfide bond (see Figure 1.5), producing a constitutively active receptor (15, 16). Very recently, Cohen expanded on this methodology by introducing Cys residues using site-directed mutagenesis and then reacting the mutants with various MTS reagents (17). We will discuss these results below. The unnatural amino acid mutagenesis approach offers an alternative and in some ways preferable strategy for introducing tethered agonists. Since the approach does not rely on cysteine modification, the tether can be incorporated at many different positions, including sites where the Cys mutant cannot produce functional receptors, and sites that are not accessible to external reagents, as might be expected at a potentially buried agonist-binding site. This strategy also removes ambiguities in tether location that can arise if more than one cysteine is present in the molecule and allows a wider variation in functionality. In addition, agonist-like functionalities are introduced directly into the receptor, eliminating possibly deleterious side reactions associated with chemical modification strategies.

In this chapter, we present our efforts to expand upon our initial observations concerning a tethered agonist in several ways, and thereby establish the generality of the approach. We show that varying the tether length produces a variation in tethered agonist efficiency; and we reveal two other sites— α Tyr 93 and γ Trp 55/ δ Trp 57—where the tethered agonist strategy is successful (18). We also discuss the results of incorporation of an isosteric but electronically neutral analog of Tyr-O3Q termed Tyr-O3tBu (Figure

2.6), in which the quaternary ammonium is replaced by a tert-butyl group. With these new findings, a more advanced, but still speculative, model for the nAChR agonist-binding site can be developed (18).

2.2 Incorporation of Tyr-OnQ into the nAChR

We attempted incorporation of the series of quaternary ammonium derivatives of tyrosine, Tyr-OnQ (n= 2, 3, 4, and 5) (see Figure 2.5 for structures), at several positions around the agonist-binding sites of the nAChR, including: α Trp 86, α Tyr 93, α Trp 149, α Trp 184, α Tyr 190, α Cys 192, α Cys 193, α Pro 194, α Tyr 198, γ Trp 55/ δ Trp 57, and γ Asp 174/ δ Asp 180. Thus, at least one site was probed on each of the five ‘loops’ (A– D, F) that have been proposed to define the ACh-binding site (Figure 1.5). Given the stoichiometry of the receptor, suppression in an α subunit incorporates two copies of the modified side chain, one associated with each of the two agonist-binding sites of the receptor. For sites in non- α subunits, we always made two mutations—one in γ and one in the analogous site in δ —so that both agonist-binding sites are comparably perturbed. Mutant proteins were expressed in *Xenopus* oocytes and whole-cell currents were measured using two-electrode voltage-clamp electrophysiology (9, 12, 19).

The hallmark of a successful experiment is the observation of large standing currents in *Xenopus* oocytes expressing the mutant channel in the absence of added ACh (Figure 2.3, identified as **a**). The standing currents are reduced in the presence of the open-channel blocker 8-(N,N-diethylamino)octyl 3,4,5-trimethoxybenzoate (TMB-8).

This establishes that the observed current is due to a nAChR, rather than a nonspecific basal current in the oocyte. Note that TMB-8 blocks the channel by binding to the open state of the receptor in the pore region at a site that is quite far removed from the agonist-binding site. As such, the mutations we are introducing should not impact the ability of TMB-8 to block constitutive current.

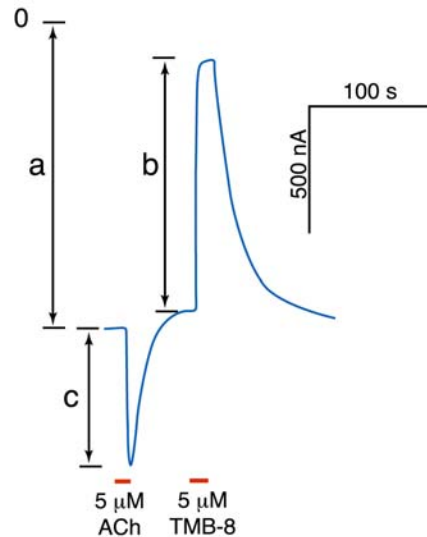


Figure 2.3. Representative recording trace (blue) of voltage-clamp currents for an individual oocyte expressing mutant nAChR with Tyr-O3Q incorporated at $\alpha 149$. The red horizontal bars indicate bath application of ACh ($5 \mu\text{M}$) and TMB-8 ($5 \mu\text{M}$). **a**: standing current due to constitutively active nAChR; **b**: standing current that is blocked by TMB-8; **c**: ACh-induced current.

In earlier studies involving Tyr-O3Q at position $\alpha\text{Trp } 149$, we also used blockade of the standing current by α -bungarotoxin as well as channel blockers such as QX-314 and NMDG; dose-dependent antagonism by curare; and single-channel measurements to associate the standing current with the nAChR (13, 14). In addition, we showed that

prolonged exposure (>3 min) to high ACh concentrations led to desensitization of both the standing currents (Figure 2.4), further evidence that the response arises directly from nAChR.

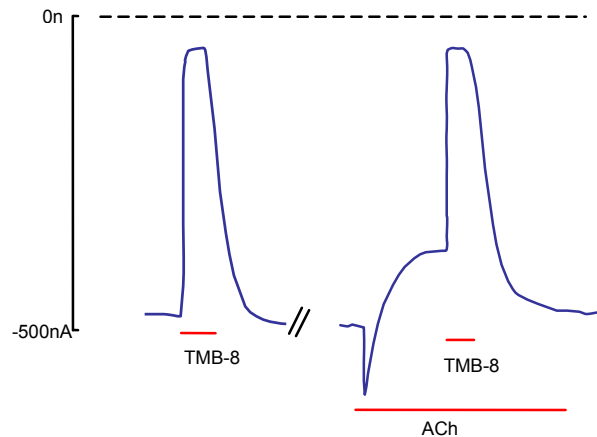


Figure 2.4. The standing current is partially occluded by additional ACh. During the first application of TMB-8 (5 μ M), the standing outward current was reduced reversibly to nearly zero. ACh (25 μ M) was then added, inducing an inward current that desensitized. During the desensitization phase, the standing current was reduced. TMB-8 was added again during the desensitization phase. The TMB-8 deflection reached the former plateau level rather than producing a net outward current. These interactions show that ACh desensitizes the conductance mechanism that produces the standing current; therefore the standing current is produced by functional nAChR.

In the present work, constitutively active receptors were observed at only three of the sites evaluated— α Trp 149, α Tyr 93, and γ Trp 55/ δ Trp 57. At the other sites, the typical outcome was that no constitutive current that could be blocked by TMB-8 was seen. In some cases, very small, TMB-8 blockable constitutive currents were seen, but only when the expression level for the receptor was especially high, as indicated by large

ACh-induced currents (see Appendix I). We are reluctant to interpret such small currents. Concerning these other sites, it is, in general, risky to interpret 'failed' nonsense suppression experiments. It could well be that the unnatural amino acid failed to incorporate into the protein at the ribosome. Alternatively, 'failure' could mean that the unnatural amino acid was incorporated at the ribosome, but after incorporation the mutant protein failed in folding, or assembly, and/or transport to the cell membrane. Or perhaps receptors containing the tethered agonists were expressed on the surface of the oocyte, but the mutant protein is nonfunctional. Generally it is difficult to distinguish among these possibilities, and for the remainder of this work we will focus on the three sites that produced constitutively active receptors.

In addition to the channel blocker TMB-8, receptors were treated with the natural agonist acetylcholine, and in all cases such treatment led to an increase in current. This establishes that a tethered quaternary ammonium group is a fairly weak agonist, a so-called partial agonist, meaning that full potency is never reached with the tether alone. Our earlier study (13) showed that, as expected, single channel conductance for the tethered system is identical to that of the native receptor, so it is the open probability that does not reach optimal values. Further supporting this view, standing currents are only observed when a mutation of Leu 262 (conventionally referred to as Leu 9') to Ser is introduced into the channel (M2) region of the β subunit. Such a mutation is quite far removed from the agonist-binding site and is well established to facilitate channel opening (13, 20, 21).

Figure 2.3 defines the key parameters for evaluating tethered agonist experiments. It begins with a standing current that by convention is considered negative. For the particular oocyte shown, the value of the standing current (**a**) was -1200 nA. Application of 5 μ M ACh causes a downward deflection, indicating an increase in current, and the magnitude of the ACh induced current is **c**. After removal of ACh and reestablishment of a (slightly shifted) baseline, TMB-8 is added, and the drop in current is labeled **b**. Numerically, **b** is equal to the difference between the standing current and the current in the presence of TMB-8. As a gauge of the effectiveness of a given tether in opening the receptor, we use the ratio of the constitutive current that is blocked by TMB-8 to the ACh-induced current (Figure 4, **b/c**). This measures the extent to which the tethered agonist opens the receptor relative to the presumed maximal response as seen with added ACh. Using this ratio minimizes complications due to variations in the expression level of the receptors in *Xenopus* oocytes. The larger the **b/c** ratio, the more effective the tethered agonist. We appreciate that this is an imperfect measure of the effectiveness of a tethered agonist, but we consider it to be a useful qualitative guideline. No quantitative significance is given to the ratios. Figure 2.5 summarizes the results of incorporation of Tyr-OnQ into the nAChR at the three sites.

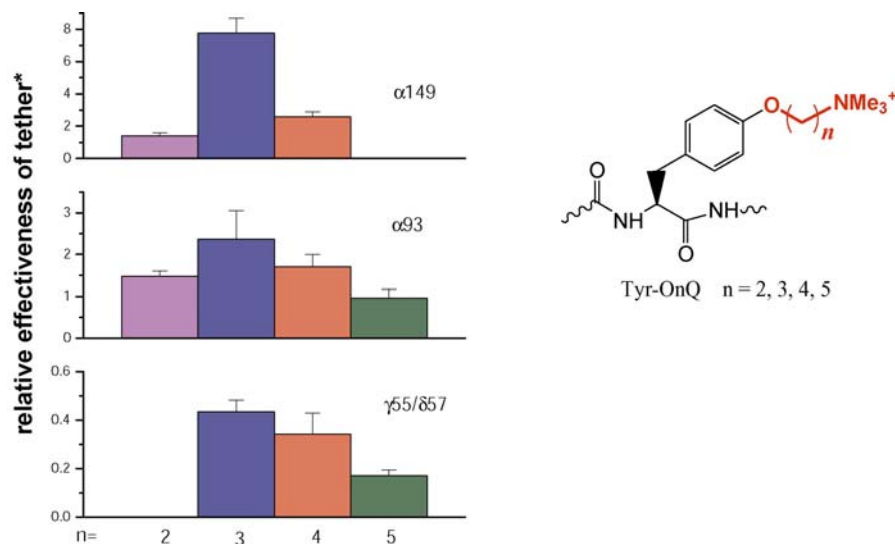


Figure 2.5. Tethered agonist relative efficiencies for Tyr-OnQ as a function of n (the number of methylene groups in the side chain) at positions $\alpha149$, $\alpha93$, and $\gamma55/\delta57$. *The value is measured as ratio of constitutive current that is blocked by TMB-8 to ACh-induced current (**b/c** per Figure 2.3). Data shown are for an ACh concentration of 25 μ M, although comparable results are seen with other concentrations.

2.3 Incorporation of an Isosteric, Neutral Tether

While Tyr-OnQ was designed to deliver a mimic of a key aspect of ACh, the quaternary ammonium group, it remained possible that the agonism seen in these experiments is due to some less specific effect, such as a simple steric disruption of the agonist-binding site. To address this concern we prepared the isosteric compound of Tyr-O3Q, where the quaternary ammonium is substituted by a tert-butyl group (Figure 2.6).

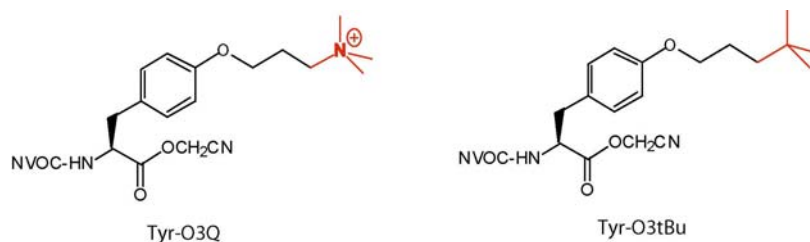


Figure 2.6. Structure of Tyr-O3Q and Tyr-O3tBu.

We incorporated Tyr-O3tBu at α 149, α 93, and γ 55/ δ 57 sites. We found that incorporation of Tyr-O3tBu at α 93 and γ 55/ δ 57 does produce constitutively active receptors. In most cases Tyr-O3tBu is less effective than Tyr-O3Q, based on both the magnitude of the constitutive currents (data not shown) and the ratio of the TMB-8-blocked current to ACh-induced current (Figure 2.7).

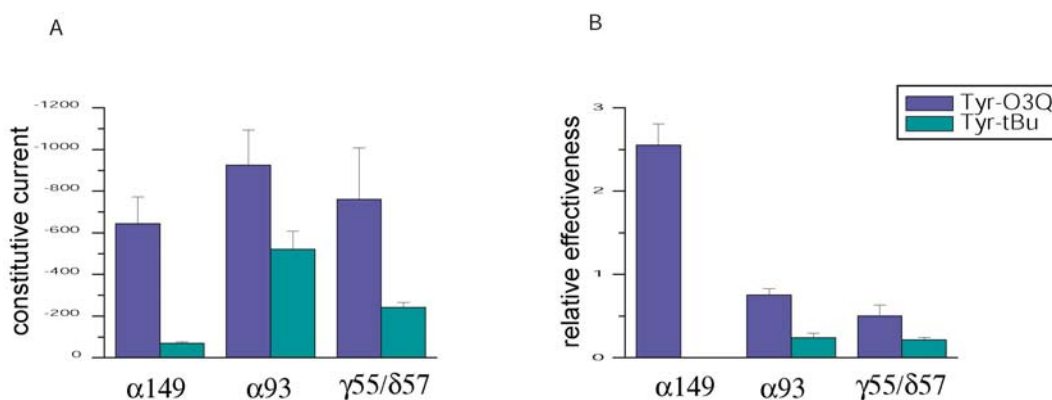


Figure 2.7. Results of incorporation of Tyr-O3tBu compared with that of Tyr-O3Q at three sites of nAChR. A. Constitutive current. B. The value plotted is the ratio of constitutive current that is blocked by TMB-8 (10 μ M) to ACh (25 μ M)-induced current, **b/c** in Figure 2.3.

Upon attempted incorporation of Tyr-O3tBu at α 149, the site at which Tyr-O3Q is most effective, no constitutive current is observed. In addition, only very small currents are observed upon application of ACh. This result could imply that receptors containing Tyr-O3tBu at α 149 are not constitutively active and cannot be activated by ACh because the tert-butyl compound is obstructing the binding site. Alternatively, the results could signal that there are no receptors expressed on the surface of the oocytes. To discriminate between these two possibilities, further investigations were undertaken to determine whether nAChR are indeed expressed on the surface of the oocytes in the Tyr-O3tBu incorporation experiments. Using either binding studies on intact oocytes with [125 I]-bungarotoxin (Figure 2.8) or Western blot analyses of oocyte membranes (Figure 2.9), we found that indeed more nAChR are expressed on the surface of the oocyte when Tyr-O3Q is incorporated than Tyr-O3tBu. In fact, the apparent expression of Tyr-O3tBu is generally not above background levels seen in control suppression experiments.

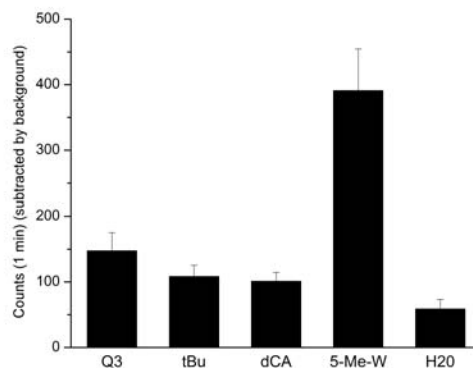


Figure 2.8. Binding of nAChR by 125 I- α -bungarotoxin measured by γ counter. (See Chapter 5 for experimental detail.) Q3, tBu and 5-Me-W are mutant receptors with Tyr-O3Q, Tyr-O3tBu and 5-methyl Trp (giving similar signal as wild type residue-Trp) incorporated at α Trp 149, respectively; dCA, unacylated tRNA was used instead of aminoacyl-tRNA; H₂O, oocytes were injected with H₂O only.

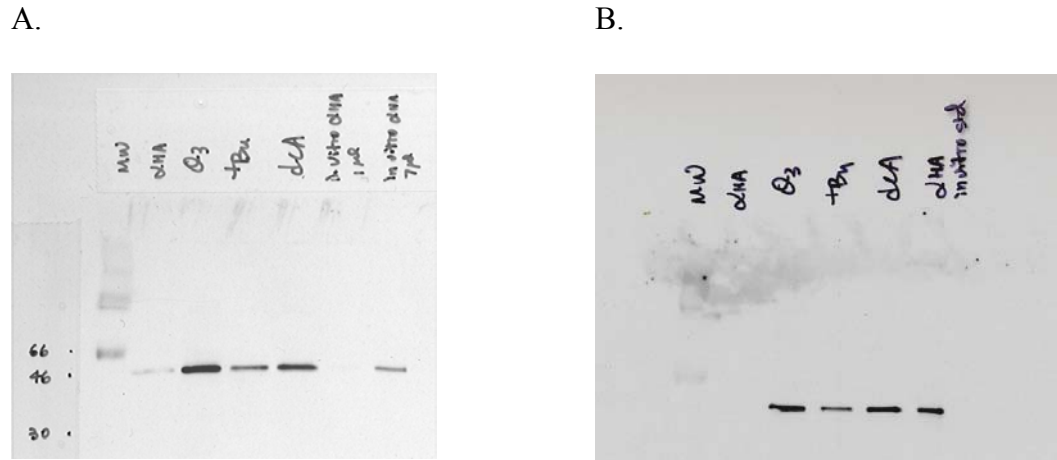


Figure 2.9. Western blots of nAChR. A. Sample prepared by stripping oocyte membrane. B. Biotinylation of surface proteins. (See Chapter 5 for experimental detail.) MW, molecular weight standard; α HA, α subunit with HA epitope; Q3 and tBu, mutant receptors with Tyr-O3Q and Tyr-O3tBu; dCA, unacylated tRNA was used instead of aminoacyl-tRNA; *in vitro* α HA, *in vitro* translation of α subunit with HA epitope using wheat germ.

2.4 Discussion

The present study shows that the tethered agonist approach, as implemented by the *in vivo* nonsense suppression methodology, is a general tool that can provide valuable information about the agonist-binding site of a neuroreceptor. Tethered agonists at three different sites give constitutively active receptors. Variations in tether length can discriminate among the different sites. In the particular case of the nAChR, we believe the results have significant implications for efforts to understand the structure of this complex protein.

In our preliminary report only Tyr-O3Q at position α 149 was studied. We now find that tether length significantly influences the effectiveness of the agonist at this position. As shown in Figure 2.5, Tyr-O3Q represents the most effective chain length. Both longer and shorter tethers are significantly less effective at inducing current—Tyr-O5Q produced no measurable constitutive current. We interpret this, in part, as a conformational effect. We concluded from our earlier studies that when ACh binds to the nAChR, the quaternary ammonium group makes van der Waals contact with the six-membered ring of α Trp 149 through a cation- π interaction (13). When Tyr-OnQ is incorporated at α 149, its aromatic ring aligns with the five-membered ring of the wild-type Trp. Note that an aromatic group is part of the Tyr-OnQ motif primarily for synthetic reasons. It is not anticipated that a cation- π interaction is involved between the tethered quaternary ammonium group and the aromatic ring of the side chain. The tether of Tyr-OnQ must curve around to position the quaternary ammonium above the site where the six-membered ring of the natural Trp would be. Modeling indicates that this is unlikely for a 2-carbon tether, but is possible for tethers of length ≥ 3 . Perhaps the tethers of Tyr-OnQ are too long when $n = 4$ or 5 , inflicting adverse steric interactions when positioning the quaternary ammonium appropriately. The strong preference for a 3-carbon tether at position α 149 suggests a fairly strict geometric requirement for achieving the maximum in constitutive activation.

We have also established that incorporation of tethered agonists at two other sites creates a constitutively active receptor. One of these sites is α 93. Previous photoaffinity and site-directed mutagenesis studies have suggested that α Tyr 93 is near the agonist-

binding site (22, 23). Our earlier evaluation of this residue using unnatural amino acid mutagenesis indicated that the OH of the Tyr forms an important hydrogen bond that affects agonist binding; however, ACh is not the acceptor of this hydrogen bond (12). As shown in Figure 2.5, Tyr-OnQ with $n = 2$ to 5 are comparably effective at $\alpha 93$, in contrast to the results for $\alpha 149$.

The other site where tethered agonists lead to a constitutively active receptor is γ Trp 55/ δ Trp 57. All the tethers with long chains (≥ 3 carbons) are modestly effective at this site. This suggests that $\gamma 55/\delta 57$ must be fairly near the agonist-binding site. However, it is likely to be further away than α Trp 149 and α Tyr 93, since the shortest tether is not effective. In fact, all tethers are less effective at γ Trp 55/ δ Trp 57 than at the other sites.

We note that the constitutive currents (Figure 2.3, **a**) are consistently larger when Tyr-OnQ is incorporated at $\alpha 149$ than at $\alpha 93$ and $\gamma 55/\delta 57$ (data not shown). This is not simply because the receptor expresses more efficiently with the tether at $\alpha 149$, since the ratio of TMB-8-blocked current to ACh-induced current shows the same trends. Apparently, Tyr-OnQ is able to position the quaternary ammonium more precisely and/or with less overall disruption of the receptor when it is delivered via $\alpha 149$ than $\alpha 93$ or $\gamma 55/\delta 57$.

Interesting results are seen with Tyr-O3tBu, a tether that is isosteric to but lacks the positive charge of Tyr-O3Q. No constitutively active or ACh-induced currents are

seen from efforts to incorporate Tyr-O3tBu at α 149. We noted above the challenges of interpreting negative results from nonsense suppression experiments. However, at the Trp α 149 site we know that (a) nonsense suppression can be quite efficient if different unnatural amino acids are employed; (b) a sterically very similar residue (Tyr-O3Q) incorporates efficiently; and (c) the desired residue, Tyr-O3tBu, does incorporate at other sites (see below) and therefore is compatible with the ribosomal machinery. Although not completely conclusive, efforts to determine whether the receptor containing Tyr-O3tBu was successfully synthesized, assembled, and transported to the surface suggest that it was not. For the reasons enumerated above, we consider it unlikely that this represents a failure of the nonsense suppression methodology. We think it more likely that a receptor with Tyr-O3tBu incorporated at position α 149 does not fold or does not assemble properly, and therefore no receptor appears on the surface. Thus, the immediate vicinity of the agonist-binding site—the region very near α Trp 149—is quite sensitive, accepting a very close analog of its natural ligand, Tyr-OnQ (n=2-4), but nothing else.

At α 93 and γ 55/ δ 57, Tyr-O3tBu is incorporated and gives measurable constitutive currents, but less than the cationic analog. While direct contact between ACh and α Trp 149 is well established, such is not the case for α Tyr 93 nor γ Trp 55/ δ Trp 57. We propose that these ‘secondary’ sites are less intimately involved in defining the agonist-binding site, but are better described as nearby. Incorporating the tether at these sites disrupts the binding region, partly through a simple steric effect, since Tyr-O3tBu works. However, a tethered quaternary ammonium is more effective, suggesting these remote sites do sense some of the binding interactions associated with the quaternary ammonium

on ACh.

It is important to appreciate that gating an ion channel is a complex process. An agonist must bind to the receptor and initiate opening of the ion channel. This is made even more complicated in the nAChR, where the ion channel and its gate are structurally remote from the agonist-binding site (24, 25). In such a system, it is envisioned that binding of agonist induces a conformational change that shifts a pre-existing equilibrium between closed and open states of the channel toward the open state. It is easy to imagine that the structural perturbation of introducing Try-OnQ or Tyr-O3tBu at one of the secondary sites could disrupt the structure of the protein in the vicinity of the agonist-binding site in the direction of the conformational change associated with opening. Note that in all cases the tethered agonist is a weak agonist, indicating that the full effect on the open/closed equilibrium elicited by ACh is never achieved with a tethered agonist. The tethered agonist essentially pushes the receptor along the path toward opening, or, stated differently, perturbs the gating equilibrium, but less effectively than the true agonist. Precisely at the agonist-binding site, α Trp 149, the structural requirements are more strict, and an optimal tether produces a large effect.

Very recently, Sullivan and Cohen described tethered agonist studies in which potential tethered agonists were incorporated by reacting Cys residues introduced by site directed mutagenesis with various MTS reagents (17). At α 149 the Cys mutation made the receptor unresponsive to ACh, which is not surprising given the crucial role of α Trp 149 in agonist binding (13). At α 93, Cys modification resulted in irreversible inhibition,

while at $\gamma 55$ there was no effect for the Cys mutants after treatment with MTS reagents. Interestingly, though, reaction of the $\alpha 198$ Tyr/Cys mutant with methanethiosulphonate ethyltrimethylammonium (MTSET) produced a constitutively active receptor. The effect was quite sensitive to the length and orientation of the tethered group, in that lengthening or shortening the tether by one methylene group negated the tethered agonist effect. The successful tether introduced by MTS modification ($C_{\alpha}CH_2SSCH_2CH_2NMe_3^+$) is much shorter than those investigated here, and so our failure to see constitutive activation with Tyr-OnQ at $\alpha 198$ is not surprising.

An emerging model of the agonist-binding site of the nAChR

Efforts to develop a detailed picture of the agonist-binding site of the nAChR continue in many labs. Efforts to date are schematized in Figure 1.5. The binding site involves several key residues located on several discontinuous ‘loops’ (26). A large number of aromatic residues are associated with the agonist-binding site, along with perhaps one anionic residue. One residue in particular, α Trp 149, has been shown to contact the agonist in the binding site (13).

Another relevant observation is the high-resolution crystal structure of acetylcholine esterase (AChE) (27), the only natural ACh binding site for which such a structure was available before the solution of AChBP structure. As was anticipated (1), a cation- π interaction is crucial for binding ACh. In fact, the esterase uses a tryptophan, Trp 84, to bind the quaternary ammonium group of ACh. In addition, the esterase

features a 20Å ‘aromatic gorge’ that leads from the surface of the enzyme to the active site and Trp 84. The gorge is lined with over a dozen conserved aromatic residues that presumably guide the ACh to the active site using cation- π interactions and other effects. This structure was revealed at about the same time that many workers were identifying the large number of aromatic residues associated with the agonist-binding site of the nAChR. The possibility that a comparable aromatic gorge would exist in the nAChR was immediately apparent. Recently, Unwin has interpreted electron densities in the vicinity of the agonist-binding site as consistent with such a gorge, but the images are not yet of sufficient resolution to be decisive (24).

If an aromatic gorge analogous to the one found in the AChE exists in the nAChR, then the results presented here put certain constraints on the model, as summarized in Figure 2.10. Certainly, the bottom of the gorge and the final resting place of ACh are defined by α Trp 149, playing the role ascribed to Trp 84 in the esterase. Note that of all the residues discussed as contributing to or being near the agonist-binding site (Figure 1.5), evidence for direct interaction with ACh exists only for α Trp 149. The relatively strict structural requirement at α Trp 149 proposed here is consistent with the absence of ACh response seen for the Cys mutant at this site (17). We propose that α Tyr 93 is near the bottom of the gorge, as evidenced by the fact that the shortest tether elicits a response at this site. The OH of α Tyr 93 is involved in a key hydrogen bond in the binding site, and we suggest this is a hydrogen bond to the protein backbone (12). Given that tethered agonists at γ 55/ δ 57 had a weaker ability to open the channel and that the two carbon tether is ineffectual, we position γ 55/ δ 57 further up the gorge. An ongoing debate

in the nAChR literature is whether the agonist-binding site is best thought of as being buried within the α subunits or whether it is at the subunit interfaces, α/γ and α/δ . Our results clearly support a role for the γ/δ subunits. However, the α/γ and α/δ subunit interfaces might be contributing to the gorge leading to the agonist-binding site, rather than actually structuring the binding site. Finally, we include α Tyr 198 as very near the agonist-binding site, based on the MTS studies of Cohen (17). Of course, the model presented in Figure 2.10 is highly speculative at this point, and we look forward to further studies, both structural and mechanistic, to refine it.

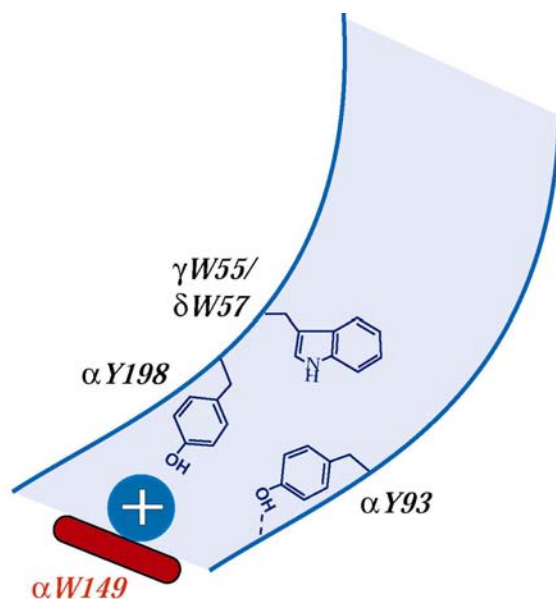


Figure 2.10. The evolving view of the nAChR agonist-binding site. Shown is a highly schematic view of an ‘aromatic gorge’ analogous to that proposed for ACh esterase. α Trp 149 lies at the bottom of the gorge and binds the quaternary ammonium group of ACh, playing the role of Trp 84 in the AChE. α Tyr 198 is near the bottom of the gorge, while α Tyr 93 lies slightly up the gorge, and its OH forms an important hydrogen bond. γ Trp 55/ δ Trp 57 lies further up the gorge.

More recently, the crystal structure of AChBP has been solved and revealed the binding site in great detail (see Chapter 3) (28). From AChBP structure five aromatic residues form an open box (Figure 3.1A), which defines much of the agonist-binding site. Among the five aromatic residues, three of them were identified by the tethered agonist approach described here. Another is the tyrosine identified by Cohen's study. In addition, an ammonium group (positively charged) from a molecule in the crystallization buffer was positioned directly over the analogous residue of α Trp 149, which is consistent with the cation- π interaction as expected. Thus, the structure of AChBP has confirmed our results very nicely.

In summary, we have shown that the tethered agonist approach via unnatural amino acid mutagenesis is a general tool for probing structure in the nAChR (18). We fully expect it will be useful in other integral membrane proteins. Using this approach we have now positioned three residues— α Trp 149, α Tyr 93, and γ Trp 55/ δ Trp 57 in loops B, A and D, respectively—very near the agonist-binding site and each with a distinct role. We anticipate that further application of this methodology will provide additional, useful insights. Indeed, in the following chapter we will describe the identification of additional residues in loops C and E very near the agonist-binding site using a new tethered agonist.

2.5 Reference

1. Dougherty, D. A., and Stauffer, D. A. (1990) *Science* 250, 1558-1560.
2. Dougherty, D. A. (1996) *Science* 271, 163-168.

3. Ma, J. C., and Dougherty, D. A. (1997) *Chem. Rev.* 97, 1303-1324.
4. Scrutton, N. S., and Raine, A. R. C. (1996) *Biochem. J.* 319, 1-8.
5. Gallivan, J. P., and Dougherty, D. A. (1999) *Proc. Natl. Acad. Sci. USA* 96, 9459-9464.
6. Mecozi, S., West Jr., A. P., and Dougherty, D. A. (1996) *Proc. Natl. Acad. Sci. USA* 93, 10566-10571.
7. Mecozi, S., West Jr., A. P., and Dougherty, D. A. (1996) *J. Am. Chem. Soc.* 118, 2307-2308.
8. Nowak, M. W., Kearney, P. C., Sampson, J. R., Saks, M. E., Labarca, C. G., Silverman, S. K., Zhong, W., Thorson, J., Abelson, J. N., Davidson, N., Schultz, P. G., Dougherty, D. A., and Lester, H. A. (1995) *Science* 268, 439-442.
9. Nowak, M. W., Gallivan, J. P., Silverman, S. K., Labarca, C. G., Dougherty, D. A., and Lester, H. A. (1998) *Meth. Enzymol.* 293, 504-529.
10. Noren, C. J., Anthony-Cahill, S. J., Griffith, M. C., and Schultz, P. G. (1989) *Science* 244, 182-188.
11. Bain, J. D., Glabe, C. G., Dix, T. A., and Chamberlin, A. R. (1989) *J. Am. Chem. Soc.* 111, 8013-8014.
12. Kearney, P. C., Nowak, N. W., Zhong, W., Silverman, S., K., Lester, H. A., and Dougherty, D. A. (1996) *Mol. Pharmacol.* 50, 1401-1412.
13. Zhong, W., Gallivan, J. P., Zhang, Y., Li, L., Lester, H. A., and Dougherty, D. A. (1998) *Proc. Natl. Acad. Sci. USA* 95, 12088-12093.
14. Zhong, W. (1998) in *Chemistry*, California Institute of Technology, Pasadena, CA.

15. Silman, I., and Karlin, A. (1969) *Science* 164, 1420-1421.
16. Chabala, L. D., and Lester, H. A. (1986) *J. Physiol.* 379, 83-108.
17. Sullivan, D. A., and Cohen, J. B. (2000) *J. Biol. Chem.* 275, 12651-12660.
18. Li, L., Zhong, W., Lester, H. A., and Dougherty, D. A. (2001) *Chem. Biol.* 8, 47-58.
19. Hille, B. (1992) *Ionic Channels of Excitable Membranes*, Sinauer Associates, Inc., Sunderland, MA.
20. Filatov, G. N., and White, M. M. (1995) *Molec. Pharm.* 48, 379-384.
21. Labarca, C., Nowak, M. W., Zhang, H., Tang, L., Deshpande, P., and Lester, H. A. (1995) *Nature* 376, 514-516.
22. Galzi, J. L., Revah, F., Black, D., Goeldner, M., Hirth, C., and Changeux, J.-P. (1990) *J. Biol. Chem.* 265, 10430-10437.
23. Karlin, A., and Akabas, M. H. (1995) *Neuron* 15, 1231-1244.
24. Miyazawa, A., Fujiyoshi, Y., Stowell, M., and Unwin, N. (1999) *J. Mol. Biol.* 288, 765-786.
25. Wilson, G. G., and Karlin, A. (1998) *Neuron* 20, 1269-1281.
26. Corringer, P.-J., Noverre, N. L., and Changeux, J.-P. (2000) *Annu. Rev. Pharmacol. Toxicol.* 40, 431-458.
27. Sussman, J. L., Harel, M., Frolow, F., Oefner, C., Goldman, A., Toker, L., and Silman, I. (1991) *Science* 253, 872-879.
28. Brejc, K., Dijk, W. J. v., Klaassen, R. V., Schuurmans, M., Oost, J. v. d., Smit, A. B., and Sixma, T. K. (2001) *Nature* 411, 269-276.

Chapter 3

**Identification of Additional Residues Near the Agonist-Binding Site by a
Tethered Agonist and Investigation of the Effect of an Intersubunit
Hydrogen Bond on the nAChR Desensitization–
Further Evidence that the N-terminal Extracellular Domain of
nAChR Is Closely Related to AChBP**

3.1 Introduction

As mentioned earlier in Chapter 1, a small soluble protein from snail glial cells—ACh binding protein (AChBP)—has been discovered and characterized (1). Its crystal structure has also been solved at 2.7 Å resolution (2). The structure reveals the essential features of a key region—the agonist-binding site of the nAChR. Moreover, the structure rationalizes almost every result from over 40 years of biochemical and electrophysiological studies of the agonist-binding site of the nAChR (3).

There is a cavity at each interface between the subunits. These cavities are lined by residues which were shown to be involved in ligand binding in nAChR by photoaffinity labeling and mutagenesis studies (4). These cavities are located close to the outside of the pentameric ring. The data do not validate (5) the suggestion that the “tunnel” seen in *Torpedo* nAChR electron microscopy pictures (6) is the access route to the ACh-binding site. The ligand-binding residues are found on both the principal subunit (plus side) and the complementary subunit (minus side). The residues on the principal subunit align with those on the α subunit of nAChR and are in loops between β strands. The residues on the complementary subunit align with those on γ or δ subunits of nAChR and are mostly within β strands. The principal side consists of residues coming from loop A (Tyr 89, i.e., α Tyr 93), loop B (Trp 143 and His 145, i.e., α Trp 149 and α Tyr 151), and loop C (Tyr 185, Cys 187, Cys 188, and Tyr 192, i.e., α Tyr 190, α Cys 192, α Cys 193, and α Tyr 198). (The aligned residue in nAChR is preceded by the Greek letter indicating the subunit.) The complementary side consists of residues coming from

loop D (Trp 53 and Gln 55, i.e., γ Trp55/ δ Trp57 and γ Glu57/ δ Asp59), loop E (Arg 104, Val 106, Leu 112, and Met 114, i.e., γ Leu 109/ δ Leu 111, γ Tyr 111/ δ Arg 113, γ Tyr 117/ δ Thr 119, and γ Leu 119/ δ Leu 121), and loop F (Tyr 164, i.e., γ Asp 177/ δ Ala 183).

All residues in the binding site have been identified by photoaffinity labeling and mutagenesis studies. All observed residues are conserved between ligand-binding subunits of nicotinic receptors except the loop F Tyr164 residue. One negatively charged residue, Asp 161, that is very close to loop F is highly conserved. The aligned residue in nAChR (γ Asp 174/ δ Asp 180) has been shown to be important in ligand binding and about 9 Å away from α Cys 192/193 (7). In the crystal structure of AChBP Asp 161 is one of the ligands of a Ca^{2+} ion near loop F. So it is suggested that Tyr 164 might contribute to the ligand-binding area because of a Ca^{2+} site that orientates its lateral chain towards to loop C. There is another residue identified by labeling studies, Trp 82 (α Trp 86), which does not participate directly in ACh-binding. Instead it is involved in hydrophobic core formation and located far (~ 15 Å) from the binding pocket.

Although the AChBP was crystallized in the absence of a specific binding site ligand, AChBP did contain a molecule of N-2-hydroxyethylpiperazine-N'-2-ethanesulphonate (HEPES) from the buffer in the binding site cavity. Each of the nitrogens of the piperazine ring is protonated, and an ammonium (positively charged) group was positioned directly over Trp143 (α Trp 149), making cation- π interactions as anticipated by our earlier studies (8). When the earlier results for nAChR are mapped onto the new structure of AChBP, the remarkable image shown in Figure 3.1B emerges.

Loops A-D do indeed form a binding site, with loops E and especially F more remote. The disulfide bond is right in the middle of the action. The binding site is shaped by the five key aromatic residues (Figure 3.1A), α Tyr 93, α Trp 149, α Tyr 190, α Tyr 198 and γ Trp 55/ δ Trp 57, which are aligned correspondingly with the AChBP residues Tyr 89, Trp 143, Tyr 185, Tyr 192 from the plus side and Trp 53 from the minus side.

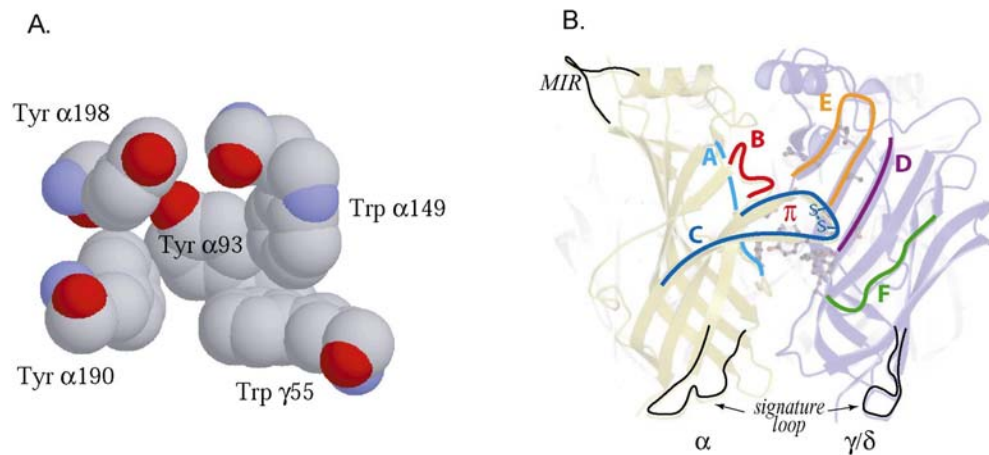


Figure 3.1. The deduced structure of the agonist-binding site of the nAChR (adapted from ref. 3). A. The open box, formed by five aromatic residues, that probably defines much of the agonist-binding site. The view is derived from A by a 90° rotation clockwise around the vertical axis. B. The key features of the nAChR agonist-binding site based on photoaffinity labeling and mutagenesis experiments are mapped onto Fig. 2b from ref. 2 (page 271). The agonist-binding site is denoted by π , emphasizing the importance of the aromatic residues in general and α Trp 149 in particular. Also highlighted are the signature loops of both subunits, and the main immunogenic region (MIR).

Undoubtedly, the crystal structure of AChBP has shed much light on our knowledge of the nicotinic receptors. The structure also confirmed all our results discussed in Chapters 2 and 4. The picture of the agonist-binding site of the nAChR is becoming more and more clear, especially for the binding of the quaternary ammonium group of ACh. However, because of the absence of ligand in the structure of AChBP, precise positioning of ligands within the binding site remains to be elucidated. For example, the relative orientation of the acetyl group of ACh is not known, although some suggestions have recently been made based on photoaffinity labeling studies (9). In addition, with the crystal structure data in hand, the next major issue is to decipher the allosteric mechanism that mediates the activation and desensitization of the nAChR ion channel from a 20–30 Å distant agonist-binding site. Finally, further evidence is desired to confirm the relevance of a small soluble protein from a snail to a receptor in the vertebrate central nervous system.

In order to gain more information on the position and orientation of ACh when it binds to the agonist-binding site, we docked the ACh molecule into the structure of AChBP. Based on the model obtained from the docking study, we found that the acetyl group of ACh is orientated toward and very close to the side chain of Met 114 (γ Leu 119/ δ Leu 121) on the complementary subunit, which is pointing toward the binding pocket. Based on this result, we designed and incorporated a new tethered agonist, lysyl-carbamylcholine. Upon incorporation into nAChR at several sites this tethered agonist produced constitutively active receptors, with significant activity seen at γ Leu 119/ δ Leu 121 as well as at α Cys192 and α Cys 193. These results demonstrated that the loop E

residues γ Leu 119/ δ Leu 121 on the complementary subunit are very close to the agonist-binding site, and also suggested the orientation of the acetyl group of ACh in binding. After re-examination of the crystal structure around the binding pocket, we found an interesting hydrogen bond between the NH of the indole side chain of Trp 143 (α Trp 149) and the carbonyl of a peptide bond of the complementary subunit. The intersubunit location suggested that this hydrogen bond might play a role in the allosteric transitions of nicotinic receptors. We therefore studied the effect of this hydrogen bond on the rate of desensitization. We found that the receptors with mutants that abolish the hydrogen bonding ability slowed the desensitization of the receptor. These results implied that this hydrogen bond might be one of the key elements that play a strategic role in the allosteric transitions of desensitization. All the above results together not only provide more interesting information on the nAChR, but also provide additional evidence that the structure of AChBP is closely related to that of N-terminal extracellular domain of the nAChR.

3.2 Docking Studies

As mentioned earlier, AChBP is a structural and functional homologue of the amino-terminal ligand-binding domain of nAChR, thus it can be used as a model in structure based modeling. The crystal structure of AChBP does not have any specific ligand bound in the binding site while on the other hand molecular docking is an important tool in studying ligand binding to receptors. We thus can use molecular

docking to get a picture of the binding mode of ligands in the binding site. Here we present our docking study of ACh to AChBP.

The crystal structure was minimized using the Dreiding force field (10) in the surface generalized Born (SGB) (11) continuum solvent after adding hydrogens and counter ions (see Chapter 5 for more details). The overall rmsd change after minimization was 0.35 Å, which showed that the Dreiding force field is suitable to describe the protein.

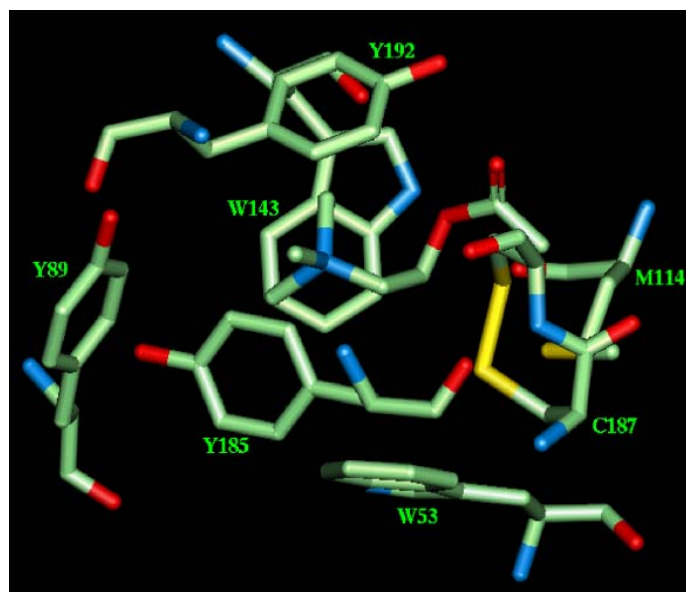
Using the HierDock docking protocol (12), the binding conformation of ACh in AChBP is obtained (see Chapter 5 for more details). Figure 3.2 shows ACh along with selected residues in the binding site of AChBP. It is seen that the quaternary ammonium group is buried deep within the pocket formed by five aromatic groups (Y89, W143, Y185, Y192 and W53 from the complimentary subunit). Interestingly, although the distances from the nitrogen atom of the quaternary ammonium to these five aromatic rings are similar (about 5 Å), the quaternary ammonium (positively charged) is only positioned directly over the face of the aromatic ring of Trp 143 (Figure 3.2A)—making the cation- π interaction as predicted by our earlier studies (8). The faces of the other four aromatic rings are not positioned correctly to allow the negative electrostatic potential resulting from the quadrupole moment to interact with the cation favorably. The implication of the docking results is that Trp 143 is unique because of orientation rather than close contact. The interaction energies between the docked ACh and all these aromatic residues are calculated and listed in Table 3.1. A test study of the binding

energy between ammonium ion and benzene has showed similar results from calculations using Dreiding force field (14.6 kcal/mol) and using *ab initio* quantum mechanics (15.38 kcal/mol), which shows the cation- π interaction can be reproduced with the Dreiding force field. As shown in Table 3.1, Trp 143 has the largest coulomb energy among the five aromatic residues, which is also consistent with the cation- π interaction. Tyr 192 has the largest total interaction energy, partly because of a weak hydrogen bond (-1.167 kcal/mol) that seems to form between its OH group and the carbonyl group of the ACh. The distance between the heavy atoms is 3.4 Å (141.5°). Because this part of the binding site is readily accessible to solvent, it is also possible that this hydrogen bond is bridged by a water molecule. Invoking a bridging water that links the OH of α Tyr 198 to the acetyl of ACh would explain the previously reported observation that O-Me-Tyr (4-MeO-Phe) at this position gives an EC₅₀ that is less than two fold different than wild-type (13). This residue cannot hydrogen bond directly to the agonist, but a water molecule could still bridge from the methoxy group to the agonist, now acting as a hydrogen bond donor at both ends of the bridge.

Residue	Total non-bond interaction energy	Van der Waals energy	Coulomb energy	H-bond
Y192	-5.575	-2.652	-1.756	-1.167
W143	-3.288	-0.571	-2.717	0.000
Y89	-2.837	-1.116	-1.721	0.000
W53	-2.211	-2.281	-0.070	0.000
Y185	-1.183	-2.230	1.047	0.000

Table 3.1. Interaction energies (kcal/mol) between ACh and the five aromatic residues in the binding site.

A.



B.

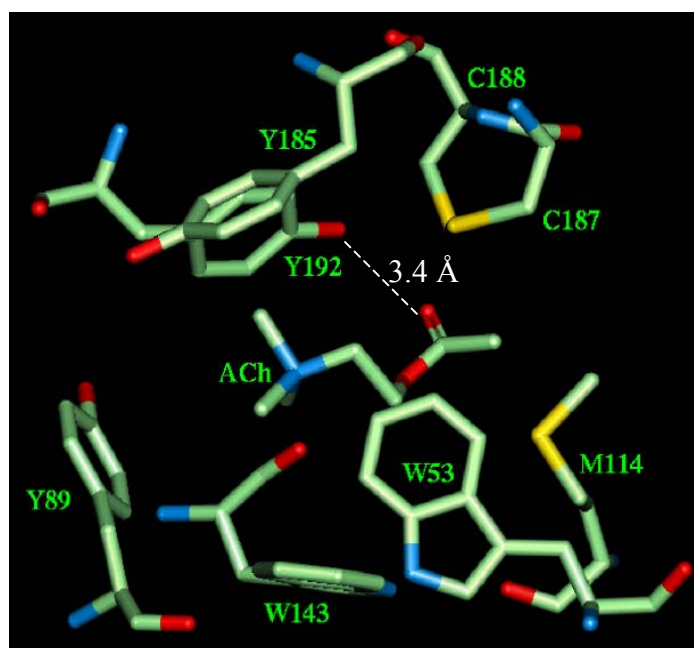


Figure 3.2. Two different views of docked ACh in the binding site of AChBP. Selected residues contributing to the agonist binding are shown. A. The quaternary ammonium of ACh is positioned directly over the face of the aromatic ring of Trp 143. B. The acetyl of ACh is oriented toward the disulfide bond and the side chain of Met 114.

Another interesting result of the docking study is the identification of the orientation of the acetyl group of ACh. As shown in Figure 3.2, the acetyl group of ACh is oriented toward the disulfide bond formed by Cys 187 and Cys 188 as well as the side chain of a residue from the complimentary subunit, Met 114. The disulfide bond between adjacent half cysteinyl residues is present in all nicotinic receptors and reduction of the disulfide bond in the nAChR affects both ligand binding and channel gating (14). On the other hand, the aligned residue of Met 114 in the nAChR family is not highly conserved and is often a large hydrophobic residue in non- α subunits. In addition, based on the docking studies Met 114 seems to have the right orientation and distance for introducing a tethered agonist, such that a properly designed tethered agonist might be able to map out the orientation of the acetyl group of ACh. Therefore, the aligned residue of Met 114 in nAChR seems to be a perfect candidate position to introduce a new tethered agonist.

3.3 Incorporation of Lysyl-carbamylcholine at γ Leu 119/ δ Leu 121 Resulted in Significant Constitutive Activity of the Receptor

With the results of the docking study, we were interested in exploring the orientation of the acetyl group of ACh when it binds to the agonist-binding site. We want to introduce the acetyl part into the tethered agonist in addition to the quaternary ammonium group, which the series of tethered agonists described in Chapter 2 contain. However, the molecule of ACh is not a good choice because it is very easily hydrolyzed. Compared with ACh, another nicotinic agonist, carbamylcholine (CCh) (Figure 3.3) is much more stable (the first order rate constant for hydrolysis of CCh is about one order of

magnitude smaller than that of ACh (15).). The equilibrium binding constants for CCh are similar to those for ACh, while doubly liganded CCh opens receptors at a slower rate than doubly liganded ACh. But compared with tetramethylammonium (TMA), CCh is a better agonist in terms of both agonist binding and channel opening (Table 3.2) (16). By incorporation of a carbamyl group to mimic the ester moiety of the agonist, which was suggested to speed both binding and channel opening (16), we might be able to not only map the orientation of the acetyl group of ACh in binding, but also increase the effectiveness of the tethered agonist. Base on the above reasons, the unnatural amino acid lysyl-carbamylcholine (Figure 3) that has been made is a perfect candidate as a new tethered agonist.

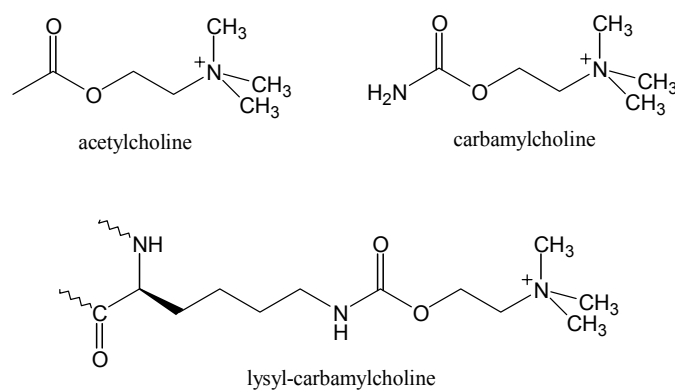


Figure 3.3. The structure of acetylcholine, carbamylcholine and lysyl-carbamylcholine.

Ligands	Channel opening rate constants (s ⁻¹)	Equilibrium binding constants (μm)
ACh	60000	20 and >650
CCh	11500	14 and 570
TMA	3000	525 and 12800

Table 3.2. The channel opening rate constants and the equilibrium binding constants of the nicotinic ligands for the embryonic mouse muscle nAChR. (Data taken from ref. 16.)

Based on the docking structure and the earlier discussion, γ Leu 119/ δ Leu 121 (the equivalent of Met 114 in AChBP) is a great position to introduce the lysyl-carbamylcholine residue. Therefore we made the mutations that contain amber codon (TAG) at γ Leu 119 and δ Leu 121. After we incorporated the lysyl-carbamylcholine into nAChR at γ Leu 119/ δ Leu 121, we observed constitutive currents as large as 2 μ A, which can be blocked by the nicotinic channel blocker TMB-8. Figure 3.4A shows the constitutive current that can be blocked by TMB-8, which varied on different experiment dates depending on the expression levels. The expression level of the mutant receptor with lysyl-carbamylcholine at γ Leu 119/ δ Leu 121 is relatively high based on ACh-induced currents (Figure 3.4B), although it varied to some extent on different experiment dates. The wild-type receptor gave ACh-induced current in the same range as the mutant receptor, but no constitutive current. We should mention that the constitutive activity for the mutant receptor was only observed with the Leu to Ser mutation at the 9' position of M2 region of the β subunit (see discussion in Chapter 2).

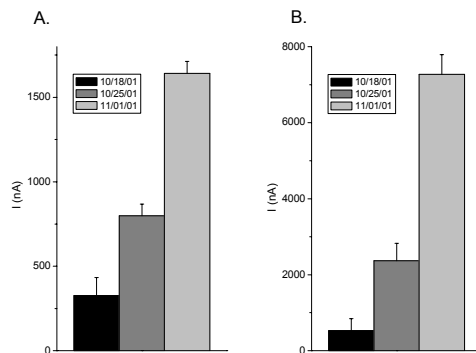


Figure 3.4. The electrophysiological results of incorporation of lysyl-carbamylcholine into nAChR at γ Leu 119/ δ Leu 121 on three different experiment dates. A. The constitutive current that can be blocked by 10 μ M TMB-8. B. The ACh (25 μ M)-induced current.

As discussed in Chapter 2, we use the ratio of the constitutive current that is blocked by TMB-8 to the ACh-induced current as a gauge of the effectiveness of a tethered agonist in activating the receptor. The concentrations of TMB-8 and ACh are always 10 μ M and 25 μ M, respectively, for measuring the currents that are used to calculate the ratios unless otherwise indicated. The ratio of TMB-8-blocked current to ACh-induced current for lysyl-carbamylcholine at γ Leu 119/ δ Leu 121 is between 0.3-0.9, varying to some extent in different experiments (Figure 3.5). Therefore its effectiveness is between what we have observed for Tyr-OnQ at α Tyr 93 and γ Trp 55/ δ Trp 57.

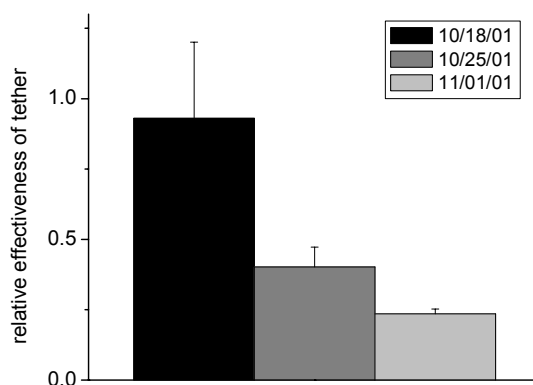


Figure 3.5. The relative effectiveness of lysyl-carbamylcholine at γ Leu 119/ δ Leu 121 on three different experiment dates.

We also incorporated Tyr-O3Q at γ Leu 119/ δ Leu 121 to compare with lysyl-carbamylcholine. It turned out that the effectiveness for the two tethered agonists was similar at this position (Figure 3.6). Note that the tether lengths (the distance between the quaternary ammonium group and the C α) in lysyl-carbamylcholine and Tyr-O3Q are very similar. One of the differences between the two tethers is the presence of the carbamyl bond in lysyl-carbamylcholine, which might be the cause of the slightly higher

activity seen for lysyl-carbamylcholine at this position. The other difference is that the side chain of lysyl-carbamylcholine is relatively more flexible than that of Tyr-O3Q.

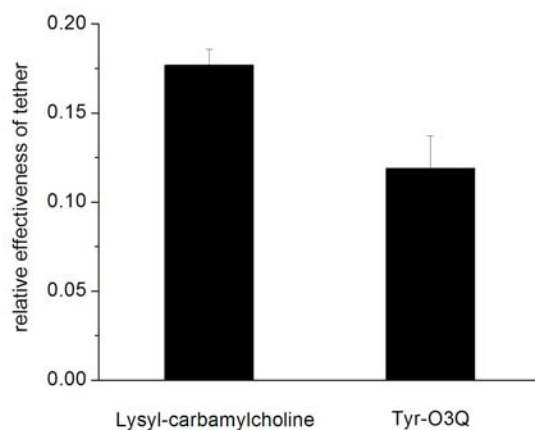


Figure 3.6. Comparison of the effectiveness of the two tethered agonists at γ Leu 119/ δ Leu 121.

Since Tyr-O3Q produced constitutively active receptors at γ Leu 119/ δ Leu 121, we decided to try the Tyr-OnQ series to see the effect of varying chain length at this position on the activity of the tethered agonist. We found that the effectiveness of the tether with 3 or 4 methylene groups were more than 10-fold higher than that of the shortest or the longest tether (Figure 3.7B). These results suggest that at position γ Leu 119/ δ Leu 121, both of the medium length tethers can be accommodated very well in the agonist-binding site and activate the receptor, while the other two tethers are either too short or too long to be positioned properly. We also tried the neutral compound Tyr-O3tBu. No constitutive current was observed, although the ACh-induced current is high (Figure 3.7A). This result implied that steric effects might not be involved here.

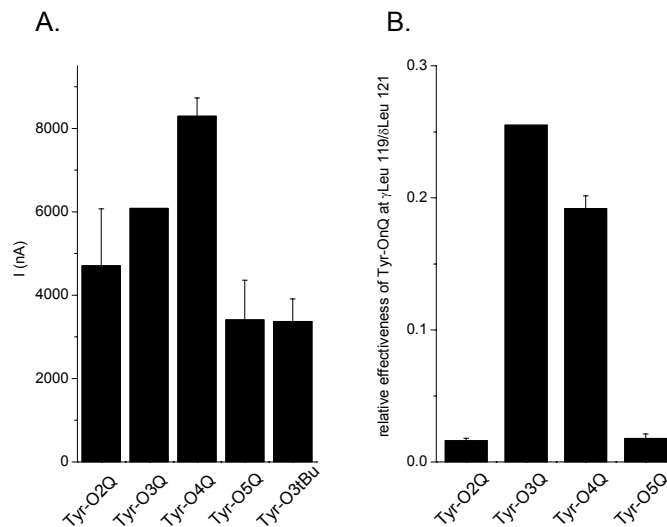


Figure 3.7. The results of incorporation of Tyr-OnQ (n=2-5) and Tyr-O3tBu at γ Leu 119/ δ Leu 121. A. The ACh (25 μ M)-induced current. B. The relative effectiveness of Tyr-OnQ.

In addition to γ Leu 119/ δ Leu 121, we also tried lysyl-carbamylcholine at several other positions around the agonist-binding site. As for the three positions that we have seen constitutive activity earlier, we found that incorporation of lysyl-carbamylcholine at α Tyr 93 and γ Trp 55/ δ Trp 57 also resulted in constitutively active receptors but not at α Trp 149. The ratios of TMB-8-blocked current to ACh-induced current are 0.25 and 0.18 for the mutant receptors with lysyl-carbamylcholine at α Tyr 93 and γ Trp 55/ δ Trp 57, respectively. Therefore at these two positions lysyl-carbamylcholine exhibited some but lower effectiveness than Tyr-O3Q (refer to Figure 2.5). The constitutive activity for both tethers at these two positions is not hard to understand, considering the similar distance between the C α and the quaternary ammonium for these two tethered agonists

and the tolerance for the tether length at these two positions (17). The somewhat lower activity can also be explained by the differences between the two tethers discussed earlier. At α Trp 149 the expression level with lysyl-carbamylcholine was relatively low based on the ACh-induced current. Still, no constitutive current was observed. We therefore consider this as a negative result, which is consistent with the previous conclusion that there is a stricter geometric requirement for receptor activation around the region very near α Trp 149 (17).

Besides the positions discussed above, we also observed constitutive activity for nAChR at α Cys 192 and α Cys 193 upon incorporation of lysyl-carbamylcholine. The expression levels are relatively low at these two positions, especially for mutant receptor with lysyl-carbamylcholine at α Cys 192. This is very likely due to the breakage of the disulfide bond between these two cysteines, since the reduction of the disulfide has been shown to affect both ligand binding and channel gating (14). At α Cys 193 the constitutive currents that could be blocked by TMB-8 were about 150 nA while the ACh-induced currents were about 300 nA, giving a ratio of about 0.5 (Figure 3.6). Therefore the effectiveness of the tether lysyl-carbamylcholine at α Cys 193 is similar to that at γ Leu 119/ δ Leu 121. At α Cys 192, although the TMB-8 blocked currents were in the same range as that at α Cys 193, the ACh-induced currents were so small that they were only about 100 nA even at 500 μ M of ACh. Thus the ratio of the TMB-8-blocked current to ACh-induced current is large. It is about 2.5 for 500 μ M ACh and should be even larger for 25 μ M of ACh (Figure 3.8). This result implied that lysyl-carbamylcholine

was a much stronger tethered agonist at α Cys 192 than at α Cys 193 and γ Leu 119/ δ Leu 121.

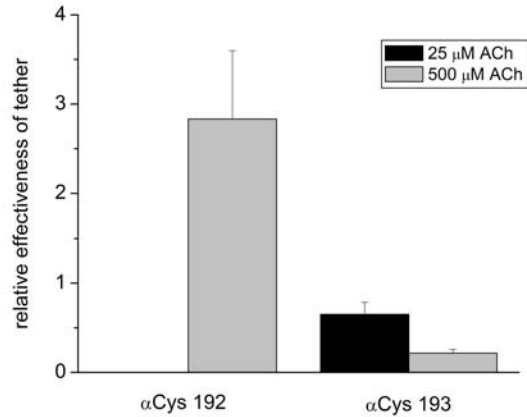


Figure 3.8. The relative effectiveness of tethered agonist lysyl-carbamylcholine at α Cys 192 and α Cys 193.

Based on all of the above results, lysyl-carbamylcholine is an effective tethered agonist at α Tyr 93, α Cys 192, α Cys 193, γ Trp 55/ δ Trp 57, and γ Leu 119/ δ Leu 121. All these residues have been identified by photoaffinity labeling studies except γ Leu 119/ δ Leu 121. Although γ Leu 119/ δ Leu 121 has been included as one of the loop E residues that contribute to the agonist binding pockets (5), there has been very little evidence that demonstrates its direct involvement in agonist binding. Neither photoaffinity labeling nor mutagenesis studies have identified this residue as being crucial for agonist binding. It has only been identified as one of the residues that contribute to α -bungarotoxin binding based on the decreased binding upon modification of the Leu to Cys mutant by MTSET (18). Here we showed that at γ Leu 119/ δ Leu 121 a tethered agonist lysyl-carbamylcholine could be positioned properly in the agonist

binding pocket and thus activate the receptor. These results confirmed that that γ Leu 119/ δ Leu 121 was very close to the agonist-binding site, which is consistent with the crystal structure of AChBP and the results of the docking study.

Among all of the positions above where incorporation of lysyl-carbamylcholine resulted in constitutively active receptors, the tether lysyl-carbamylcholine is more effective at α Cys 192, α Cys 193, and γ Leu 119/ δ Leu 121 than at α Tyr 93 and γ Trp 55/ δ Trp 57. This result suggested that the tether lysyl-carbamylcholine could be positioned better at α Cys 192, α Cys 193, and γ Leu 119/ δ Leu 121 than at α Tyr 93 and γ Trp 55/ δ Trp 57. This is consistent with the docking model, in which the acetyl group of ACh is oriented in the way that it makes close contact with residues Cys 187, Cys 188 and Met 114 (α Cys 192, α Cys 193, and γ Leu 119/ δ Leu 121), while the quaternary ammonium group of ACh is located in a box formed by the five aromatic residues (Figure 3.2). A recent photoaffinity labeling study has identified α Tyr 190, α Cys 192, α Cys 193, and α Tyr 198 as the residues that might contribute to the binding of the ester moiety of ACh (9). But the labeling molecule used (DCTA, (diazocyclohexadienoyl-propyl)-trimethylammonium) is less closely related to ACh than lysyl-carbamylcholine in terms of structure. In our study we obtained negative results at α Tyr 190 and α Tyr 198. Our results suggested among the loop C residues, α Cys 192 and α Cys 193 could position the carbamylcholine moiety of the tether chain more properly than α Tyr 190 and α Tyr 198 and therefore activate the receptor. Combined with the docking study, our results implied that the acetyl group of ACh was very likely oriented towards the side chain of α Cys 192, α Cys 193, and γ Leu 119/ δ Leu 121.

The above results also provide further evidence that supports the close relevance of AChBP to nAChR. In addition, the success of a new tethered agonist at a new position has showed that the tethered agonist approach indeed can be a general and very useful tool in mapping the structure of ion channel proteins.

3.4 Investigation of the Effect of an Intersubunit Hydrogen Bond on Desensitization

Careful examination of the crystal structure of AChBP revealed an intersubunit hydrogen bond between the NH of the indole side chain of Trp 143 (α Trp 149) and the peptide carbonyl of Met 114 (γ Leu 119/ δ Leu 121) on the complementary subunit. As discussed earlier in Chapter 1, the subunit interface might play a crucial role in the allosteric mechanism that mediates the activation and desensitization of the nAChR. It has been inferred (5) that AChBP was crystallized in a frozen “desensitized” (D) state, based on the high affinity of AChBP for nicotinic ligands and Hill coefficients that are either equal to or below unity (*I*). This led to the hypothesis that the basal (B) activatable conformation of nAChR derives from the AChBP structure by a reorganization of the quaternary structure. Therefore, this hydrogen bond at the interface of two subunits might play a key role in allosteric transitions of desensitization of the nAChR by stabilizing the more compact conformation of the D state.

We therefore decided to explore this interesting hydrogen bond further. Based on the above hypothesis, we think that incorporation of tryptophan analogs that abolish the hydrogen bonding abilities of the indole side chain at α Trp 149 may destabilize the

desensitized state of the nAChR. Here the nonsense suppression methodology provides us an indispensable tool that allows us to introduce unnatural amino acids with very subtle changes compared with their natural analog into the receptors. This would not have been possible with traditional site-directed mutagenesis. We have incorporated several tryptophan analogs, including N-methyl tryptophan (N-Me-Trp), 1-naphthylalanine (1-Np-Ala) and 2-naphthylalanine (2-Np-Ala) (Figure 3.9).

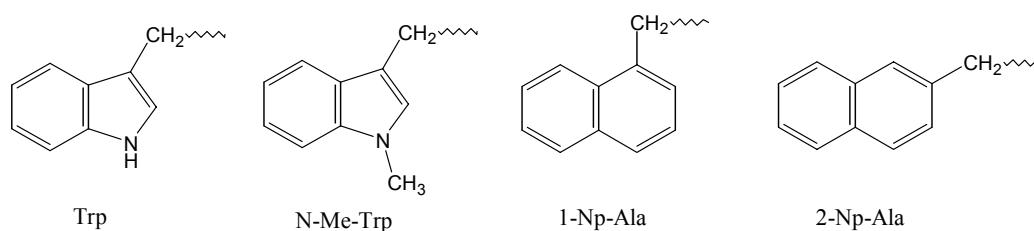


Figure 3.9. Structures of tryptophan and its analogs.

We incorporated tryptophan and its analogs into nAChR at Trp 149 and measured the current response to ACh using two-electrode voltage clamp. The receptor was desensitized by prolonged exposure to ACh. Figure 3.10 shows representative traces in this set of experiments. The desensitization phase was fit using a two exponential fit in Clampfit, and the weighted rate constants were calculated. As shown in figure 3.11 in most cases the desensitization rate constants for wild-type receptor are about 2.5-6 fold larger than those of the mutant receptors lacking the hydrogen bonding abilities. Thus, the receptor desensitizes more slowly in the absence of the hydrogen bond between the indole side chain of Trp 149 and the carbonyl backbone on the neighboring subunit. These results suggested that this intersubunit hydrogen bond is very likely one of the key elements in stabilizing the desensitized state of the receptor. Considering the strategic

location of this hydrogen bond—not only intersubunit but also within the binding pocket—it seems reasonable to propose that it is involved in transducing the binding event into a conformational change, and therefore plays a pivotal role in the allosteric mechanism of the receptor desensitization.

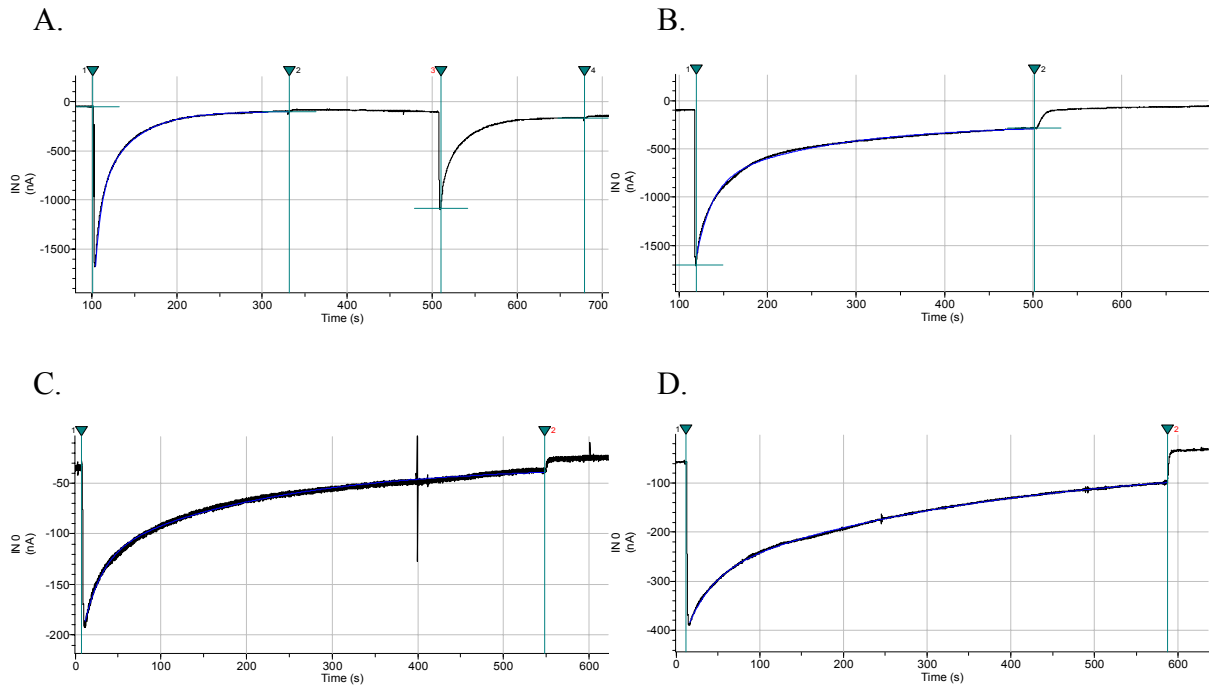


Figure 3.10. Representative traces in the desensitization experiments. (A) Wild type (Trp), (B) 1-Np-Ala, (C) N-Me-Trp, (D) 2-Np-Ala. The green cursors indicate the start and the end of the application of ACh. The concentrations of ACh used are 200 μM for wild type and mutant with 1-Np-Ala, and 400 μM for mutant with N-Me-Trp and 2-Np-Ala. The traces are in black and the fitting curves are in blue. For wild-type receptor (A) two applications of ACh were performed, only the first one was fit.

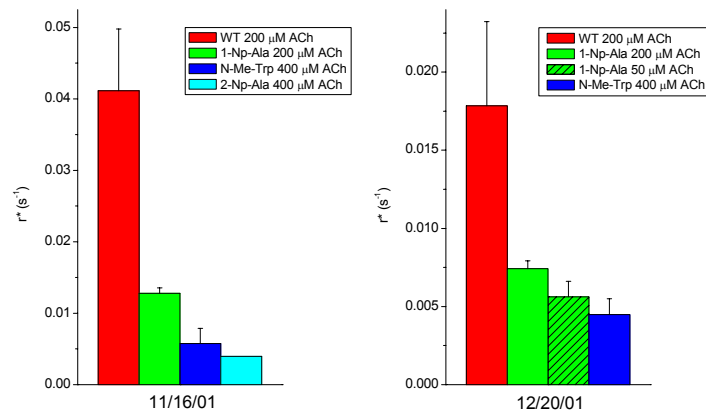


Figure 3.11. The weighted rate constants for desensitization of wild-type and mutant nAChRs. The concentrations of ACh used are indicated. (Weighted rate constants are calculated as following: $r^* = 1/[\tau_1 \times A_1 / (A_1 + A_2) + \tau_2 \times A_2 / (A_1 + A_2)]$, where τ_1 and τ_2 are the time constants for the slow and fast phase respectively in the two exponential fit, A_1 and A_2 are the amplitudes, respectively.)

The expression levels of the mutant receptors with different tryptophan analogs varied. The mutant with 1-Np-Ala expressed very well, giving large ACh-induced currents (2000-3000 nA at 200 μM of ACh) in the same range as wild-type receptor (Figure 3.12). However, the mutants with N-Me-Trp and 2-Np-Ala expressed relatively poorly, with only 200-300 nA ACh-induced current at 400 μM of ACh. Occasionally even no ACh current was seen, such as for the mutant receptor with 2-Np-Ala in the experiment conducted on December 20 (Figure 3.12).

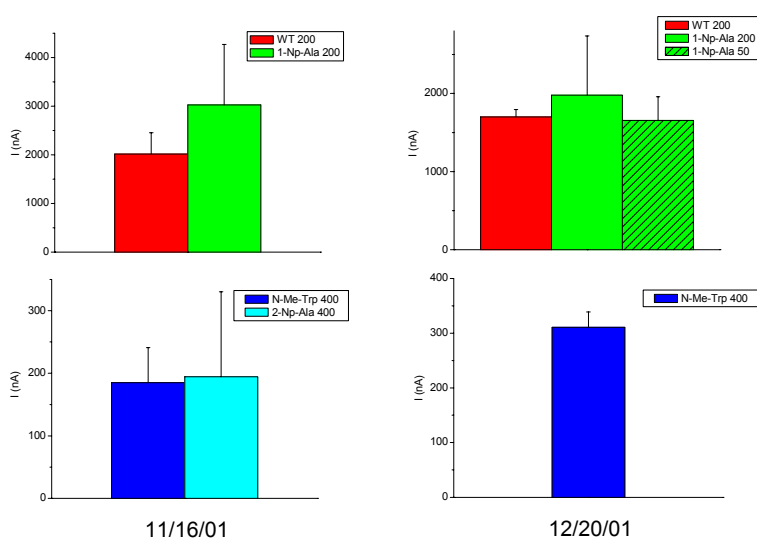


Figure 3.12. ACh-induced current for wild-type and mutant nAChRs with tryptophan analogs at α Trp 149. The concentrations of ACh (μ M) used are indicated.

The mutant nAChRs with these tryptophan analogs at α Trp 149 have actually been studied before in searching for the cation- π interaction, and the EC_{50} values for these mutant receptors have been measured (8). During our experiments we observed deviations of the EC_{50} values from the previous data. Thus we repeated the measurements. Figure 3.13 shows the representative dose response curves for these mutant nAChRs with unnatural tryptophan analogs at α Trp 149. As shown in Table 3.3, the EC_{50} value for 1-Np-Ala mutant is about 5-fold lower than that of wild-type receptor, while the EC_{50} value for 2-Np-Ala mutant is 5-fold higher, and the EC_{50} for N-Me-Trp is in between. Compared with wild-type EC_{50} the trends of the EC_{50} changes for the three mutants are different although they all lack the hydrogen bonding ability. Therefore the differences in EC_{50} values between the mutants and wild type are due to some other

structural aspects; further experiments will be needed to distinguish among the possible reasons. It is worth mentioning that the mutant with 1-Np-Ala at α Trp 149 is the first mutant that has been found to be substantially more active than wild-type nAChR.

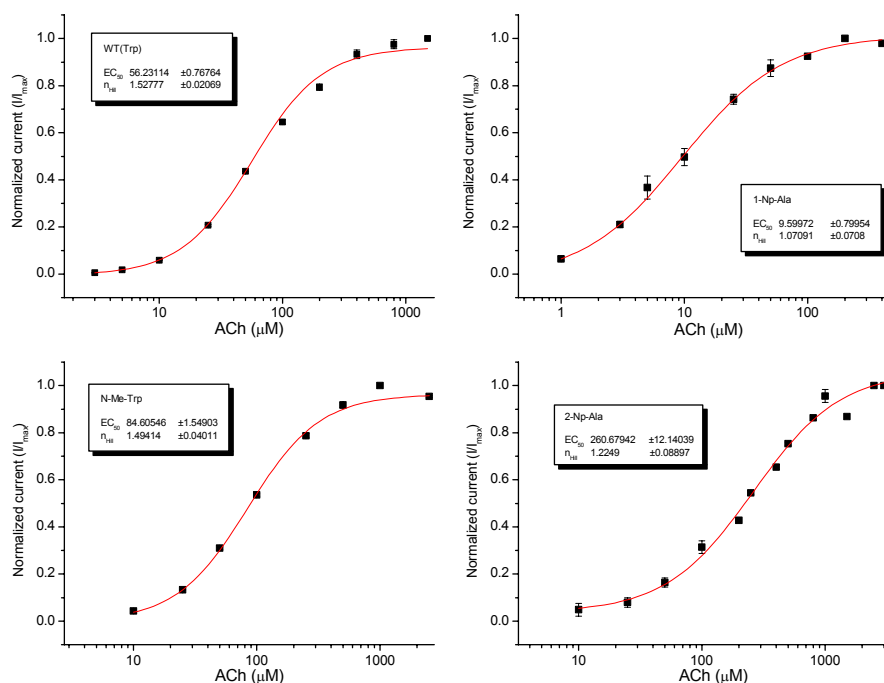


Figure 3.13. Representative dose-response measurements for wild-type and mutant nAChRs with tryptophan analogs at α Trp 149.

Side Chain	EC ₅₀	Hill coefficient
Trp	56.2±0.77	1.5±0.02
1-Np-Ala	9.6±0.80	1.1±0.07
N-Me-Trp	84.6±1.5	1.5±0.04
2-Np-Ala	260.7±12.1	1.2±0.09

Table 3.3. The EC₅₀ values and Hill coefficients for wild-type and mutant nAChRs with tryptophan analogs at α Trp 149.

3.5 Conclusions and Future Directions

The high-resolution structure of AChBP has certainly advanced our understanding of the nAChR. Here we present a docking study of ACh to AChBP in conjunction with several experiments that were designed based on the docking model and in return confirmed the docking structure. Incorporation of a new tethered agonist, lysyl-carbamylcholine, which contains a carbamyl group to mimic the acetyl group of ACh in addition to the quaternary ammonium group, resulted in constitutively active receptors with significant effectiveness at α Cys 192, α Cys 193, and γ Leu 119/ δ Leu 121. We therefore concluded that all these three residues, including the loop E residues γ Leu 119/ δ Leu 121 on the complementary subunits, are very near the agonist-binding site. In addition, we investigated the role of an intersubunit hydrogen bond between the NH of the indole side chain of Trp 143 and the carbonyl of the peptide backbone on the complementary subunit. The mutant receptor with tryptophan analogs that lack the hydrogen bonding abilities desensitized more slowly than wild-type receptor. These results suggested that this intersubunit hydrogen bond is very likely one of the key elements in stabilizing the desensitized state of the receptor, and therefore play a strategic role in the allosteric mechanism of the receptor desensitization.

All the results discussed above revealed new interesting information on both agonist binding and allosteric control of the nAChR. In addition, it provided further evidence that the soluble protein AChBP from snail glial cells is closely related to and

can be used to deduce the N-terminal extracellular domain of the vertebrate neurotransmitter receptor nAChR.

There are several other experiments that can be done to further explore different aspects of the project. First of all, the carbamylcholine derivatives of ornithine and homolysine, which are one carbon shorter and one carbon longer, respectively, than lysyl-carbamylcholine, can be prepared and incorporated into nAChR to investigate the effect of varying tether chain length on the effectiveness of the tether, therefore mapping out the geometric requirements in agonist binding. Based on the result with Tyr-OnQ at γ 119/ δ 121, we may predict that the one carbon longer tether may work as well as lysyl-carbamylcholine while the shorter one may not. Also, the nAChR is known for its pharmacological diversity. It would be very interesting to see how nicotine binds to the agonist-binding site using molecular docking since nicotine has been thought to bind the receptor differently compared with ACh. Finally, it has been shown that substitution of amino acid with an α -hydroxy acid to make the amide-to-ester mutation makes the carbonyl a poorer hydrogen bond acceptor (19). We can therefore study the interesting hydrogen bond further by replacing the residue C-terminal to γ Leu 119/ δ Leu 121, whose peptide bond carbonyl is the hydrogen bond acceptor, with an α -hydroxy acid. This should weaken the hydrogen bond and therefore affect the receptor desensitization.

3.6 Reference

1. Smit, A. B., Syed, N. I., Schaap, D., Minnen, J., Klumperman, J., Kits, K. S., Lodder, H., Schors, R. C., Elk, R., Sorgedragger, B., Brejc, K., Sixma, T. K., and Geraerts, W. P. M. (2001) *Nature* 411, 261-268.
2. Brejc, K., Dijk, W. J. v., Klaassen, R. V., Schuurmans, M., Oost, J. v. d., Smit, A. B., and Sixma, T. K. (2001) *Nature* 411, 269-276.
3. Dougherty, D. A., and Lester, H. A. (2001) *Nature* 411, 252-254.
4. Corringier, P.-J., Novere, N. L., and Changeux, J.-P. (2000) *Annu. Rev. Pharmacol. Toxicol.* 40, 431-458.
5. Grutter, T., and Changeux, J. P. (2001) *Trends Biochem. Sci.* 26, 459-463.
6. Miyazawa, A., Fujiyoshi, Y., Stowell, M., and Unwin, N. (1999) *J. Mol. Biol.* 288, 765-786.
7. Czajkowski, C., and Karlin, A. (1995) *J. Biol. Chem.* 270, 3160-3164.
8. Zhong, W., Gallivan, J. P., Zhang, Y., Li, L., Lester, H. A., and Dougherty, D. A. (1998) *Proc. Natl. Acad. Sci. USA* 95, 12088-12093.
9. Grutter, T., Ehret-Sabatier, L., Kotzyba-Hibert, F., and Goeldner, M. (2000) *Biochemistry* 39, 3034-3043.
10. Mayo, S. L., Olafson, B.D., and Goddard III, W.A. (1990) *J. Phys. Chem.* 94, 8897-8909.
11. Ghosh, A., Rapp, C. S. and Friesner, R. A. (1998) *J. Phys. Chem. B* 102, 10983-10990.

12. Floriano, W. B., Vaidehi, N., Goddard, W. A., Singer, M. S., and Shepherd, G. M. (2000) *Proc Natl Acad Sci USA* 97, 10712-6.
13. Kearney, P. C., Nowak, N. W., Zhong, W., Silverman, S., K., Lester, H. A., and Dougherty, D. A. (1996) *Mol. Pharmacol.* 50, 1401-1412.
14. Kao, P. N., and Karlin, A. (1986) *J. Biol. Chem.* 261, 8085-8088.
15. Ferdous, A. J., Dickinson, N. A., and Waigh, R. D. (1991) *J. Pharm. Pharmacol.* 43, 860-862.
16. Zhang, Y., Chen, J., and Auerbach, A. (1995) *J. Physiol.* 486, 189-206.
17. Li, L., Zhong, W., Zacharias, N., Gibbs, C., Lester, H. A., and Dougherty, D. A. (2001) *Chem. Biol.* 8, 47-58.
18. Sine, S. M. (1997) *J. Biol. Chem.* 272, 23521-23527.
19. Koh, J. T., Cornish, V. W., and Schultz, P. G. (1997) *Biochemistry* 36, 11314-11322.

Chapter 4

Efforts Toward Preparing a Short Tethered Agonist and Its Introduction into nAChR by Chemical Modification

4.1 Introduction

As mentioned in Chapter 2, Sullivan and Cohen observed constitutively active receptors upon modification of cysteine at α Tyr 198 by MTSET (1). They introduced cysteine mutants by traditional mutagenesis and used sulfhydryl-reactive reagents to tether primary or quaternary amines at several positions around the agonist-binding site of the nAChR. In most cases, the tethered amines acted as irreversible antagonists. But at α Tyr 198, MTSET modification of cysteine resulted in activation of the receptor. The effect was very sensitive to the length and orientation of the tethered group, in that lengthening or shortening the tether by one methylene group negated the activation effect. The inward current resulting from the MTSET treatment of cysteine at α 198 was as large as a few microamps. This effect was seen even without the additional Leu9'Ser mutation required in our studies (see Chapter 2), which could indicate quite efficient activation. This tethered agonist is much shorter than those discussed earlier in Chapters 2 and 3. It would be interesting to see whether we could observe constitutive activation in the absence of the Leu9'Ser mutation by incorporating this tether at α Tyr 198 by nonsense suppression. We therefore decided to make this shorter and more flexible tethered agonist-MTSET modified cysteine, i.e., S-[(2-trimethylammonium)-ethyl]-cysteine (Figure 4.1).

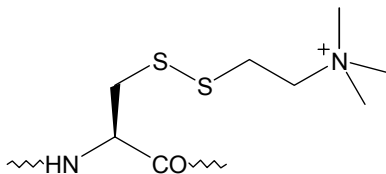


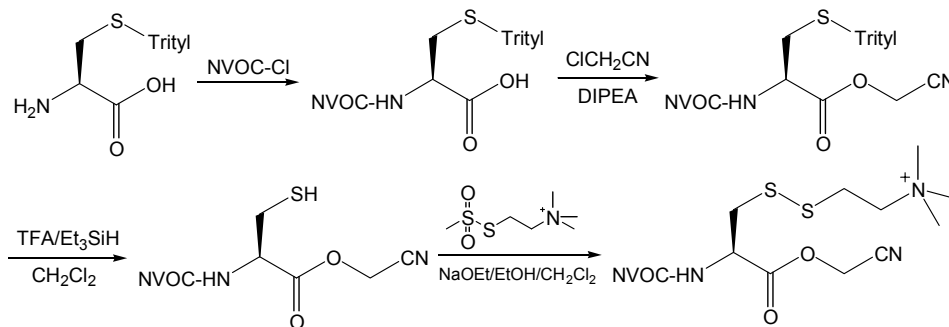
Figure 4.1. The structure of MTSET-modified cysteine.

4.2 Efforts toward Preparing a Short Tethered Agonist–MTSET-Modified Cysteine

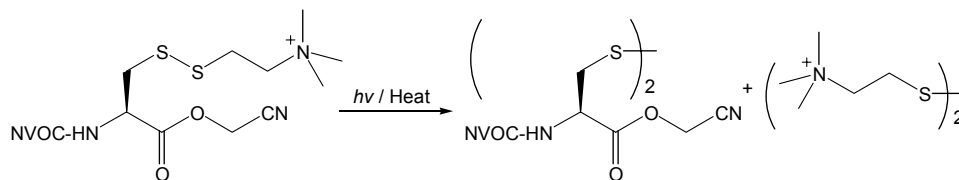
For use in the unnatural amino acid methodology, the synthetic target is the amino acid with the side chain in place, the amino group protected, and the carboxylate activated as a cyanomethyl ester (2, 3). The purpose of activation of the carboxylate group is to facilitate the coupling of the amino acid with the dinucleotide dCA (5'-phospho-2'-deoxyribocytidylriboadenosine) to form the dCA-amino acid complex, which is then ligated to tRNA (see chapter 5 for details). The amino group of the amino acid is protected by a nitroveratryloxycarbonyl (NVOC) group that will be removed by photolysis right before injecting the tRNA-amino acid into a *Xenopus* oocyte. The step to put on the NVOC group is straightforward and usually done at the beginning of the synthesis, while the formation of the cyanomethyl ester is usually carried out in the final step and is challenging in certain cases.

The planned synthetic route to MTSET-modified cysteine is outlined in Scheme 4.1. It does not seem to be problematic. Indeed, everything worked fine until the last step. MTSET has been widely used in biological studies, but it has not been reported to be used in organic synthesis. There are only a few instances of literature (4-6) for the preparation of disulfides with thio and methanethiosulfonates containing a primary or a secondary amine. I tried several conditions for the reaction with MTSET: CsCO₃/DMF, CsF/CH₃CN and C₂H₅OH/CH₂Cl₂ with or without C₂H₅ONa. It turned out the reaction went best in C₂H₅OH/CH₂Cl₂ with C₂H₅ONa. Although the reaction did go based on HPLC and the mass spectra showed the right peak, ¹H NMR indicated that the product

was not pure, but rather a mixture. One major component of the mixture was the free acid – N-NVOC-S-[(2-trimethylammonium)-ethylthio]-cysteine. This suggested that the cyanomethyl ester was easily hydrolyzed. In addition, there were some other complications of the reaction. One of them was the disproportionation of the disulfide (Scheme 4.2). We observed the disproportion product based on mass spectra and ^1H NMR after separating one peak in HPLC. We attempted the coupling reaction with dinucleotide dCA using the crude product and failed. The major peak in HPLC after the coupling reaction was N-NVOC-S-[(2-trimethylammonium)-ethylthio]-cysteine, again the hydrolyzed product of the cyanomethyl ester.

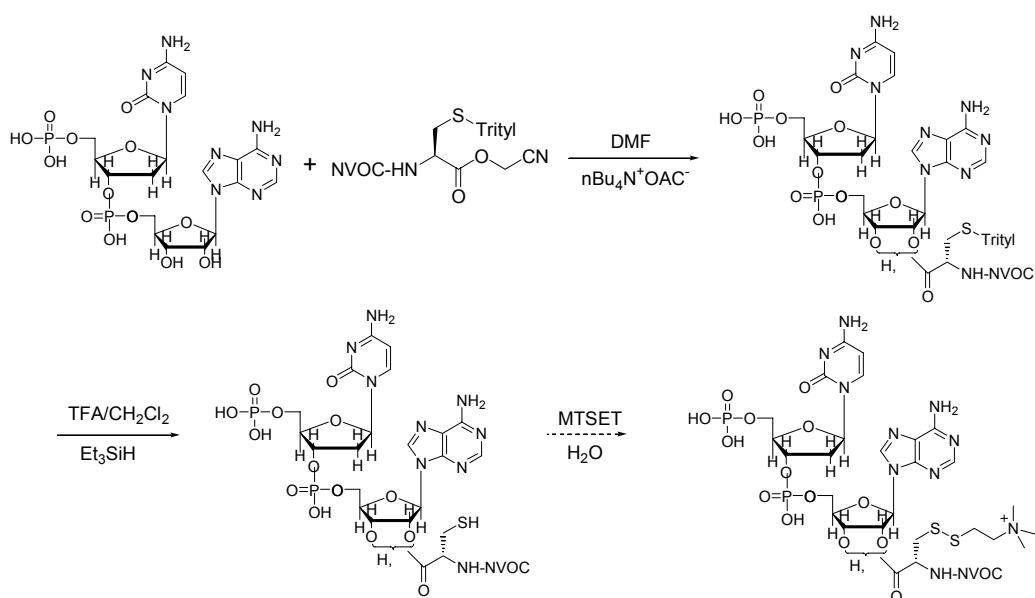


Scheme 4.1. The synthetic route for N-NVOC-S-[(2-trimethylammonium)-ethylthio]-cysteine cyanomethyl ester.



Scheme 4.2. The disproportionation of the disulfide of N-NVOC-S-[(2-trimethylammonium)-ethylthio]-cysteine cyanomethyl ester.

Since we had made N-NVOC-S-trityl-cysteine cyanomethyl ester, we also tried its coupling with dCA followed by the deprotection of the trityl group and the reaction of MTSET with dCA-cysteine (Scheme 4.3). However, the disadvantage of this procedure is that mass spectroscopy is the only informative way for characterization of the product. In addition, the phosphoester bond in dCA was vulnerable to the TFA used for the deprotection of the trityl group, which led to a low yield. We did not observe the final product, which was very likely because of the instability of the ester bond between the amino acid and the dinucleotide.



Scheme 4.3. Synthesis of dCA- N-NVOC-S-[(2-trimethylammonium)-ethylthio]-cysteine beginning with the coupling of N-NVOC-S-trityl-cysteine cyanomethyl ester with dCA followed by the deprotection of trityl group and the reaction of MTSET.

We think the instability of the cyanomethyl ester is due to the electronic effect of the quaternary ammonium group on the carbonyl of the ester bond (Figure 4.2) even though the 9-membered ring is not greatly favored. Such a mechanism has been

proposed to explain the instability of ACh (7, 8). In addition, the compound containing a quaternary ammonium group tends to be very hygroscopic. Actually, we had encountered difficulties in our earlier efforts to make amino acids containing quaternary ammonium groups with a short side chain, such as those shown in Figure 4.3 (9). When we prepared the Tyr- OnQ series and lysyl-carbamylcholine, we found that we had to form the cyanomethyl ester first and then add the quaternary ammonium group at the final stage using a two step amination sequence (see Chapter 5 and ref. 5 for more details). The advantage of this strategy is that the final product, the amino acid containing the quaternary ammonium group, just precipitated from the reaction solution and could be used in the following coupling reaction with dCA without further purification by HPLC. For the synthesis of the MTSET-modified cysteine here, we could use a similar procedure. However, it is still possible that it wouldn't work here, since the success in the preparation of Tyr-OnQ and lysyl-carbamylcholine could be because they are not as labile as MTSET-modified cysteine, due to the longer chain length and the rigidity of the chain, especially in the case of Tyr-OnQ. After we tried a few alternative ways to couple the amino acid with dCA without forming the cyanomethyl ester and failed (see below), we decided to test the potential application of this unnatural amino acid by some biological experiment (see section 4.3) before we make further efforts in its synthesis.

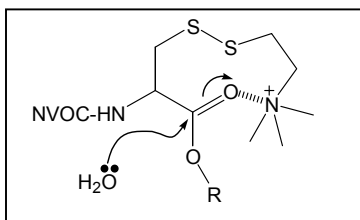


Figure 4.2. A schematic of the electronic effect of the quaternary ammonium on the instability of the ester bond.

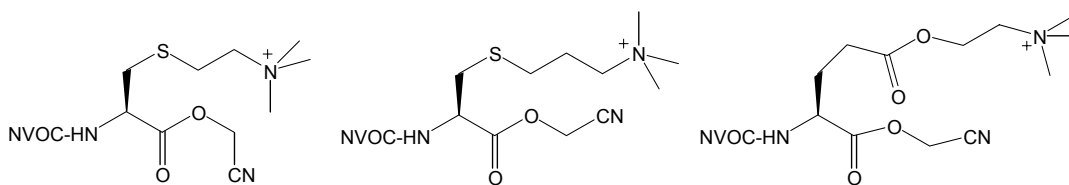
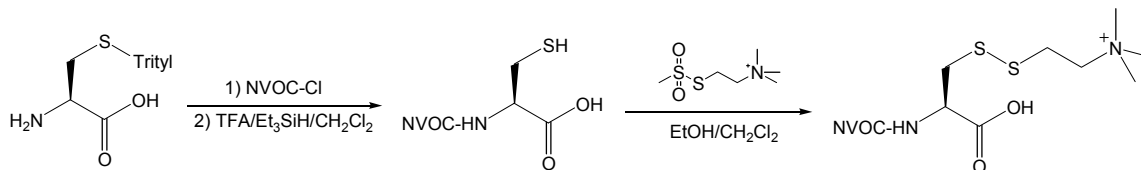


Figure 4.3. Amino acids containing a short chain with a quaternary ammonium group at the end.

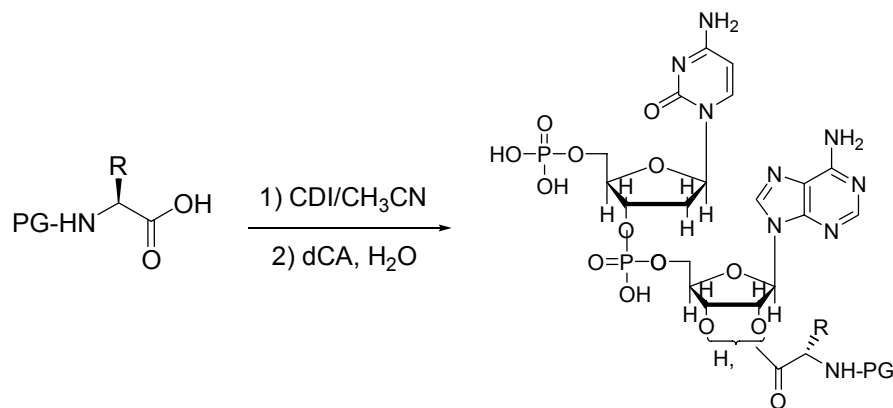
After the failures to make the cyanomethyl ester, we decided to try some alternative methods to couple the amino acid with dinucleotide dCA just using N-NVOC-S-[(2-trimethylammonium)-ethylthio]-cysteine since it is straightforward to prepare it (Scheme 4.4).



Scheme 4.4. Synthesis of N-NVOC-S-[(2-trimethylammonium)-ethylthio]-cysteine.

Chamberlin and coworkers reported the method of coupling N-protected amino acids with dinucleotide dCA using carbonyldiimidazole (CDI) to activate the carboxylate group in aqueous solution (Scheme 4.5) (10, 11). The reason they use water as solvent is to avoid a possible side-reaction, the acylation of the 4-amino group of cytidine (12). It was reported as a one-pot procedure without isolating the amino acid imidazolide, but the yield was very low, only 6% (10). I tried this reaction using both N-NVOC-S-[(2-trimethylammonium)-ethylthio]-cysteine and a model amino acid, $^{\alpha}\text{N-NVOC-}^{\epsilon}\text{N-Boc-L-Lysine}$. The reaction worked for the model amino acid, although the yield was extremely low (1%). However, we didn't observe the coupling product for N-NVOC-S-[(2-

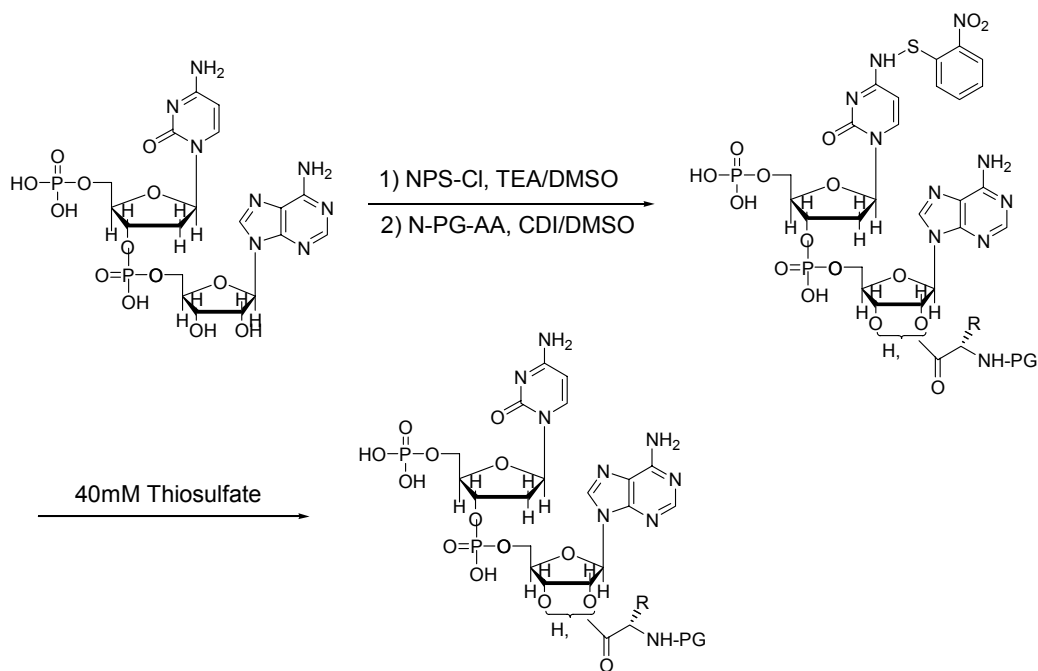
trimethylammonium)-ethylthio]-cysteine. We think the imidazolide formed after the activation of N-NVOC-S-[(2-trimethylammonium)-ethylthio]-cysteine with CDI was hydrolyzed back to the acid.



Scheme 4.5. The method of coupling the N-protected amino acid with dinucleotide dCA using CDI in aqueous solution.

When Schultz and coworkers first reported the *in vitro* nonsense suppression method for unnatural amino acid incorporation, the method for dCA-AA coupling they used involved the protection of the 4-amino group of the cytosine in dCA with a nitrophenylthio (NPS) group and then coupling of the N-protected amino acid with NPS-dCA using CDI followed by the deprotection of the NPS group with thiosulfate (Scheme 4.6) (13, 14). Although the coupling reaction was run in dry DMSO, the deprotection step was carried out in an aqueous solution of thiosulfate. We obtained the same results as the other procedure: the reaction worked for the model amino acid ^αN-NVOC-^εN-Boc-L-Lysine, but not for N-NVOC-S-[(2-trimethylammonium)-ethylthio]-cysteine. We think that this procedure suffers from the complications associated with the protection

and deprotection of dCA, but the failure is mainly due to the instability of ester bond between the amino acid and the ribose of the dinucleotide.



Scheme 4.6. The method of coupling the N-protected amino acid with NPS-protected dinucleotide dCA using CDI in anhydrous DMSO.

After we encountered these hurdles in obtaining the MTSET-modified cysteine and its complex with dinucleotide dCA, we decided to test the potential application of this short tethered agonist with biological experiments before we put further efforts into the synthesis.

4.3 MTSET-Modification of Cysteine Incorporated by Nonsense Suppression Resulted in Constitutively Active Receptors

One major purpose of attempting to incorporate this short tethered agonist into nAChR was to obtain strong constitutive activity, which therefore could be observed without using the Leu9'Ser mutation in M2 of the β subunit. This was based on the significant effect of activation seen in Cohen and coworkers' results (*1*). However, we should mention that the cysteine mutation was introduced by traditional site-directed mutagenesis in their work. One of the limitations of the unnatural amino acid mutagenesis methodology is the relatively low suppression efficiency compared with traditional site-directed mutagenesis. Actually, the amount of surface receptors determined by ^{125}I - α -bungarotoxin binding was about 4 fmol for wild-type receptors and 2 fmol for the cysteine mutants. This is more than 10 times the amount we can obtain by nonsense suppression. This means that we probably wouldn't be able to observe strong activation after we incorporate the MTSET-modified cysteine into nAChR by nonsense suppression if the expression level is not high enough. Assuming the expression levels for mutant receptors with cysteine or MTSET-modified cysteine incorporated by nonsense suppression methodology are similar, the signal from chemical modification of cysteine by MTSET should be similar to that from incorporation of MTSET-modified cysteine. We therefore incorporated a cysteine residue by nonsense suppression at α 198 to test how much activation we could obtain by MTSET modification, both in the presence and in the absence of the Leu9'Ser mutation. Figure 4.4 shows the representative traces in the electrophysiological experiment.

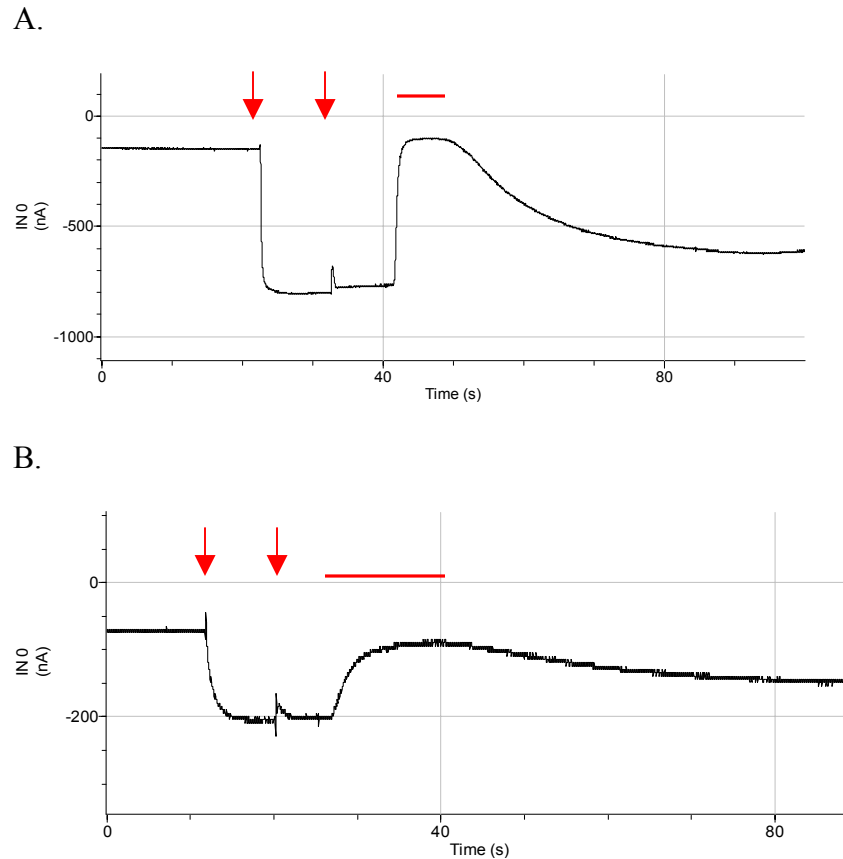


Figure 4.4. The representative traces in the electrophysiological experiment. The red arrow indicates the application of 100 μM MTSET by pipette tip. The red bar indicates the application of 10 μM TMB-8. A. Mutant receptor with cysteine at $\alpha 198$ and Leu9'Ser mutation in β subunit. B. Mutant receptor with cysteine at $\alpha 198$ only.

As we can see, MTSET-modification of the mutant nAChR with cysteine at $\alpha 198$ resulted in a large inward current that could be reversibly inhibited by TMB-8, which indicated a constitutively active receptor. This constitutive activity was seen for mutant receptor with or without the Leu9'Ser mutation. However, the resulting inward current for the mutant with the Leu9'Ser mutation was about 10 times larger than that without it (Figure 4.5). On one hand, these results confirmed the results seen by Cohen and

coworkers. On the other hand, it suggested that incorporation of MTSET-modified cysteine into nAChR by nonsense suppression would not result in significant activation unless in the presence of the Leu9'Ser mutation due to the relatively low expression level of the receptor.

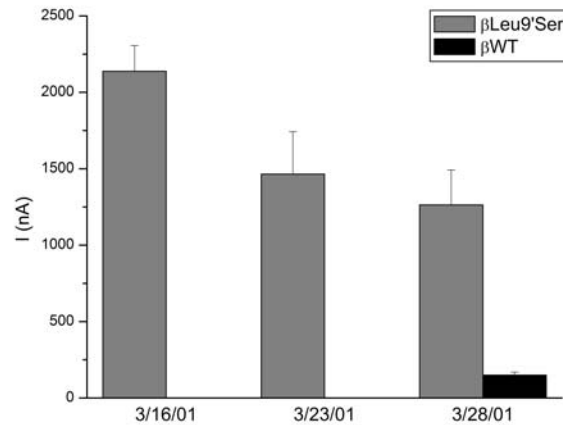


Figure 4.5. The inward current resulted from the MTSET-modification of the mutant nAChR with cysteine at α 198 in the presence or absence of the Leu9'Ser mutation in β subunit.

In conclusion, we were not able to prepare a short tethered agonist, MTSET-modified cysteine, nor the dCA-amino acid, due to the strong tendency toward the hydrolysis of these compounds. Incorporation of a cysteine residue by nonsense suppression followed by chemical modification with MTSET resulted in constitutively active receptors. However, the strong activity was only observed in the presence of Leu9'Ser mutation, suggesting that the effectiveness of the tethered agonist was limited by the relatively low expression of receptors by *in vivo* nonsense suppression methodology.

4.4 Reference

1. Sullivan, D. A., and Cohen, J. B. (2000) *J. Biol. Chem.* 275, 12651-12660.
2. Ellman, J., Mendel, D., Anthonycahill, S., Noren, C. J., and Schultz, P. G. (1991) *Meth. Enzym.* 202, 301-336.
3. Robertson, S. A., Ellman, J. A., and Schultz, P. G. (1991) *J. Am. Chem. Soc.* 113, 2722-2729.
4. Bruice, T. W., and Kenyon, G. L. (1982) *J. Protein Chem.* 1, 47-58.
5. Singh, P. K., and Field, L. (1988) *J. Chem. Eng. Data* 33, 67-68.
6. Field, L., Kim, H. K., and Bellas, M. (1967) *J. Med. Chem.* 10, 1166-7.
7. Davis, W., and Ross, W. C. J. (1950) *J. Chem. Soc.*, 3056.
8. Davis, W., and Ross, W. C. J. (1951) *J. Chem. Soc.*, 2706.
9. Zhong, W. (1998) in *Chemistry*, California Institute of Technology, Pasadena, CA.
10. Steward, L. E., Collins, C. S., Gilmore, M. A., Carlson, J. E., Ross, J. B. A., and Chamberlin, A. R. (1997) *J. Am. Chem. Soc.* 119, 6-11.
11. Steward, L. E., and Chamberlin, A. R. (1998) *Methods Mol. Biol.* 77, 325-54.
12. Gottikh, B. P., Krayevsky, A. A., Tarussova, N. B., Purygin, P. P., and Tsilevich, T. L. (1970) *Tetrahedron* 26, 4419-33.
13. Robertson, S. A., Noren, C. J., Anthony-Cahill, S. J., Griffin, M. C., and Schultz, P. G. (1989) *Nucleic Acids Res.* 17, 9649-9660.
14. Noren, C. J., Anthony-Cahill, S. J., Griffith, M. C., and Schultz, P. G. (1989) *Science* 244, 182-188.

Chapter 5

Methods in Molecular Biology, Electrophysiology and Molecular Docking, and Synthesis of Amino Acids

5.1 Methods in Molecular Biology and Electrophysiology

Mutagenesis and mRNA Synthesis

The site-directed mutagenesis of the nAChR TAG mutants was carried out using the QuikChange kit (Stratagene, La Jolla, CA). The α , β , γ and δ subunits of nAChR were subcloned into the expression vector pAMV, which is optimized for oocyte expression (1). The cDNA plasmid was linearized with *NotI*, and mRNA was prepared by *in vitro* transcription of the linearized cDNA plasmid using the Ambion (Austin, TX) mMESSAGE mMACHINE T7 Kit.

tRNA Synthesis and Ligation of dCA-Amino Acid to tRNA

The gene construction of the *Tetrahymena thermophila* tRNA^{Gln} CUA having a G at position 73 (THG73) has been described previously (1, 2). The gene contains an upstream T7 RNA polymerase promoter and a downstream *FokI* restriction site. Template DNA for *in vitro* transcription of tRNA lacking the 3'-terminal bases C75 and A76 was prepared by linearizing pTHG73 with *FokI*. *In vitro* transcription of the linearized plasmid was performed using the Ambion (Austin, TX) MEGAscript T7 kit. The α -NH₂-protected dCA-amino acid or dCA was enzymatically ligated to the THG73 *FokI* runoff transcripts using T4 RNA ligase to form a full-length aminoacyl-THG73 or a full-length but unacylated THG73-dCA as described previously (1).

Oocyte Microinjection

Oocytes were removed from *Xenopus laevis* as described (3) and maintained at 18°C, in ND96 solution (pH 7.5 adjusted by NaOH), which contains 96 mM NaCl, 2 mM KCl, 1.8 mM CaCl₂, 1 mM MgCl₂, 5 mM HEPES, 2.5 mM sodium pyruvate, 0.5 mM theophylline and 10 µg/ml Gentamycin. Before microinjection, the NVOC-aminoacyl-tRNA was deprotected by irradiating the sample for 5 minutes with a 1000 W xenon arc lamp (Oriol) operating at 400 W equipped with WG-335 and UG-11 filters (Schott, Duryea, PA). The deprotected aminoacyl-tRNA was immediately mixed with the desired mRNA and microinjected into *Xenopus* oocytes. Each oocyte was injected with 50 nl of a 1:1 (volume) mixture of deprotected aminoacyl-tRNA (25-50 ng) and mRNA (12.5–18 ng of total at a concentration ratio of 20:1:1:1 for αTAG:β:γ:δ or 2:1:10:10 for α:β:γTAG:δTAG). Since the presence of constitutively active channels would be expected to compromise the health of the oocytes through a large leak current, 2µM - 5µM TMB-8 (RBI, Natick, MA) was added to the incubation solution to block any leak current that might occur through the nAChR.

It is worth mentioning that TMB-8 may have the effect of preventing the receptor from desensitization. In our last experiments, when we were recording from oocytes expressing the mutant receptor with Tyr-O3Q at αTrp 149, we noticed that the standing current was initially small but continuously increased upon application of TMB-8, and the blocked current by TMB-8 also increased at the same scale and thus could reach the same plateau independent of the increasing standing current. This observation suggested

that the receptor was rescued from desensitization by treatment with TMB-8. This is consistent with the fact that we didn't add TMB-8 in the oocyte incubation media in these last experiments, while in our earlier experiments we incubated the oocytes in ND96 with TMB-8, and the oocytes showed large standing currents.

Electrophysiology

Electrophysiological recordings were carried out 24-48 hours after injection. Whole-cell currents from oocytes were measured using a Geneclamp 500 amplifier and pCLAMP software (Axon Instruments, Foster City, CA) in the two-electrode voltage-clamp configuration. The first electrode simply measures the electrical potential across the oocyte's membrane. Using a feedback loop, current is injected via the second electrode to maintain the transmembrane potential at any desired value (that is, the membrane potential is "clamped" to the chosen value). Microelectrodes were filled with 3 M KCl and had resistances ranging from 0.5 to 1.5 M Ω . Oocytes were continuously perfused with a nominally calcium-free bath solution consisting of 96 mM NaCl, 2 mM KCl, 1 mM MgCl₂, and 5 mM HEPES (pH 7.5), while impaled with two electrodes. Microscopic ACh-induced and TMB-8-blocked currents were recorded in response to bath application of ACh and TMB-8 at the desired concentration at a holding potential of -80 mV. All numerical and plotted data are from measurements obtained from 4-8 oocytes and are reported as mean \pm standard error. Individual dose-response relations were fit to the Hill equation, $I/I_{\max} = 1/[1 + (EC_{50}/[A])^{nH}]$, where I is the current for the agonist concentration $[A]$, I_{\max} is the maximal current, EC_{50} is the concentration to elicit a

half-maximal response, and n_H is the Hill coefficient.

Bungarotoxin Binding and Western Blot Analysis

^{125}I - α -bungarotoxin binding experiments were performed as described (4). Oocytes were incubated in 400 μl of calcium-free ND96 solution containing 10 mg/ml BSA (Sigma) for 10 minutes and then ^{125}I - α -bungarotoxin (Amersham) was added to a final concentration of 1 nM. After incubation for 2 hours, the oocytes were washed extensively and then counted in a Beckman LS5000 γ -counter.

Western blot analyses were carried out as described (5). A hemagglutinin (HA) epitope was subcloned into the intracellular loop between the third and fourth transmembrane domains of the α subunit. The vitelline/plasma membranes were manually stripped from oocytes expressing nAChR (6). Alternatively, the oocytes were treated with sulfo-NHS-LC-biotin (Pierce) and then homogenized. After removing the yolks of the oocytes by centrifuge, the remaining supernatant was incubated with streptavidin-agarose beads (Sigma). The protein was then eluted from the beads by adding SDS buffer. In either case, the samples were analyzed by SDS-PAGE, followed by immunoblotting with the anti-hemagglutinin antibody (BabCO, cat # MMS-101R), and visualized using an ECL detection kit (Amersham).

5.2. Methods for Molecular Docking

Structure Preparation

The coordinates of the AChBP crystal structure were downloaded from the Protein Data Bank (pdb id: 1I9B). Hydrogens were added to the protein using Biograf. The whole protein including the HEPES ligands was then minimized using MPSim (7) with the Dreiding force field (8). The CMM nonbond method (9) was used to allow efficient yet fast energy evaluation. The surface generalized Born (SGB) implicit solvation model (10) was applied to simulate the solvation effect of the bulk solvent. Protein was described using CHARMM22 (11) charges, with counterions (Na^+ and Cl^-) added to neutralize charged residues. The final structure after minimization was used in the docking simulation.

For the HEPES and acetylcholine ligands, Mullikan charges based on molecular orbitals from quantum mechanics were used. The quantum mechanics calculations were done using Jaguar 4.0 (Schrödinger Inc, Portland, OR) at the HF level with the 6-31G ** base set. The geometry was optimized by using forces calculated with Poisson Boltzmann continuum solvation (12).

Docking Protocol

The HierDock protocol (13) was used in docking acetylcholine into the binding site of AChBP. It is based on DOCK 4.0 (14), and has been used in screening of unnatural amino acids binding to aminoacyl-tRNA synthetases (15) and odor ligands binding to olfactory receptors (13). The HierDock protocol combines the fast Monte Carlo conformation search and a good force field scoring function with solvation to accurately get the binding conformation of a ligand in a receptor. It has a procedure for screening a binding site if that information is unknown for a certain ligand to the receptor. Because the acetylcholine binding site is well known in this case, the binding site screening procedure has been skipped. The rest of the procedures are:

(1) A negative image of the receptor's Connolly molecular surface in the binding site was generated and filled with a set of overlapping spheres. A probe radius of 1.4 Å and a surface density of 5 dots/Å² were used. The binding site was defined as the cube occupied by the HEPES ligand in the crystal structure plus a 5 Å margin in each dimension. An energy grid was then generated for the binding region plus a 10 Å margin for each dimension. This energy grid was used later to evaluate ligand conformations and orientations.

(2) Ligand conformations were generated using a Monte Carlo procedure and matched to spheres in the binding site. The total number of conformations was set to 5000. Each conformation was then passed through a bump filter. A bump was defined as

an overlap of two atoms between ligand and receptor with distance less than 75% of the combined van der Waals value. Conformations with more than three bumps were rejected without further evaluation. The ligand conformation was then minimized and the binding energy was calculated using the energy grid. The top 50 conformations with the best binding energies were saved for further evaluation. These steps were done using DOCK version 4.0 (14).

(3) DOCK is considered a coarse grain search procedure because it lacks precision in conformation evaluation. A subsequent fine grain binding energy calculation was done using MPSim, a full molecular mechanics and molecular dynamics suite with full force field capability. First each of the 50 conformations out of DOCK was minimized in the presence of the receptor. The 5 conformations with the lowest energies were selected to run 5 cycles of annealing dynamics to get better binding interaction between the ligand and receptor. Each cycle of annealing dynamics consisted of heating the system from 50 K to 600K and cooling from 600K to 50K in steps of 20K for 0.5 ps. These annealing MD calculations included the SGB continuum solvation with a dielectric constant of 80 and a solvent radius of 1.4 Å. Each cycle of annealing dynamics generated a minimized ligand conformation, thus totally 25 conformations were generated and the one with the lowest energy was selected to be the docked ligand conformation. The binding energy was calculated using the following definition:

$$-\Delta\Delta G_{binding} = (\Delta G_{ligand} + \Delta G_{receptor}) - \Delta G_{complex} ,$$

where $\Delta G_{complex}$ is the total energy of the protein with the ligand bound in this case being AChBP with ACh bound to it including solvation, ΔG_{ligand} and $\Delta G_{receptor}$ are the energies

of the ligand and receptor including solvation. The receptor and the ligand structures were optimized in Molecular Dynamics with SGB solvation.

5.3. Synthesis of Amino Acids and dCA-Amino Acids

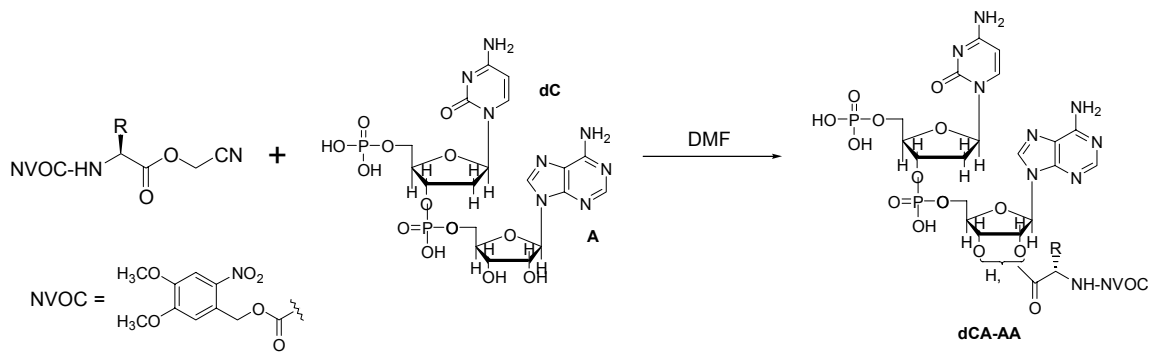
Materials

Reagents were purchased from Aldrich, Sigma, or other commercial sources. Anhydrous THF was distilled from sodium benzophenone; anhydrous methylene chloride, toluene and acetonitrile were distilled from CaH₂; anhydrous acetone was distilled from CaSO₄; anhydrous DMF was obtained from Fluka. BakerDRY solvents (ultra low water) in CYCLE-TAINER from J. T. Baker were also used for anhydrous THF, methylene chloride, ethyl ether and acetonitrile. Flash chromatography was on 230-400 mesh silica gel with the solvent indicated. All NMR shifts are reported as δ ppm downfield from TMS. ¹H NMR spectras were recorded at 300 MHz in CDCl₃ using a GE QE-300 or Varian 300 spectrometer. FAB-MS determinations were performed at the University of Nebraska, Lincoln. Electrospray ionization (ESI), quadruple mass spectrometry was performed at the Caltech Protein/Peptide Micro Analytical Laboratory. High performance liquid chromatography (HPLC) separations were performed on a Waters dual 510 pump liquid chromatography system equipped with a Waters 490E variable wavelength UV detector for semi-preparative HPLC and a Waters 996 PDA (photodiode array) UV detector for analytical HPLC. Waters Prep Nova-Pak HR C₁₈ column (7.8x300 mm) was used for semi-preparative HPLC and Waters Nova-Pak C₁₈

column (3.9x150 mm) was used for analytical HPLC. Nitroveratryloxycarbonyl chloride (NVOC-Cl) and NVOC-Tyrosine t-butyl ester were prepared as described earlier (16).

General Procedure for Coupling of Amino Acid to dCA

This method is essentially as described (16, 17). The N-protected amino acid cyanomethyl ester (~30 μmol , 3 equivalents) was mixed with the tetrabutylammonium salt of the dCA dinucleotide (~10 μmol , 1 equivalent) in 400 μl of dry DMF. The reaction mixture was kept stirring for 1-3 hours under argon. The reaction was monitored by reverse phase analytical HPLC with a gradient from 25 mM ammonium acetate (pH 4.5) to CH_3CN . The crude product was isolated using reverse-phase semi-preparative HPLC. The desired fractions containing the aminoacyl dinucleotide were combined, frozen, and lyophilized. The lyophilized solid was redissolved in 10 mM aqueous acetic acid/acetonitrile and lyophilized a second time to remove ammonium ions, which inhibits T4 RNA ligase in the ligation of dCA-amino acid to the tRNA. The products were characterized by mass spectrometry and quantified by UV/Vis spectra, assuming $\epsilon_{350} \sim 6350$ per nitroveratryl group.



Scheme 5.1. Synthesis of dCA-amino acid.

dCA-NVOC-O-2-(trimethylammonium)ethyl tyrosine (dCA-NVOC-Tyr-O2Q).

Prepared as above using NVOC-O-2-(trimethylammonium)ethyl tyrosine cyanomethyl ester (**3a**) as starting material. FAB-MS: $[M^+]$, calc'd for $C_{43}H_{56}N_{11}O_{21}P_2$: 1124.3128; found: 1124.2.

dCA-NVOC-O-4-(trimethylammonium)butyl tyrosine (dCA-NVOC-Tyr-O4Q).

Prepared as above using NVOC-O-4-(trimethylammonium)butyl tyrosine cyanomethyl ester (**3b**) as starting material. FAB-MS: $[M^+]$, calc'd for $C_{45}H_{60}N_{11}O_{21}P_2$: 1152.3440; found: 1152.3.

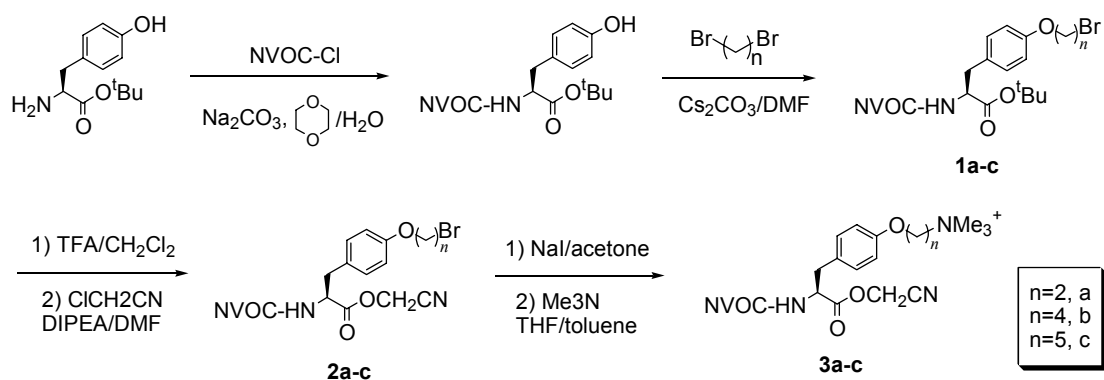
dCA-NVOC-O-5-(trimethylammonium)pentyl tyrosine (dCA-NVOC-Tyr-O5Q).

Prepared as above using NVOC-O-5-(trimethylammonium)pentyl tyrosine cyanomethyl ester (**3c**) as starting material. FAB-MS: $[M^+]$, calc'd for $C_{46}H_{62}N_{11}O_{21}P_2$: 1166.3596; found: 1166.4.

dCA-N $_{\alpha}$, N $^5_{(in)}$ -di-NVOC-5-amino tryptophan. Prepared as above using N $_{\alpha}$, N $^5_{(in)}$ -di-NVOC-5-amino tryptophan cyanomethyl ester (**8**) as starting material. FAB-MS: calc'd for $C_{50}H_{55}N_{13}O_{26}P_2$: 1316.0114; found $[M-H]^-$: 1314.2.

dCA-N-NVOC-S-trityl cysteine. Prepared as above using N-NVOC-S-trityl cysteine cyanomethyl ester as starting material. ESI-MS: calc'd for $C_{51}H_{54}N_{10}O_{20}P_2S$: 1221.0626; found $[M-H]^-$: 1219.4, $[M-2H]^{2-}$: 609.2.

Synthesis of Tyr-OnQ



Scheme 5.2. Synthesis of Tyr-OnQ.

NVOC-O-(2-bromoethyl) tyrosine t-butyl ester (1a). To a mixture of 0.690 ml (8 mmol, 16 equivalents) of 1, 2-dibromoethane and 330 mg (1 mmol, 2 equivalents) of Cs_2CO_3 in 15 ml of anhydrous DMF was added a solution of 238 mg (0.5 mmol) of NVOC-tyrosine t-butyl ester in 10 ml of DMF slowly over 10 hours using a syringe pump. After stirring overnight, the reaction mixture was quenched by adding 30 ml of water and extracted by 3 x 30 ml of ethyl acetate. The combined organic layers were washed with water once, dried (over Na_2SO_4), rotary-evaporated, and chromatographed (30:70 ethyl acetate:petroleum ether), providing 61 mg (21%) of product. ^1H NMR (CDCl_3) δ 7.69 (s, 1H), 7.05 (d, 2H), 6.95 (s, 1H), 6.81 (d, 2H), 5.54 and 5.46 (AB, 1H), 5.32 (d, 1H), 4.48 (m, 1H), 4.24 (t, 2H), 3.93 (s, 6H), 3.61 (t, 2H), 3.03 (m, 2H), 1.41 (s, 9H).

NVOC-O-(4-bromobutyl) tyrosine t-butyl ester (1b). This compound was prepared by the procedure described above except using 1, 4-dibromobutane as starting material.

Yield 67%. $^1\text{H NMR}$ (CDCl_3) δ 7.68 (s, 1H), 7.06 (d, 2H), 6.94 (s, 1H), 6.77 (d, 2H), 5.53 and 5.45 (AB, 1H), 5.35 (d, 1H), 4.46 (m, 1H), 3.94 (m, 2H), 3.92 (s, 6H), 3.46 (t, 2H), 3.01 (m, 2H), 2.02 (m, 2H), 1.90 (m, 2H), 1.40 (s, 9H).

NVOC-O-(5-bromopentyl) tyrosine t-butyl ester (1c). This compound was prepared by the procedure described above except using 1, 5-dibromopentane as starting material.

Yield 58%. $^1\text{H NMR}$ (CDCl_3) δ 7.52 (s, 1H), 6.94 (d, 2H), 6.82 (s, 1H), 6.65 (d, 2H), 5.61 (d, 1H), 5.32 (m, 2H), 4.35 (m, 1H), 3.96 (m, 2H), 3.77 (s, 6H), 3.28 (t, 2H), 2.91 (m, 2H), 1.77 (m, 2H), 1.65 (m, 2H), 1.40 (m, 2H), 1.27 (s, 9H).

NVOC-O-(4-Bromobutyl) tyrosine cyanomethyl ester (2b). To a solution of 290 mg (0.48 mmol) of azeotropically dried (with toluene) **1b** in 1.7 ml of dry CH_2Cl_2 was slowly added 2.8 ml of TFA (37.2 mmol, 77.5 equivalents). The mixture was stirred under argon at room temperature for two hours. TFA was removed by passing argon through the reaction solution. The residue was rotary-evaporated with toluene twice (2x10 ml), dried under vacuum and then used directly in the next step. To this crude product was added 5 ml of anhydrous DMF, 0.67 ml (10.5 mmol, 21.8 equivalents) of chloroacetonitrile and 96 μL of diisopropylethylamine. The mixture was stirred at room temperature overnight. After about 14 hours the reaction was quenched by adding 10 ml of 0.1 M KH_2PO_4 and 10 ml of water and then extracted with 2x50 ml of ethyl acetate. The combined organic layers were washed with water, dried (over Na_2SO_4) and rotary-evaporated. Flash chromatography (1:3 to 2:3 ethyl acetate:petroleum ether) gave 210 mg (74%) of product. $^1\text{H NMR}$ (CDCl_3) δ 7.66 (s, 1H), 7.03 (d, 2H), 6.89 (s, 1H), 6.80 (d, 2H), 5.51 and 5.41

(AB, 1H), 5.38 (d, 1H), 4.72 (m, 3H), 3.94 (m, 2H), 3.91 (s, 6H), 3.58 (t, 1H), 3.45 (t, 1H), 3.07 (m, 2H), 2.01 (m, 2H), 1.92(m, 2H).

NVOC-O-(2-Bromoethyl) tyrosine cyanomethyl ester (2a). This compound was prepared by the procedure described above using **1a** as starting material. Yield 58%. ¹H NMR (CDCl₃) δ 7.70 (s, 1H), 7.07 (d, 2H), 6.92 (s, 1H), 6.87 (d, 2H), 5.56 and 5.45 (AB, 1H), 5.29 (d, 1H), 4.76 (m, 3H), 4.27 (t, 2H), 3.95 (s, 6H), 3.63 (t, 2H), 3.10 (m, 2H).

NVOC-O-(5-Bromopentyl) tyrosine cyanomethyl ester (2c). This compound was prepared by the procedure described above using **1c** as starting material. Yield 69%. ¹H NMR (CDCl₃) δ 7.61 (s, 1H), 7.01 (d, 2H), 6.86 (s, 1H), 6.77 (d, 2H), 5.53 (d, 1H), 5.46 and 5.37 (AB, 1H), 4.71 (m, 3H), 3.89 (m, 2H), 3.87 (s, 6H), 3.51 (t, 1H), 3.38 (t, 1H), 3.05 (m, 2H), 1.87 (m, 2H), 1.75 (m, 2H), 1.56 (m, 2H).

NVOC-O-4-(trimethylammonium)butyl tyrosine cyanomethyl ester (NVOC-Tyr-O4Q) (3b). 200 mg (0.337 mmol) of **2b** was mixed with 650 mg (4.333 mmol, 12.5 equivalents) of sodium iodide in 10 ml of acetone at room temperature. The reaction was kept stirring in the dark overnight. Acetone was then rotary-evaporated off, and the solid was partitioned between water and methylene chloride (30 ml each). The aqueous layer was extracted with methylene chloride once. Organic layers were combined, washed with water once, dried (over Na₂SO₄), and rotary-evaporated to give 200 mg (93%) of yellowish solid NVOC-O-(4-iodobutyl) tyrosine cyanomethyl ester. Half of this product was carried on to make **3b**. The solution of the iodide in 7 ml of dry toluene and 12 ml of

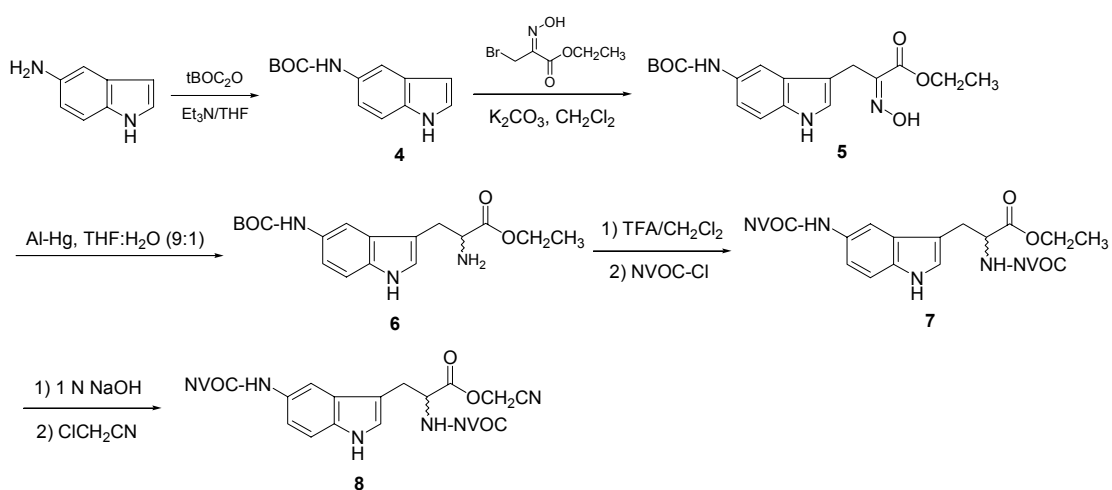
dry THF was cooled to 0 °C in an ice/NaCl bath. Then trimethylamine was passed through the solution via a metal needle for about 5 minutes. The solution was allowed to warm up to room temperature and stirred in the dark for 32 hours. Precipitate formed on the inner wall of the flask. Argon was passed through to get rid of the amine, which was trapped by 6 N HCl. When most of the amine was removed (indicated as neutral by wet pH paper), the solution was decanted and the solid was rinsed with ethyl acetate three times and dried under vacuum. Yield 70 mg (68%). ^1H NMR (CDCl_3) δ 7.74 (s, 1H), 7.23 (d, 2H), 7.13 (s, 1H), 6.91 (d, 2H), 6.46 (d, 1H), 5.46 and 5.39 (AB, 1H), 4.85 (s, 2H), 4.52 (m, 1H), 4.05 (t, 2H), 3.96 (s, 3H), 3.93 (s, 3H), 3.39 (m, 2H), 3.10 (s, 9H), 3.00 (m, 2H), 1.98 (m, 2H), 1.85 (m, 2H).

NVOC-O-2-(trimethylammonium)ethyl tyrosine cyanomethyl ester (NVOC-Tyr-O2Q) (3a). This compound was prepared by the procedure described above using **2a** as starting material. Yield 85%. ^1H NMR (CDCl_3) δ 7.73 (s, 1H), 7.26 (d, 2H), 7.11 (s, 1H), 6.94 (d, 2H), 6.41 (d, 1H), 5.44 and 5.37 (AB, 1H), 4.83 (s, 2H), 4.55 (m, 1H), 4.41 (m, 2H), 3.95 (s, 3H), 3.92 (s, 3H), 3.74 (m, 2H), 3.20 (s, 9H), 3.01 (m, 2H).

NVOC-O-5-(trimethylammonium)pentyl tyrosine cyanomethyl ester (NVOC-Tyr-O5Q) (3c). This compound was prepared by the procedure described above using **2c** as starting material. Yield 74%. ^1H NMR (CDCl_3) δ 7.72 (s, 1H), 7.20 (d, 2H), 7.11 (s, 1H), 6.87 (d, 2H), 6.47 (d, 1H), 5.44 and 5.37 (AB, 1H), 4.83 (s, 2H), 4.51 (m, 1H), 4.00 (t, 2H), 3.92 (s, 3H), 3.90 (s, 3H), 3.31 (m, 2H), 3.13 (m, 2H), 3.08 (s, 9H), 1.98 (m, 2H), 1.83 (m, 2H), 1.53 (m, 2H).

Synthesis of 5-Amino Tryptophan

Besides the tryptophan analogs with electron-withdrawing groups discussed in Chapter 2, we also made 5-amino tryptophan as one with an electron-donating group. The synthetic strategy (Scheme 5.3) was based on the method developed by Roberts and coworkers (18). We have used this route previously to make many tryptophan analogs (19). This strategy simplified the synthesis of tryptophan analogs to the synthesis of the corresponding indole derivatives.



Scheme 5.3. Synthesis of 5-amino tryptophan.

5-(*tert*-butoxycarbonylamino)indole (4). A heterogeneous solution of 1.0 g of 5-amino indole in 15 ml of dry THF was stirred for 15 minutes before 1.816 g (1.1 eq) of Di-*tert*-butyl dicarbonate (taken from refrigerator right before weighing) was added. The mixture was stirred for one and a half hours before it was quenched with 15 ml of saturated NaCl. The aqueous layer was extracted with 20 ml of THF twice and the

organic layers were combined, washed with saturated NaCl, dried over Na₂SO₄ and rotary-evaporated. Flash chromatography (ethyl acetate: petroleum ether 1:3) gave 1.188 g (68%) of product. ¹H NMR (CDCl₃) δ 1.56 (s, 9H), 6.49 (s, 1H), 6.51 (t, 1H), 7.14 (d, 1H), 7.21 (t, 1H), 7.35 (d, 1H), 7.72 (s, 1H), 8.14 (s, 1H).

5-(*tert*-butoxycarbonylamino)- α -hydroxyimino-tryptophan ethyl ester (5). To a solution of 129 mg (1eq) of ethyl 3-bromo-2-hydroxyimino-propanoate (*19*) and 494 mg (3.5 eq) of **4** in 6 ml of dry CH₂Cl₂ was added 98 mg of anhydrous Na₂CO₃. The reaction was kept stirring for 2 hours before it was quenched by 10 ml of CH₂Cl₂ and 10 ml of H₂O. The aqueous layer was extracted with CH₂Cl₂. The organic layers were combined, washed with H₂O, dried over Na₂SO₄ and rotary-evaporated to give a white solid. Flash chromatography (ethyl acetate: petroleum ether 1:1) gave 118 mg (53%) of product. ¹H NMR (CDCl₃) δ 1.28 (t, 3H), 1.51 (s, 9H), 4.04 (s, 2H), 4.24 (q, 2H), 6.50 (s, 1H), 7.08 (d, 1H), 7.22 (d, 1H), 7.24 (d, 1H), 7.72 (s, 1H), 7.96 (b, 1H), 8.85 (s, 1H).

5-(*tert*-butoxycarbonylamino) tryptophan ethyl ester (6). To a 25 ml flask containing 118 mg of **5** was added 9 ml of THF and 1 ml of H₂O. Two aluminum pellets were weighed (778 mg), treated with 8% NaOH for 3 minutes, rinsed with water and then treated with 2% HgCl₂ for 5 minutes. The pellets were then added to the solution of **5**. Gray precipitate appeared gradually. The reaction was kept stirring overnight and then 15 ml of THF was added. The mixture was filtered and the filtrate was dried over Na₂SO₄ and rotary-evaporated to give light yellow sticky oil. Yield (83%). ¹H NMR

(CDCl₃) δ 1.24 (t, 3H), 1.51 (s, 9H), 3.01 (dd, 1H), 3.20 (dd, 1H), 3.73 (m, 3H), 4.15 (q, 2H), 6.48 (b, 1H), 7.02 (s, 1H), 7.13 (d, 1H), 7.23 (d, 1H), 7.61 (s, 1H), 8.08 (s, 1H).

N α , N⁵_(in)-di-NVOC-5-amino tryptophan ethyl ester (7). To a 10 ml flask containing 86 mg of **6** was added 1 ml of dry CH₂Cl₂ and 102 mg of p-dimethoxybenzene, followed by 1 ml of TFA. After stirring at room temperature for 1 hour, argon was bubbled through the flask to remove CH₂Cl₂ and TFA and a sticky solid was obtained. 2 ml of CH₂Cl₂ was added and the solution was rotary-evaporated. Then 1 ml of toluene was added and the mixture was vacuum pumped for a few hours to yield an orange-brown sticky solid which was reacted with NVOC-Cl using the standard procedure. 120 mg (67%) of product was obtained. ¹H NMR (CDCl₃) δ 1.23 (t, 3H), 3.31 (m, 2H), 3.87, 3.94 and 3.98 (s, 12H), 4.17 (m, 2H), 4.72 (q, 1H), 5.50 (s, 2H), 5.59 (s, 2H), 5.40 (d, 1H), 6.92 (s, 1H), 7.03 (s, 1H), 7.10 (d, 1H), 7.26 (d, 1H), 7.60 (s, 1H), 7.69 (s, 2H), 7.73 (s, 1H), 8.07 (s, 1H).

N α , N⁵_(in)-di-NVOC-5-amino tryptophan cyanomethyl ester (8). To a 25 ml flask containing 120 mg of **7** was added 10 ml of dioxane and 2 ml of H₂O, followed by 1 ml of 1N NaOH. After stirring for 4 hours, the reaction was stopped. 30 ml of CH₂Cl₂, 10 ml of 1M KH₂PO₄ (pH 4) and 20 ml of H₂O were added. The aqueous layer was separated and adjusted to pH 4 with KH₂PO₄. Aqueous layer was extracted with 20 ml of CH₂Cl₂. The organic layers were combined, washed with H₂O, dried over Na₂SO₄ and rotary-evaporated. The crude product was used directly to prepare the cyanomethyl ester using the standard procedure. Yield 42%. ¹H NMR (CDCl₃) δ 3.32 (m, 2H), 3.90, 3.93 and

3.95 (s, 12H), 4.65 (b, 1H), 4.70 (m, 1H), 4.84 (m, 1H), 5.37 (d, 2H), 5.48 (d, 2H), 5.59 (s, 2H), 6.91 (s, 1H), 7.08 (s, 1H), 7.10 (d, 1H), 7.32 (d, 1H), 7.60 (s, 1H), 7.68 (s, 2H), 7.72 (s, 1H), 8.12 (s, 1H).

Synthesis of MTSET-Modified Cysteine

N-NVOC-S-trityl cysteine. This compound was prepared from S-trityl cysteine and NVOC-Cl using the standard procedure. Yield 58%. ^1H NMR (acetone- d^6) δ 2.70 (m, 2H), 3.86 (s, 3H), 3.93 (s, 3H), 4.16 (m, 1H), 5.46 (s, 2H), 6.98 (d, 1H), 7.19 (s, 1H), 7.35 (m, 15H), 7.71 (s, 1H).

N-NVOC-S-trityl cysteine cyanomethyl ester. This compound was prepared from N-NVOC-S-trityl cysteine and chloroacetonitrile using the standard procedure. Yield 88%. ^1H NMR (acetone- d^6) δ 2.65 (dd, 2H), 3.90 (s, 3H), 3.94 (s, 3H), 4.13 (m, 1H), 4.93 (s, 2H), 5.47 (s, 2H), 7.18 (s, 1H), 7.25-7.44 (m, 15H), 7.73 (s, 1H).

N-NVOC-cysteine cyanomethyl ester. The deprotection of the trityl group was carried out using a procedure reported by Pearson et al (20). To a 50 ml flask containing 600 mg of N-NVOC-S-trityl cysteine cyanomethyl ester was added 3 ml of CH_2Cl_2 , 0.6 ml (4 eq) of triethylsilane and 1.5 ml (20 eq) of TFA. The reaction mixture turned green yellow right away and was stirred for 50 minutes. Argon was passed through to remove TFA. CH_2Cl_2 was added and then rotary-evaporated and vacuum pumped. Flash chromatography (30:70 ethyl acetate: petroleum ether) gave 78% product. ^1H NMR

(CDCl₃) δ 1.47 (t, 1H), 3.06 (m, 2H), 3.96 (s, 3H), 4.01 (s, 3H), 4.80 (m, 3H), 5.51 and 5.60 (AB, 2H), 5.75 (d, 1H), 7.01 (s, 1H), 7.72 (s, 1H).

N-NVOC-cysteine. This compound was prepared as above using N-NVOC-S-trityl cysteine as starting material. Yield 96%. ¹H NMR (CD₃CN) δ 1.85 (t, 1H), 2.97 (m, 2H), 3.91 (s, 3H), 3.97 (s, 3H), 4.44 (m, 1H), 5.46 (s, 2H), 7.17 (s, 1H), 7.72 (s, 1H).

N-NVOC-S-(2-trimethylammonium)ethylthio cysteine. To a 5 ml flask was added 35 mg of N-NVOC-cysteine and 40 mg (1.5 eq) of MTSET followed by 2.5 ml of dry ethanol and 1 ml of dry acetonitrile. TLC showed the reaction was complete after 10 minutes. The reaction mixture was stirred for another 10 minutes and then frozen and lyophilized. The yellow solid obtained was dissolved in ~1:1 H₂O:acetonitrile in portions right before HPLC injection. The product was purified by semi-preparative HPLC, eluting with a gradient of from 25 mM NH₄OAc to acetonitrile and eluted at ~25% of acetonitrile. The fractions were combined and lyophilized. Yield 70%. ¹H NMR (D₂O) δ 2.83 (dd, 1H), 2.96 (s, 11H), 3.14 (dd, 1H), 3.48 (m, 2H), 3.71 (s, 3H), 3.77 (s, 3H), 4.16 (q, 1H), 4.64 (s, 2H), 5.10 and 5.27 (AB, 2H), 6.88 (s, 1H), 7.51 (s, 1H). ESI-MS: calc'd for C₁₈H₂₈N₃O₈S₂: 478.57; found [M]⁺: 478.2.

N-NVOC-S-(2-trimethylammonium)ethylthio cysteine cyanomethyl ester. The reaction was run in a similar way as above except that ~1 eq of sodium ethoxide was also added. The reaction was monitored by analytical HPLC with a gradient from 25 mM NH₄OAc to acetonitrile. The product was separated by semi-preparative HPLC but MS

and ^1H NMR indicated a mixture of expected product and its hydrolyzed byproduct. ^1H NMR (D_2O) δ 3.15 (d or t). ESI-MS: calc'd for $\text{C}_{20}\text{H}_{29}\text{N}_4\text{O}_8\text{S}_2$: 517.606; found $[\text{M}]^+$: 517.2 and 478.2.

4-N-o-Nitrophenyl sulfenyl-2'-deoxycytidylyl(3'-5')adenosine-5'-phosphate (NPS-dCA). This compound was prepared according to the reported literature (21). To a 25 ml flask was added 192 mg of the tetrabutylammonium salt of dCA and 6ml of dry DMSO. To this solution was added 3x44.3 mg (~4 eq) of o-nitrophenyl sulfenyl chloride and 3 x 33 μl (~4eq) of triethylamine at 0, 1.5 and 3 hours. The reaction was quenched after 5 hours with a solution of 257 mg of NH_4OAc in 2-3 ml of H_2O and lyophilized to a yellow solid. The product was purified by preparative HPLC, eluting with a gradient of 0-40% acetonitrile in aqueous 25 mM NH_4OAc . The appropriate fractions were collected, combined and lyophilized. Yield 48%. ^1H NMR (500 MHz) (D_2O) δ 1.88 (m, 1H), 2.32 (m, 1H), 3.89 (s, 2H), 4.01 (m, 2H), 4.14 (s, 1H), 4.20 (s, 1H), 4.39 (t, 1H), 4.55 (t, 1H), 5.85 (d, 1H), 5.96 (m, 1H), 6.11 (b, 1H), 7.08 (d, 2H), 4.34 (b, 1H), 7.78 (d, 1H), 7.91 (s, 1H), 7.95 (b, 1H), 8.25 (s, 1H). ESI-MS: calc'd for $\text{C}_{25}\text{H}_{29}\text{N}_9\text{O}_{15}\text{P}_2\text{S}$: 789.57; found $[\text{M-H}]^-$ 788.0 and $[\text{M-2H}]^{2-}$ 393.4.

5.4 Reference

1. Nowak, M. W., Gallivan, J. P., Silverman, S. K., Labarca, C. G., Dougherty, D. A., and Lester, H. A. (1998) *Meth. Enzymol.* 293, 504-529.

2. Saks, M. E., Sampson, J. R., Nowak, M. W., Kearney, P. C., Du, F., Abelson, J. N., Lester, H. A., and Dougherty, D. A. (1996) *J. Biol. Chem.* 271, 23169-23175.
3. Quick, M., and Lester, H. A. (1994) in *Ion Channels of Excitable Cells* (Narahashi, T., Ed.) pp 261-279, Academic Press, San Diego, CA.
4. Gallivan, J. P., Lester, H. A., and Dougherty, D. A. (1997) *Chem. Biol.* 4, 739-749.
5. England, P. M., Zhang, Y., Dougherty, D. A., and Lester, H. A. (1999) *Cell* 96, 89-98.
6. Ivanina, T., Peters, T., Thornhill, W. B., Levin, G., Dascal, N., and Lotan, I. (1994) *Biochemistry* 33, 8786-8792.
7. Lim, K.-T., Brunett, S., Iotov, M., McClurg, R. B., Vaidehi, N., Dasgupta, S., Taylor, S. and Goddard, W. W., III. (1997) *J. Comput. Chem.* 18, 501-521.
8. Mayo, S. L., Olafson, B.D., and Goddard III, W.A. (1990) *J. Phys. Chem.* 94, 8897-8909.
9. Ding, H. Q., Karasawa, N. and Goddard, W. A., III. (1992) *J. Chem. Phys.* 97, 4309-4315.
10. Ghosh, A., Rapp, C. S. and Friesner, R. A. (1998) *J. Phys. Chem. B* 102, 10983-10990.
11. MacKerell, A. D., Bashford, D., Bellott, M., Dunbrack, R. L., Evanseck, J.D., Field, M.J., Fischer, S., Gao, J., Guo, H., Ha, S., Joseph-McCarthy, D., Kuchnir, L., Kuczera, K., Lau, F.T.K., Mattos, C., Michnick, S., Ngo, T., Nguyen, D.T., Prodhom, B., Reiher, W.E., Roux, B., Schlenkrich, M., Smith, J.C., Stote, R., Straub, J., Watanabe, M.,

- Wiorcikiewicz-Kuczera, J., Yin, D., and Karplus, M. (1998) *J. Phys. Chem. B* 102, 3586-3616.
12. Tannor, D. J., Marten, B., Murphy, R., Friesner, R.A., Sitkoff, D., Nicholls, A., Ringnalda, M., Goddard III, W.A., and Honig, B. (1994) *J. Am. Chem. Soc.* 116, 11875-11882.
13. Floriano, W. B., Vaidehi, N., Goddard, W. A., Singer, M. S., and Shepherd, G. M. (2000) *Proc. Natl. Acad. Sci. USA* 97, 10712-6.
14. Ewing, T. J. A., and Kuntz, I. D. (1997) *Journal of Computational Chemistry* 18, 1175-1189.
15. Wang, P., Vaidehi, N., Tirrell, D.A., and Goddard III, W. A. (2002) *J. Am. Chem. Soc.* (in press).
16. Kearney, P. C., Nowak, N. W., Zhong, W., Silverman, S., K., Lester, H. A., and Dougherty, D. A. (1996) *Mol. Pharmacol.* 50, 1401-1412.
17. Robertson, S. A., Ellman, J. A., and Schultz, P. G. (1991) *J. Am. Chem. Soc.* 113, 2722-2729.
18. Gilchrist, T. L., Lingham, D. A., and Roberts, T. G. (1979) *J. C. S. Chem. Comm.*, 1089-1090.
19. Zhong, W. (1998) in *Chemistry*, California Institute of Technology, Pasadena, CA.
20. Pearson, D. A., Blanchette, M., Baker, M. L., and Guindon, C. A. (1989) *Tetrahedron Lett.* 30, 2739-2742.
21. Robertson, S. A., Noren, C. J., Anthony-Cahill, S. J., Griffin, M. C., and Schultz, P. G. (1989) *Nucleic Acids Res.* 17, 9649-9660.

Appendix I. Summary of results of incorporation of Tyr-OnQ at different positions around the agonist-binding site of nAChR

Site	Exp. Date	Tethered Agonists Tried	# of Oocytes Recorded	Leakage Current (nA)	TMB-8 Blockable Current	ACh-induced Current						Note	Summary of Results
α86	10/14/98	Q3	6	-925	0	25 μM						* In 10/14/98 Exp. Control (Q3 α149) expressed well, but leaky.	At α86, only Q3 tried. Neither constitutive current nor ACh (25 μM) current seen.
						0							
α184	10/14/98	Q3	6	-1001	0	1 μM	5 μM	25 μM	100 μM	500 μM	*		At α184, all tethers tried, no constitutive current, all gave ACh current, but dCA current is high.
						228	681	756		842			
	10/1/98	Q2	6	-114	0		338	533	551				
		Q3	7	-121	0		568	877	993				
		Q4	5	-155	0		752	1071	1175				
		Q5	3	-150	0		610	848	998				
		dCA	7	-117	0		1255	1522	1698				
	10/2/98	Q2	5	-248	0		252	715					
		Q3	5	-502	0		588	1754					
		Q4	5	-423	0		401	1161					
Q5		5	-158	0		145	435						
dCA		5	-284	0		263	654						
α190	10/14/98	Q3	10	-372.5	0	25 μM						*	At α190, only Q3 tried, Neither constitutive current nor ACh (25 μM) current seen.
α198	10/14/98	Q3	8	-189	0	25 μM	500 μM				*		At α198, all tethers tried, only Q4 showed small constitutive current. All give ACh current, dCA current high.
						0	0						
	9/3/99	Q2	5	-48	0		19	170				Control (Q4, α93) expressed normally.	
		Q3	5	-82	0		29	219					
		Q4	8	-162.5	94		76	503.75					
		Q5	6	-145	0		19	177.5					
		dCA	5	-169	0		175	1209					

α192	3/3/99	Q5	6	-95	0	25 μM				§. In 3/3/99 exp. Control(Q4,α93) expressed OK.	At α192, only Q5 tried, small ACh current, no constitutive current.
						0.5 μM	5 μM	25 μM	11.25		
α193	2/24/99	Q3	3	-1368	0	0.5 μM	5 μM	25 μM	†. In 2/24/99 exp. Control(Q3,α93) expressed poorly.	At α193, all tethers tried, only Q4 showed very small constitutive current once when expressed well. All gave ACh current.	
	3/3/99	Q4	9	-152	48.5	8	102.5	375	§		
	3/11/99	Q2	5	-966	0	19	97.5	All tethers expressed low due to low tRNA concentration.	Control(Q3,α93)		
		Q3	6	-119	0	20	117.5				
		Q4	3	-795	0	5	45				
		Q5	4	-1152.5	0		0				
		dCA	5	-76	0		71				
	2/24/99	Q3	4	-266	0	0.5 μM	5 μM	25 μM	†		
	α194	3/3/99	Q5	9	-216	90.5	142.5	767.5	1385	§	At α194, all tethers tried, and all showed small constitutive current once in different exp. (3/3 and 7/1) when expression is very high (based on ACh Current).
			Q2	8	-64	0	932.5	6991	7980		
3/19/99		Q3	7	-55	0	152.5	37.8	Express low, probably need high tRNA concentration.	Control(Q4,α93)		
		Q4	5	-123	0	19	129	Expresses low due to low tRNA conc.			
		Q5	9	-78	5	225	155	Control (Q4, α93) expressed poorly.			
		dCA	8	-62	0	91	0				
		Q2	7	-81	0		248				
4/1/99		Q3	8	-91	0		129		Leaky oocytes.		
		Q4	6	-132.5	0		248				
7/1/99		Q5	10	-86	0		155		Control (Q4, α93) expressed poorly.		
	dCA		6	-72.5	0	1544	0				
	Q2	1	-4440	80	600	2100		Leaky oocytes.			
	Q3	2	-2487.5	75	995	4207.5					
	Q4	4	-501	11.25	822.5	3507.5					
dCA	2	-402.5	0	395	2235						

γ174/ δ180	8/19/99	Q2	5	-106	-19	5 μM	125 μM	500 μM	Application of TMB-8 led to very small inward current.	At γ174/δ180, all tethers tried, no constitutive current, all gave ACh current, but dCA current high.
		Q2	5	-106	-19	722	1045	1633		
		Q3	5	-233	0	126	217	304		
		Q4	5	-148	-12.5	1749	2600	3553		
		Q5	5	-77	-15	107	185	252		
		dCA	6	-74	0	2507.5				